The Discovery of Drug-like Modulators for Dynamic Transcriptional Coactivators via Novel Screening Strategies

by

Ayza Croskey

A dissertation submitted in partial fulfillment
of the requirements for the degree of
Doctorate of Philosophy
(Chemical Biology)
in the University of Michigan
2025

Doctoral Committee:

Professor Anna K. Mapp, Chair
Professor Charles L. Brooks III
Professor Tomasz Cierpicki
Associate Professor Wenjing Wang

Ayza Croskey

cayza@umich.edu

ORCID iD: 0000-0002-0806-0097

© Ayza Croskey 2025

Dedication

To all the little Black kids who look beyond their present and the first-generation college students who dare to dream big

Acknowledgements

I've had so many wonderful people in my life through this journey, and I am so appreciative of all their contributions in my life. There's so much I can say but I prefer to share all of my specific sappy sentiments in-person; however, I do want to say to everyone who has been with me and supported me throughout this journey that I love and appreciate you.

Table of Contents

Dedication ii

Acknowledgements iii

List of Tables vii

List of Figures viii

List of Appendices xii

Abstract xiii

Chapter 1 The Challenge in Modulating Transcriptional Coactivator Domains and the Opportunity in Their Dynamics 1

1.1 Intrinsic disorder and molecular recognition 1

1.2 The importance of dynamic transcriptional coactivators 2

1.3 Activator binding domains 5

1.4 Presently known probes/inhibitors for the dynamic ABDs 8

1.5 The primary screening methods for targeting IDR-containing domains 10

1.6 Dissertation Summary 13

1.7 References 14

Chapter 2 Targeting Loop Dynamics in the Search for Modulators for CBP KIX 21

2.1 Abstract 21

2.2 Introduction 22

2.3 Results and Discussion 24

2.3.1 Buffering conditions facilitate the thermostability evaluation of the CBP KIX domain 24

2.3.2 High-throughput conformational stability assessment of CBP KIX in the presence of a diverse chemical library 27

2.3.3 A dual approach to examine modulator effects on the CBP KIX domain and its PPIs 29

2.3.4 Investigation of the oxyclozanide scaffold and its key interactions 34

2.4 Conclusions 37

2.5 Materials and Methods 37

2.6 References 49

Chapter 3 Setting the Stage for Targeting and Investigating the MED15 KIX Motifs 54

3.1 Abstract 54

3.2 Introduction 54

3.3 Results and Discussion 57

3.3.1 Optimization of assay conditions for cgMED15 and ARC105/MED15 KIX motifs 57

3.3.2 Identification of diverse modulators for cgMed15 KIX and Arc105 KIX and exploration of oxyclozanide's inhibition of alpha helical domains 60

3.3.3 Examination of the conformational and ligand landscape of ARC105 KIX 63

3.4 Conclusions 65

3.5 Materials and Methods 66

3.6 References 69

Chapter 4 Uncovering Colorimetric Dye Sensors that Engage Conformationally Dynamic ABDs and Detect Their Binding Events 71

4.1 Abstract 71

4.2 Introduction 71

4.3 Results and Discussion 75

4.3.1 Identifying colorimetric tools for two conformationally dynamic coactivator domains Med25 AcID and CBP KIX 75

4.3.2 Examination of significant ABD conformational stabilization with the colorimetric dye Erythrosin B 81

4.4 Conclusions 82

4.5 Materials and Methods 83

4.6 References 86

Chapter 5 Conclusions and Future Directions 90

5.1 Conclusions 90

5.2 Future Directions 93

5.2.1 Structure-guide development of a more potent mixed mechanism inhibitor 93

5.2.2 All-around probing of the MED15 KIX motifs 94

5.2.3 Mechanistic insights into the colorimetric dyes 94

5.3 References 97

Appendices 99

List of Tables

Table 1.1 Current probes for CBP KIX, Med25 AcID, Arc105 KIX, and cgMed15 KIX. ... 8

Table A.1 Sequences of activator peptides used in this study. 99

Table A.2 Summary of masses of activator peptides used in this study. 100

Table D.1 Dye concentrations for the initial colorimetric array screening 126

List of Figures

Figure 1.1 An illustration of the difference in the conformational landscape of structured and intrinsically disordered proteins. 2

Figure 1.2 Transcriptional coactivators are central hub proteins of transcription. 3

Figure 1.3 A pictural representation of the CREB-Binding Protein 4

Figure 1.4 A pictural representation of the Mediator complex 5

Figure 1.5 Structures of the CBP KIX domain (top) and the Med25 AcID domain (bottom) with their binding partners. 6

Figure 1.6 Structures of the Arc105 (left) and cgMed15 (right) KIX domains and their corresponding transactivation domains *Oaf-1 binds under the condition that it has been activated. 7

Figure 2.1 CBP KIX buffer composition screening. 26

Figure 2.2 The optimized buffer conditions enable the examination of CBP KIX binding events via DSF. 27

Figure 2.3 Dual-site inhibitor MybLLtide serve as the optimal positive control effector for HTS. 28

Figure 2.4 The DSF screening of a diverse library against CBP KIX 29

Figure 2.5 Examination of the modulators by HSQC NMR identified those initiated significant shifts in the backbone 30

Figure 2.6 Visualization of the key residues perturbed by modulator binding 32

Figure 2.7 Establishment of the dual fluorescence polarization assay for CBP KIX 33

Figure 2.8 Discovery of a mixed mechanism inhibitor in oxyclozanide 34

Figure 2.9 Assessment of the oxyclozanide analogs 35

Figure 2.10 Mapping the key interactions between oxyclozanide and CBP KIX 36

Figure 3.1 An illustration of the sequence and structural similarities within the KIX motifs. 56

Figure 3.2 Assay optimization steps and the proof-of-concept for DSF application against MED15 KIX motifs 59

Figure 3.3 Use of the 29 CBP KIX modulators in DSF screening for MED15 KIX motifs 61

Figure 3.4 Recognition of oxyclozanide a pan-inhibitor for KIX motifs 62

Figure 3.5 Expanding the conformational landscape and ligandibility of ARC105 KIX .. 65

Figure 4.1 Examples of dyes and tags found in colorimetry and fluorimetry 74

Figure 4.2 Three dye candidates were identified from the colorimetric array as potential tools. 77

Figure 4.3 Absorbance spectra for the three candidates in the presence and absence of each ABD. 79

Figure 4.4 PCA plots of the dye sensors in the presence of varied concentrations of ABD. 80

Figure 4.5 A comparative assessment of significant ABD binding events. 82

Figure 5.1 The KIX motif modulators identified in this work 92

Figure 5.2 The surface view of oxyclozanide docked with CBP KIX 94

Figure 5.3 The colorimetric dyes identified for model domains Med25 AcID and CBP KIX 97

Figure A.1 Chromatogram and MS Spectrum for FITC-MLL 101

Figure A.2 Chromatogram and MS Spectrum for Unlabeled MLL 102

Figure A.3 Chromatogram and MS Spectra for TR-MLL 103

Figure A.4 Chromatogram and MS Spectra for FITC-Myb 104

Figure A.5 Chromatogram and MS Spectra for unlabeled Myb 105

Figure A.6 Chromatogram and MS Spectra for FITC-Myb32 106

Figure A.7 Chromatogram and MS Spectrum for FITC-Pdr1 107

Figure A.8 Chromatogram and MS Spectrum for Ac-Pdr1 108

Figure A.9 Chromatogram and MS Spectra for FITC-SREBP1a 109

Figure A.10 Chromatogram and MS Spectrum for Ac-SREBP1a 110

Figure A.11 Chromatogram and MS Spectra for FITC-Oaf1 111

Figure A.12. Analytical HPLC trace of FITC-MLL monitored at 214 and 495 nm. 113

Figure A.13. Analytical HPLC trace of β-Ala-MLL monitored at 214 nm. 113

Figure A.14 Analytical HPLC trace of TR-MLL monitored at 280 and 595 nm. 114

Figure A.15 Analytical HPLC trace of β-Ala-Myb monitored at 214 and 280 nm. 114

Figure A.16 Analytical HPLC trace of FITC-Myb32 monitored at 280 and 495 nm. 115

Figure A.17 Analytical HPLC trace of FITC-Pdr1 monitored at 214 and 495 nm. 115

Figure A.18 Analytical HPLC trace of Ac-Pdr1 monitored at 214 nm. 116

Figure A.19 Analytical HPLC trace of FITC-SREBP-1a monitored at 214 and 280 nm. 116

Figure A.20 Analytical HPLC trace of Ac-SREBP-1a monitored at 214 nm. 117

Figure A.21 Analytical HPLC trace of FITC-Oaf-1 monitored at 214 and 280 nm. 117

Figure B.1 Med25 AcID is a thermostable dynamic ABD 118

Figure B.2 DSF screening is not feasible with CBP KIX in Med25 AcID Buffer 118

Figure B.3 Sodium phosphate concentration can shift TAD binding affinity 119

Figure B.4 Analysis of the regional chemical shifts for the significant CBP KIX modulators 119

Figure C.1 Preliminary DSF assessment with cgMed15 KIX and SYPRO Orange 120

Figure C.2 Top conditions for bis-ANS in Med25 AcID DSF assessment 121

Figure C.3 The strong CBP IBiD and ACTR interaction is effectively inhibited by oxyclozanide. 121

Figure C.4 Med25 AcID PPIs are largely unaffected by oxyclozanide 122

Figure C.5 FP Direct Binding Experiments with the known native ligands of cgMed15 KIX and Arc105 KIX 122

Figure C.6 Arc105 KIX Direct Binding with alternative TADs and TAD Sequence comparison 123

Figure C.7 Garcinolic Acid inhibits Arc105 KIX interactions to similar degrees. 123

Figure D.1 The 23 dyes utilized in the colorimetric array screening 124

Figure D.2 PCA of the absorbance spectra for each ABD as single concentration compared to the dye alone 125

List of Appendices

Appendix A: Sequences and Characterization of Synthesized Peptides.....99

Appendix B: Supplemental Data for Chapter 2 – Targeting Loop Dynamics in the Search for Modulators for CBP KIX 118

Appendix C: Supplemental Data for Chapter 3 – Setting the Stage for Targeting and Investigating the MED15 KIX Motifs.....120

Appendix D: Supplemental Data for Chapter 4 – Uncovering Colorimetric Dye Sensors that Engage Conformationally Dynamic ABDs and Detect Their Binding Events 124

Abstract

Intrinsic disorder is key to molecular recognition, and the prevalence of intrinsically disordered regions (IDRs) is advantageous in forming networks composed of transient interactions, which is pivotal for processes such as transcription. More specifically, transcriptional coactivators are central players that mediate the protein-protein interactions (PPIs) that regulate gene expression and cell differentiation. These proteins can undergo conformational shifts that allow them to recognize diverse binding partners. Dysregulation of the PPIs formed between coactivators and associated transcription factors is commonly seen in numerous pathological states. Thus, the key transcription factor-interacting domains within coactivators are optimal targets for drug discovery efforts. Deploying traditional high-throughput screening approaches has had limited success in identifying drug-like molecules that effectively modulate these domains. Here we propose that dye-based methods have significant potential at the forefront of screening strategies for dynamic coactivator domains. We demonstrate that prioritizing target engagement effectively distinguishes modulators that engage the IDRs of coactivator domains and inhibit their PPIs via orthosteric and allosteric mechanisms.

This dissertation presents the development and implementation of screening methods that identify inhibitors and probes that engage flexible loop dynamics in coactivator domains. As a starting point, the conformationally dynamic KIX domain within the coactivator CBP used as a model dynamic domain. Thermostabilization

served as a common thread amongst the previously identified mixed mechanism inhibitors for CBP KIX, implicating the value of thermostability assessment in the discovery of these molecules for dynamic domains. Thus, we demonstrated that DSF is suited for CBP KIX screening. Further, we conducted a screen of a diverse compound library, leading to the identification of several probes that engage and stabilize CBP KIX. Structural evaluation of probe binding revealed engagement of the flexible loop between the alpha-1 and -2 helices. Functional assessment of these probes discovered a global inhibitor for CBP KIX, oxyclozanide. Thus, we investigated its scaffold and confirmed its binding mode as a mixed mechanism inhibitor that engages the crucial flexible loop.

Next, we hypothesized that the structural and sequential conservation of the KIX motifs would enable the discovery of novel ligands for the investigation of KIX motifs in humans and yeast. DSF platforms were developed and implemented for Arc105 and cgMed15 KIX. Of the hits from CBP KIX screen that were tested, we discovered structurally diverse modulators for both domains as well as established oxyclozanide as a inhibitor across KIX motifs, establishing a scaffold for development. Finally, assessment of the dynamics and peptide binding exemplify the Arc105 KIX's malleability and set the stage for further studies of KIX motifs.

Finally, we sought to discover more accessible screening tools for dynamic domains in colorimetric dyes. With a rich history in analyte detection, the colorimetric array enabled the assessment of a diverse set of dyes against Med25 AcID and CBP KIX via two primary analysis methods, elucidating three dyes. Secondary analysis pinpointed erythrosin B as a versatile colorimetric tool. Further assessment of erythrosin B for Med25 AcID and CBP KIX binding events with mixed mechanism inhibitors

displayed a relationship between significant protein stabilization and dye response, suggesting its potential for screening conformationally fluid domains. In summary, coactivator domains demand novel approaches for investigating and targeting their dynamic behavior. There is significant potential in the identified strategies, scaffolds, and tools outline in this work that will facilitate the targeting of dynamic domains.

Chapter 1 The Challenge in Modulating Transcriptional Coactivator Domains and the Opportunity in Their Dynamics

1.1 Intrinsic disorder and molecular recognition

The eukaryotic proteome consists of proteins that contain varying combinations of ordered and disordered regions.[1] Proteins without significant intrinsic disorder are called structured proteins, and proteins with entirely disordered that do not adopt any tertiary structure are referred to as intrinsically disordered proteins (IDPs). While ordered proteins usually have a single, well-defined conformation representing a global free-energy minimum with the potential to bind small molecules with high affinity, the free-energy landscape of disordered proteins is characterized by numerous local minima.[2] These minima correspond to the many conformations within the structural ensemble populated by disordered protein. (Figure 1.1) Regions of disorder are found to be abundant in proteins associated with signaling, cancer, cardiovascular disease, neurodegenerative disease, and diabetes.[3]

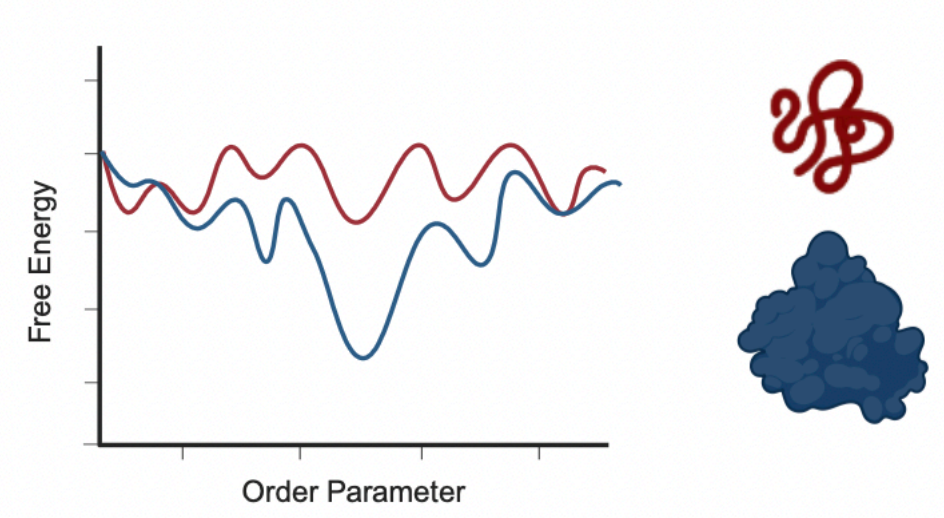


Figure 1.1 An illustration of the difference in the conformational landscape of structured and intrinsically disordered proteins. Secondary and especially tertiary protein structure significantly impact a protein's free energy of binding. The order parameter on the x-axis represents the degree of order within a protein structure. The free energy on the y-axis represents the free energy of ligand binding.

1.2 The importance of dynamic transcriptional coactivators

Transcription is the process that initiates gene expression and cell differentiation. This process is regulated by protein complexes made up of dynamic protein substructures. These substructures undergo conformational shifts, which allows them to achieve and regulate selectivity for different binding partners.[4] This is particularly useful in the formation of transcriptional protein-protein interactions (PPIs), which are often transient and dynamic.[5] Transcriptional coactivators stand at the center of these PPIs by binding RNA Polymerase II, transcription factors/activators, epigenetic modulators, and even other coactivators.[6–9] Coactivators act as major regulatory proteins by mediating the interactions within transcriptional complexes in the activation of RNA polymerase II activity and the recruitment of histone-modifying enzymes to DNA chromatin. (Figure 1.2) The dysregulation of the interactions between transcriptional coactivators and transcriptional machinery is a common motif observed in disease[10–17]

and depending on the coactivator, there are varying degrees of knowledge surrounding its interactions. Thus, targeting the key interacting domains within coactivators would aid in the investigation of these interactions and the development of therapeutics for a range of diseases.

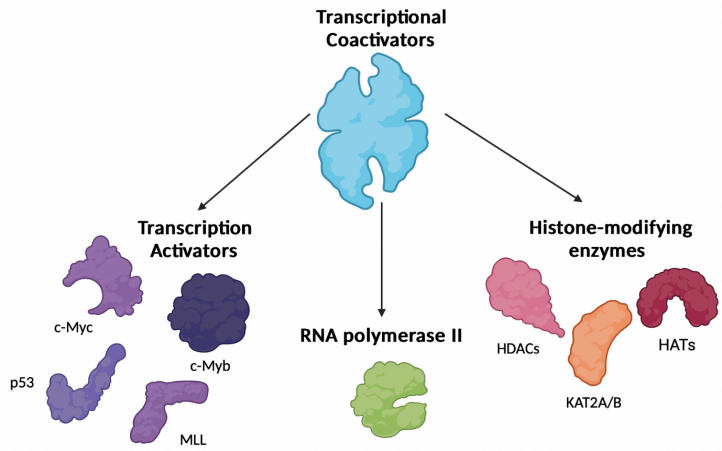


Figure 1.2 Transcriptional coactivators are central hub proteins of transcription. These proteins directly and indirectly mediate the interactions of all aspects of transcription.[6-8]

The cAMP-response element-binding protein (CREB)-binding protein along with its paralog p300, which exhibits a 75% sequence similarity, act as “master coactivators” of gene regulation in many multicellular organisms.[16,18,19] These large, multi-domain proteins contain stretches of IDRs and several helical protein-binding domains that interact with a large variety of transcription machinery. Both are composed of N-terminal nuclear receptor interaction domain (NRID), three cysteine–histidine rich regions (CH1, -2 and -3), four zinc finger domains (TAZ1, PHD, ZZ, and TAZ2), a kinase-inducible domain interacting (KIX) domain, a bromodomain (BD), a histone acetyltranferase (HAT), and an interferon binding domain (IBiD).[18,20–27] (Figure 1.3; PDB 1U2N, 4I9O, 5W0I, 5KJ2, 1TOT, 1F81, and 1JJS) Utilizing these domains, CBP and p300 can

regulate epigenetics and act as a bridge between upstream transcription factors and the basal transcriptional machinery.

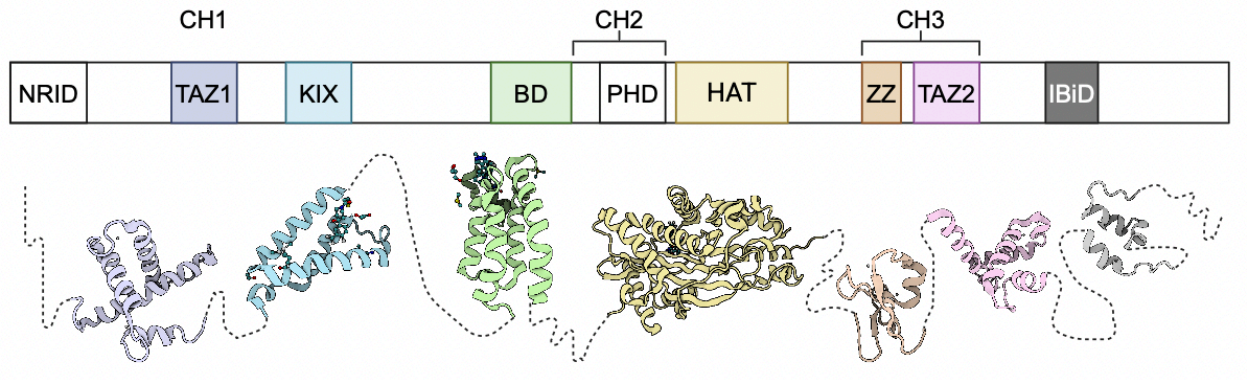


Figure 1.3 A pictural representation of the CREB-Binding Protein. With CBP being a large multi-domain protein, the structures of many of its domains have been independently solved to facilitate exploration of their roles in transcription. PDB IDs: 1U2N, 4I9O, 5W0I, 5KJ2, 1TOT, 1F81, and 1JJS.

Much like CBP and p300, the Mediator complex is considered to be a “master regulator” of gene expression in eukaryotes. Unlike CBP/p300, the Mediator is a large protein complex composed of 20-30 subunits that make up four modules (head, middle, tail, and kinase). It acts as a functional bridge between enhancers and promoters.[28] Of the modules, the tail subunits serve as the primary targets for transcriptional factors within the complex.[29] (Figure 1.4; PDB 8TQW) The tail undergoes conformational changes prompted by binding of activators and repressors to convey regulatory information to RNA polymerase II.

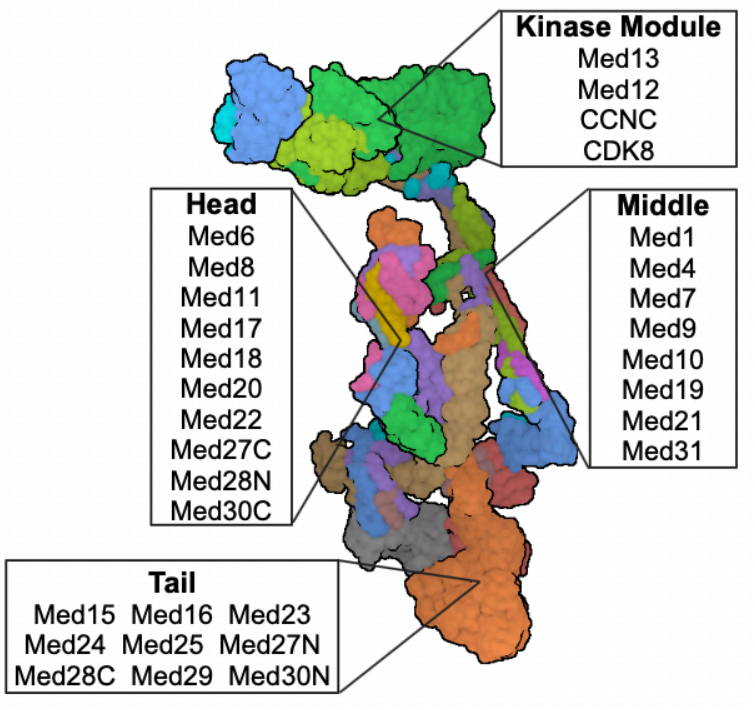


Figure 1.4 A pictural representation of the Mediator complex. The subunits of each module of the Mediator complex uniquely participate in the transcriptional process, however, the knowledge about the roles of each subunit is variable. PDB ID: 8TQW

1.3 Activator binding domains

CBP/p300 and the tail module of the Mediator complex are key facets in transcriptional activation. Activators directly interact with domains on the coactivator known as the activator binding domains (ABDs). These domains typically interact with a variety of transcriptional activators that share very little sequential similarity, thus requiring the domains to be conformationally malleability to accommodate a diverse set of partners.

The dynamic, highly conserved ABD known as the KIX domain within CBP/p300 is known to bind numerous transcriptional activators. This helical bundle composed of three α-helices connected by IDRs has two canonical binding surfaces by which it binds activators and regulates their associated genes.[30–33] Past structural studies of

CBP/p300 KIX bound to various transactivation domains (TADs) of known interacting activators as well as the covalent modification of CBP/p300 KIX have revealed a subset of conformations that KIX adopts upon binding a ligand. (Figure 1.5; PDB 2LXT) Supplemented with computational studies, a wide distribution of lowly-populated configurational states for apo CBP KIX were identified. Activator Interacting Domain (AcID), similarly to CBP KIX, is an ABD of the Med25 subunit in the Mediator complex tail that engages with a plethora of transcriptional activators via two binding faces. AcID contains a seven-stranded β-barrel core flanked with dynamic loops and three α-helices.[7,14,34] During ligand binding, it undergoes significant conformational changes throughout the domain, (Figure 1.5; PDB 2L23) suggesting that intrinsic mobility is indicative of this class of proteins.

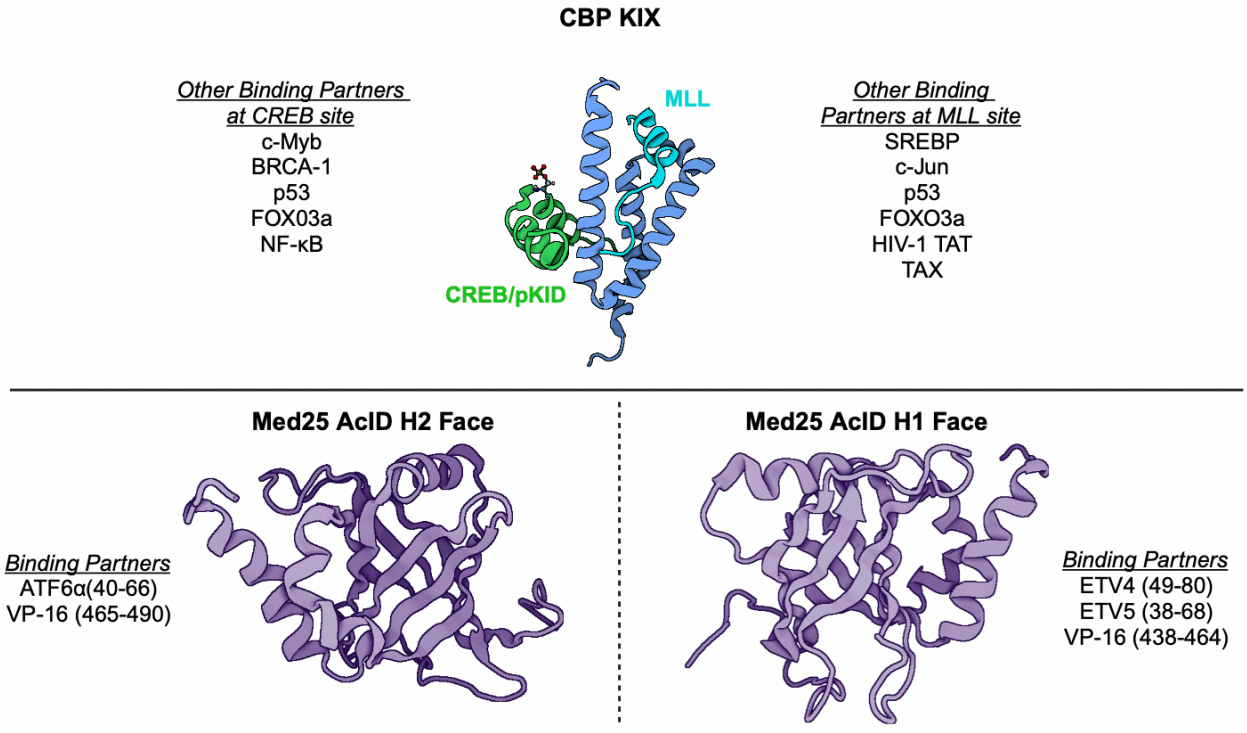


Figure 1.5 Structures of the CBP KIX domain (top) and the Med25 AcID domain (bottom) with their binding partners. PDB IDs: 2LXT and 2L23.

The extensive studies of CBP KIX and Med25 AcID set the precedent and opened the door to studying related yet under-studied ABDs. The KIX domain is one of the most crucial molecular recognition domains for gene regulation in mammals and yeast. In addition to CBP/p300, this domain can namely be found in yeast and human Med15, another subunit of the Mediator complex tail. There is a lack of conservation of the KIX α3 helix that affords activator binding specificity for the Med15 domains, thus there is a significant discrepancy in the knowledge of Med15 KIX interactions.[35] The Med15 KIX in the *candida glabrata* yeast strain (specified as cgMed15 KIX) reportedly interacts with transcriptional activators Pdr-1 and conditionally Oaf-1,[36,37] while the human Med15 KIX (also known Arc105 KIX) has a single identified activator, SREBP-1a.[11,38,39] (Figure 1.6; PDB 2GUT and 4D7X) Given the limited information on these KIX domains, investigation of them would be prudent.

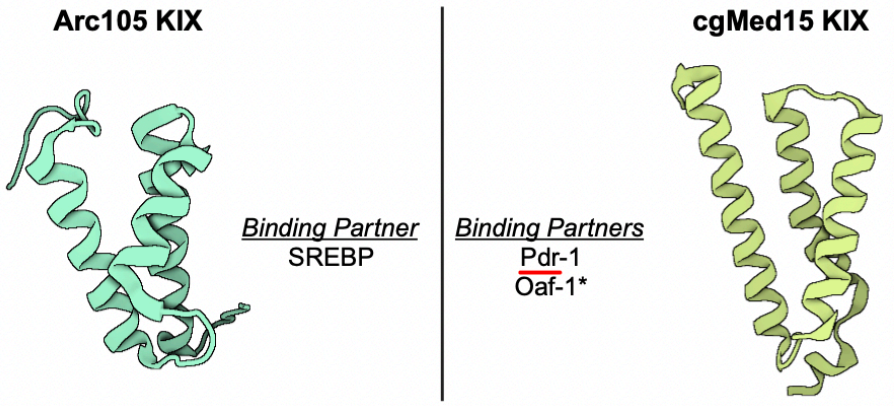


Figure 1.6 Structures of the Arc105 (left) and cgMed15 (right) KIX domains and their corresponding transactivation domains *Oaf-1 binds under the condition that it has been activated. PDB IDs: 2GUT and 4D7X.

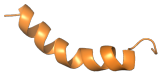
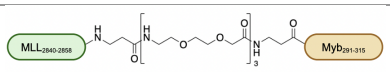
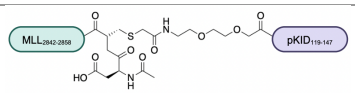
These activator binding domains are linked to multiple pathologies. Dysregulation of the ternary complex of the transcriptional activators c-Myb and MLL with the CBP KIX

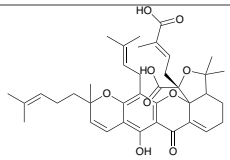
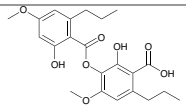
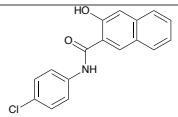
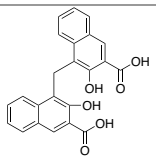
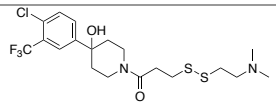
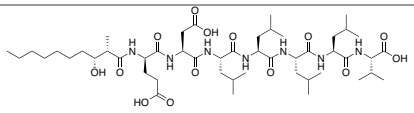
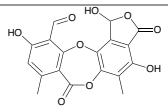
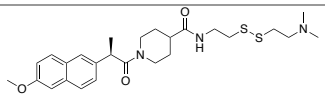
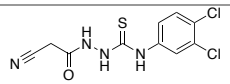
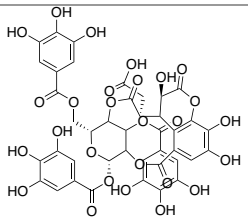
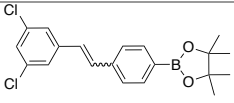
domain of leads to leukemogenesis in pediatric and adult patients with MLL fusion proteins.[40] Additionally, CBP KIX interactions are dysregulated in several other cancer and some neurological disorders.[41,42] Med25 AcID similarly complexes with the ETV/PEA3 factors underpin metastatic phenotypes in several cancers.[7,14,34,43] Multi-drug resistance, which is prevalent in pathogenic fungi like *candida glabrata*, is subject to antifungal/xenobiotic-dependent regulation by the cgMed15 KIX and Pdr-1 interaction.[12,37,44] Deregulation of Arc105 KIX interaction with SREBP-1a has been shown to be connected to obesity.[11,13,39,45] The disease associations of these ABDs serve as a driving force in the search for probes and therapeutics.

1.4 Presently known probes/inhibitors for the dynamic ABDs

The dynamics of ABDs make targeting them a difficult task; nonetheless, inhibitors of different classes have been discovered for these domains. (Table 1.1)

Table 1.1 Current probes for CBP KIX, Med25 AcID, Arc105 KIX, and cgMed15 KIX.

Name	Structure	Target Domain	Classification	Ref
MybMIM		CBP KIX	Peptidomimetic	46
MybLL-tide		CBP KIX	Peptidomimetic	47
CREBLL-tide		CBP KIX	Peptidomimetic	48

Garcinolic Acid		CBP KIX	Natural Product	[49]
Sekikaic Acid		CBP KIX	Natural Product	[50]
Naphthol AS-E		CBP KIX	Small Molecule	[51]
Pamoic Acid		CBP KIX	Small Molecule	[52]
Compound 1-10		CBP KIX	Covalent Small Molecule	[21]
LPPM-8		Med25 AcID	Peptidomimetic	[34]
Norstictic Acid		Med25 AcID	Natural Product	[43]
Compound 22		Med25 AcID	Covalent Small Molecule	[7,53]
iKIX1		cgMed15 KIX	Covalent Small Molecule	[37]
Chebulinic acid		cgMed15 KIX	Natural Product	[44]
BF175		Arc105 KIX	Covalent Small Molecule	[11]

Most of the reported inhibitors fall into three broad classes: peptidomimetics; natural products; and covalent small molecules. Although these inhibitors can serve as candidates for probing interactions, each class has their own associated drawbacks that present as roadblocks in therapeutic development. Peptide-based inhibitors suffer from low bioavailability, poor membrane permeability, as well as chemical and physical instability.[54] Natural product inhibitors pose a challenge in regard to the lengthy process of determining the compound of interest from an extract, frequent incompatibility with traditional target-based assays, and the difficulty of synthetic optimization.[55] Covalent small molecule inhibitors are very useful in assessing configurational changes; however, they tend to exhibit high reactivity and toxicity.[56] With these drawbacks, there is a need for additional non-covalent small molecules that can be useful probes that can lead to therapeutic development.

1.5 The primary screening methods for targeting IDR-containing domains

To advance the druggability and exploration of IDR-containing domains, it is important to define a primary screening method that is broadly applicable for the discovery of modulators. The most common primary methods used to target ABDs are fluorescence polarization (FP) and nuclear magnetic resonance (NMR). Both are biophysical means of determining ligand engagement with a protein of interest (POI). FP typically utilizes a competitive approach in which compounds compete for the binding site of a fluorescently labeled ligand known to engage the POI. This is a method to determine significant site-specific changes in domain binding, and FP defines the

functionality of a probe,[57] which is essential for therapeutic development. NMR, on the other hand, is highly sensitive to all shifts in the POI that result from compound interaction. It is a method to map overall changes in the domain, and NMR contributes to binding mode determination,[58] which is valuable in probing a novel domain's interactions. Both methods have methods have merit in the search for modulators of ABDs; nevertheless, neither method presents itself as the optimal primary screening method of these dynamic domains. In a high throughput screen, the site specificity of FP limits the scope of potential compounds of interest (COI) to those that significantly inhibit known orthosteric sites. Unfortunately, NMR is low-to medium-throughput such that large library screening would be time-consuming and costly. Thus, the development of deliberate screening approaches for recognizing dynamic changes would be invaluable to therapeutic development and elucidation of domain interactions for dynamic ABDs.

Although the dynamic and heterogenous nature of ABDs make modulating and characterizing their dynamics particularly challenging, stabilizing the IDRs in their native disordered ensemble or allosterically modulating the protein domain conformation are viable options for approaching protein domains with significant IDRs. In recent years, alternative screening strategies like computational screening and differential scanning fluorimetry (DSF) have gained traction as valuable modes of identifying probes for dynamic substructures. Computational modeling has often been utilized to study protein dynamics and supplement experimental data in binding site determination.[59,60] Advancements in molecular dynamics (MD) force fields expand the potential for simulating various protein states. This optimizes the development of native-like models

of IDR-containing domains to used be in virtual screening and drug design.[61–63] While significant strides have been made in computational modeling, there is a caveat. The more structural data available for conformational sampling, the higher the accuracy of the conformational ensembles in model-building. Hence, domains with little to no experimental conformation data are not optimal candidates for computation-based primary screening.

Although virtual screening requires structural precedents, DSF presents as an effective method for truly enigmatic domains. Historically, this method has primarily been utilized to confirm engagement of a previously identified ligand;[49] however, more recent studies have found it at the forefront of high-throughput screening (HTS). DSF is a fast, simple, and affordable method that monitors changes in protein unfolding. In this method, changes in the fluorescent dye emission are measured during protein denaturation upon temperature increase.[64–67] Changes in protein activity such as complex formation affect protein thermal stability, altering the apparent melting temperature (T_M). Due to the relationship between thermal and conformational stability, DSF has been used to identify conformational stabilizers for some so-called "undruggable" domains.[68–70] Thus, DSF positions itself as an ideal primary screening mode for dynamic ABDs, and while the other previously mentioned screening modes are not suited for the primary position, they can make notable contributions to therapeutic development and/or illumination of interactions in a directed screening approach.

1.6 Dissertation Summary

Despite the importance of dynamic domains, there is a lack of sufficient approaches for targeting them and investigating their interactions. My thesis work focuses on developing and implementing screening approaches to define probes that exploit the conformational dynamics of ABDs.

CBP KIX occupies a wide distribution of conformational states, making effectively drugging its interactions very difficult; however, placing stabilization at the helm of CBP KIX modulator discovery can mitigate that issue. In chapter 2, I illustrate the merit of differential scanning fluorimetry (DSF) in screening particularly difficult dynamic domains like CBP KIX. In addition, I develop an DSF-led screening strategy as an effective method for identifying small molecules that engage the dynamics of the CBP KIX motif. This work encompasses the conformational stability assessment of CBP KIX in the presence of a diverse chemical library, identification of the stabilizers' primary binding mode, discovery of functional stabilizer, and the key interactions of the functional stabilizer. Using thermostability, fluorescence polarization (FP), bioNMR, SAR, and computation, I demonstrate that this workflow yields a synthetically tractable mixed mechanism small molecule inhibitor.

The KIX domains with the Med15 subunit at the tail of the Mediator complex have a high structural similarity to CBP KIX; however, currently, there has been very little probing of these homologs. In chapter 3, I employ a similar workflow as developed in Chapter 2 to define modulators of other members of the KIX family, Arc105 KIX and cgMed15 KIX. A screen of the CBP KIX conformational modulators using thermostability and fluorescence polarization experimentation defined novel modulators of Arc105 and cgMed15 KIX to further probe their interactions.

As exemplified in previous chapters, dyes can be powerful tools in the examination of dynamic domains. In chapter 4, I demonstrate the value of the colorimetric dye tools as accessible means of screening of model ABDs. Most significantly, these studies led to the identification of a colorimetric dye for screening ABD binding.

In chapter 5, I present a summary of how my findings have contributed to the current knowledge about targeting dynamic behaviors in drug discovery and expanded upon the probes for dynamic domains. Additionally, I discuss how this work can impact the development of more focused screening strategies for challenging protein targets.

1.7 References

1. Van Der Lee R, Buljan M, Lang B, et al. Classification of intrinsically disordered regions and proteins. *Chem Rev*. 2014;114(13):6589-6631. doi:10.1021/cr400525m

2. Krieger JM, Fusco G, Lewitzky M, et al. Conformational recognition of an intrinsically disordered protein. *Biophys J*. 2014;106(8):1771-1779. doi:10.1016/j.bpj.2014.03.004

3. Metallo SJ. Intrinsically disordered proteins are potential drug targets. *Curr Opin Chem Biol*. 2010;14(4):481-488. doi:10.1016/j.cbpa.2010.06.169

4. Liu J, Perumal NB, Oldfield CJ, Su EW, Uversky VN, Dunker AK. Intrinsic disorder in transcription factors. *Biochemistry*. 2006;45(22):6873-6888. doi:10.1021/bi0602718

5. Mapp AK, Pricer R, Sturlis S. Targeting transcription is no longer a quixotic quest. *Nat Chem Biol*. 2015;11(12):891-894. doi:10.1038/nchembio.1962

6. Ghosh R, Kaypee S, Shasmal M, Kundu TK, Roy S, Sengupta J. Tumor Suppressor p53-Mediated Structural Reorganization of the Transcriptional Coactivator p300. *Biochemistry*. 2019;58(32):3434-3443. doi:10.1021/acs.biochem.9b00333

7. Henderson AR, Henley MJ, Foster NJ, et al. Conservation of coactivator engagement mechanism enables small-molecule allosteric modulators. *Proc Natl Acad Sci U S A*. 2018;115(36):8960-8965. doi:10.1073/pnas.1806202115

8. Waters L, Yue B, Veverka V, et al. Structural diversity in p160/CREB-binding protein coactivator complexes. *J Biol Chem*. 2006;281(21):14787-14795. doi:10.1074/jbc.M600237200

9. Knutson BA, Hahn S. Domains of Tra1 Important for Activator Recruitment and Transcription Coactivator Functions of SAGA and NuA4 Complexes. *Mol Cell Biol*. 2011;31(4):818-831. doi:10.1128/mcb.00687-10

10. Bhagwat AS, Vakoc CR. Targeting Transcription Factors in Cancer. *Trends Cancer*. 2015;1(1):53-65. doi:10.1016/j.trecan.2015.07.001

11. Zhao X, Xiaoli, Zong H, et al. Inhibition of SREBP transcriptional activity by a boron-containing compound improves lipid homeostasis in diet-induced obesity. *Diabetes*. 2014;63(7):2464-2473. doi:10.2337/db13-0835

12. Thakur JK, Arthanari H, Yang F, et al. A nuclear receptor-like pathway regulating multidrug resistance in fungi. *Nature*. 2008;452(7187):604-609. doi:10.1038/nature06836

13. Hua X, Ge S, Zhang L, et al. MED15 is upregulated by HIF-2α and promotes proliferation and metastasis in clear cell renal cell carcinoma via activation of SREBP-dependent fatty acid synthesis. *Cell Death Discov*. 2024;10(1). doi:10.1038/s41420-024-01944-1

14. Vojnic E, Mourão A, Seizl M, et al. Structure and VP16 binding of the Mediator Med25 activator interaction domain. *Nat Struct Mol Biol*. 2011;18(4):404-410. doi:10.1038/nsmb.1997

15. de Thonel A, Ahlskog JK, Daupin K, et al. CBP-HSF2 structural and functional interplay in Rubinstein-Taybi neurodevelopmental disorder. *Nat Commun*. 2022;13(1). doi:10.1038/s41467-022-34476-2

16. Goodman RH, Smolik S. CBP/p300 in cell growth, transformation, and development. *Genes Dev*. 2000;(14):1553-1577.

17. Wood MA, Attner MA, Oliveira AMM, Brindle PK, Abel T. A transcription factor-binding domain of the coactivator CBP is essential for long-term memory and the expression of specific target genes. *Learn Mem*. 2006;13(5):609-617. doi:10.1101/lm.213906

18. Kalkhoven E. CBP and p300: HATs for different occasions. In: *Biochemical Pharmacology*. Vol 68. ; 2004:1145-1155. doi:10.1016/j.bcp.2004.03.045

19. Gou P, Zhang W. Protein lysine acetyltransferase CBP/p300: A promising target for small molecules in cancer treatment. *Biomed Pharmacother*. 2024;171. doi:10.1016/j.biopha.2024.116130

20. Breen ME, Mapp AK. Modulating the masters: chemical tools to dissect CBP and p300 function. *Curr Opin Chem Biol*. 2018;45:195-203. doi:10.1016/j.cbpa.2018.06.005

21. Wang N, Majmudar CY, Pomerantz WC, et al. Ordering a dynamic protein Via a small-molecule stabilizer. *J Am Chem Soc*. 2013;135(9):3363-3366. doi:10.1021/ja3122334

22. De Guzman RN, Wojciak JM, Martinez-Yamout MA, Dyson HJ, Wright PE. CBP/p300 TAZ1 domain forms a structured scaffold for ligand binding. *Biochemistry*. 2005;44(2):490-497. doi:10.1021/bi048161t

23. Legge GB, Martinez-Yamout MA, Hambly DM, et al. ZZ domain of CBP: An unusual zinc finger fold in a protein interaction module. *J Mol Biol*. 2004;343(4):1081-1093. doi:10.1016/j.jmb.2004.08.087

24. De Guzman RN, Liu HY, Martinez-Yamout M, Dyson HJ, Wright PE. Solution structure of the TAZ2 (CH3) domain of the transcriptional adaptor protein CBP. *J Mol Biol*. 2000;303(2):243-253. doi:10.1006/jmbi.2000.4141

25. Romero FA, Murray J, Lai KW, et al. GNE-781, A Highly Advanced Potent and Selective Bromodomain Inhibitor of Cyclic Adenosine Monophosphate Response Element Binding Protein, Binding Protein (CBP). *J Med Chem*. 2017;60(22):9162-9183. doi:10.1021/acs.jmedchem.7b00796

26. Lasko LM, Jakob CG, Edalji RP, et al. Discovery of a selective catalytic p300/CBP inhibitor that targets lineage-specific tumours. *Nature*. 2017;550(7674):128-132. doi:10.1038/nature24028

27. Lin CH, Hare BJ, Wagner G, Harrison SC, Maniatis T, Fraenkel E. A Small Domain of CBP/p300 Binds Diverse Proteins: Solution Structure and Functional Studies. *Mol Cell*. 2001;8:581-590.

28. El Khattabi L, Zhao H, Kalchschmidt J, et al. A Pliable Mediator Acts as a Functional Rather Than an Architectural Bridge between Promoters and Enhancers. *Cell*. 2019;178(5):1145-1158.e20. doi:10.1016/j.cell.2019.07.011

29. Chao TC, Chen SF, Kim HJ, et al. Structural basis of the human transcriptional Mediator regulated by its dissociable kinase module. *Mol Cell*. 2024;84(20):3932-3949.e10. doi:10.1016/j.molcel.2024.09.001

30. Yang K, Stanfield RL, Martinez-Yamout MA, Dyson HJ, Wilson IA, Wright PE. Structural basis for cooperative regulation of KIXmediated transcription pathways by the HTLV-1 HBZ activation domain. *Proc Natl Acad Sci U S A*. 2018;115(40):10040-10045. doi:10.1073/pnas.1810397115

31. Law SM, Gagnon JK, Mapp AK, Brooks CL. Prepaying the entropic cost for allosteric regulation in KIX. *Proc Natl Acad Sci U S A*. 2014;111(33):12067-12072. doi:10.1073/pnas.1405831111

32. Lee CW, Arai M, Martinez-Yamout MA, Dyson HJ, Wright PE. Mapping the interactions of the p53 transactivation domain with the KIX domain of CBP. *Biochemistry*. 2009;48(10):2115-2124. doi:10.1021/bi802055v

33. Tollinger M, Kloiber K, Ágoston B, et al. An isolated helix persists in a sparsely populated form of KIX under native conditions. *Biochemistry*. 2006;45(29):8885-8893. doi:10.1021/bi0607305

34. Pattelli ON, Valdivia EM, Beyersdorf MS, et al. A Lipopeptidomimetic of Transcriptional Activation Domains Selectively Disrupts the Coactivator Med25 Protein–Protein Interactions. *Angew Chem - Int Ed*. 2024;63(21). doi:10.1002/anie.202400781

35. Thakur JK, Yadav A, Yadav G. Molecular recognition by the KIX domain and its role in gene regulation. *Nucleic Acids Res*. 2014;42(4):2112-2125. doi:10.1093/nar/gkt1147

36. Kumar V, Waseem M, Dwivedi N, Maji S, Kumar A, Thakur JK. KIX domain of AtMed15a, a Mediator subunit of Arabidopsis, is required for its interaction with different proteins. *Plant Signal Behav*. 2018;13(2). doi:10.1080/15592324.2018.1428514

37. Nishikawa JL, Boeszoermenyi A, Vale-Silva LA, et al. Inhibiting fungal multidrug resistance by disrupting an activator-Mediator interaction. *Nature*. 2016;530(7591):485-489. doi:10.1038/nature16963

38. Kato Y, Habas R, Katsuyama Y, Näär AM, He X. A component of the Arc/Mediator complex required for TGFb/Nodal signaling. *Nature*. 2002;418(6898):641-646. doi:10.1038/nature00921

39. Yang F, Vought BW, Satterlee JS, et al. An ARC/Mediator subunit required for SREBP control of cholesterol and lipid homeostasis. *Nature*. 2006;442(7103):700-704. doi:10.1038/nature04942

40. Pattabiraman DR, Mcgirr C, Shakhbazov K, et al. Interaction of c-Myb with p300 is required for the induction of acute myeloid leukemia (AML) by human AML oncogenes. Published online 2014. doi:10.1182/blood-2012

41. Rouaux C, Loeffler JP, Boutillier AL. Targeting CREB-binding protein (CBP) loss of function as a therapeutic strategy in neurological disorders. In: *Biochemical Pharmacology*. Vol 68. ; 2004:1157-1164. doi:10.1016/j.bcp.2004.05.035

42. Chatterjee S, Angelakos CC, Bahl E, et al. The CBP KIX domain regulates long-term memory and circadian activity. *BMC Biol*. 2020;18(1). doi:10.1186/s12915-020-00886-1

43. Garlick JM, Sturlis SM, Bruno PA, et al. Norstictic Acid Is a Selective Allosteric Transcriptional Regulator. *J Am Chem Soc*. 2021;143(25):9297-9302. doi:10.1021/jacs.1c03258

44. Waseem M, Das S, Mondal D, Jain M, Thakur JK, Subbarao N. Identification of novel inhibitors against Med15a KIX domain of Candida glabrata. *Int J Biol Macromol*. 2023;253. doi:10.1016/j.ijbiomac.2023.126720

45. Näär AM, Beaurang PA, Robinson KM, et al. Chromatin, TAFs, and a novel multiprotein coactivator are required for synergistic activation by Sp1 and SREBP-1a in vitro. *Genes Dev*. 1998;(12):3020-3031.

46. Ramaswamy K, Forbes L, Minuesa G, et al. Peptidomimetic blockade of MYB in acute myeloid leukemia. *Nat Commun*. 2018;9(1). doi:10.1038/s41467-017-02618-6

47. Joy ST, Henley MJ, De Salle SN, et al. A Dual-Site Inhibitor of CBP/p300 KIX is a Selective and Effective Modulator of Myb. *J Am Chem Soc*. 2021;143(37):15056-15062. doi:10.1021/jacs.1c04432

48. Liu Y, Joy ST, Henley MJ, et al. Inhibition of CREB Binding and Function with a Dual-Targeting Ligand. *Biochemistry*. 2024;63(1):1-8. doi:10.1021/acs.biochem.3c00469

49. Breen ME, Joy ST, Baruti OJ, et al. Garcinolic acid distinguishes between GACKIX domains and modulates interaction networks. *ChemBioChem*. Published online August 2023. doi:10.1002/cbic.202300439

50. Majmudar CY, Højfeldt JW, Arevang CJ, et al. Sekikaic acid and lobaric acid target a dynamic interface of the coactivator CBP/p300. *Angew Chem - Int Ed*. 2012;51(45):11258-11262. doi:10.1002/anie.201206815

51. Uttarkar S, Dukare S, Bopp B, Goblirsch M, Jose J, Klempnauer KH. Naphthol AS-E phosphate inhibits the activity of the transcription factor Myb by blocking the interaction with the KIX domain of the coactivator p300. *Mol Cancer Ther*. 2015;14(6):1276-1285. doi:10.1158/1535-7163.MCT-14-0662

52. Best JL, Amezcua CA, Mayr B, et al. Identification of small-molecule antagonists that inhibit an activator:coactivator interaction. *Proc Natl Acad Sci U S A*. 2004;101(51):17622-17627.

53. Henley MJ, Linhares BM, Morgan BS, Cierpicki T, Fierke E □ CA, Mapp AK. Unexpected specificity within dynamic transcriptional protein-protein complexes. *Proc Natl Acad Sci U S A*. 2020;117(44):27346-27353. doi:10.1073/pnas.2013244117/-/DCSupplemental

54. Wang L, Wang N, Zhang W, et al. Therapeutic peptides: current applications and future directions. *Signal Transduct Target Ther*. 2022;7(1). doi:10.1038/s41392-022-00904-4

55. Atanasov AG, Zotchev SB, Dirsch VM, et al. Natural products in drug discovery: advances and opportunities. *Nat Rev Drug Discov*. 2021;20(3):200-216. doi:10.1038/s41573-020-00114-z

56. Kathman SG, Statsyuk AV. Covalent tethering of fragments for covalent probe discovery. *MedChemComm*. 2016;7(4):576-585. doi:10.1039/c5md00518c

57. Sijbesma E, Somsen BA, Miley GP, et al. Fluorescence Anisotropy-Based Tethering for Discovery of Protein-Protein Interaction Stabilizers. *ACS Chem Biol*. 2020;15(12):3143-3148. doi:10.1021/acschembio.0c00646

58. Egner JM, Jensen DR, Olp MD, et al. Development and Validation of 2D Difference Intensity Analysis for Chemical Library Screening by Protein-Detected NMR Spectroscopy. *ChemBioChem*. 2018;19(5):448-458. doi:10.1002/cbic.201700386

59. Bhattacharya S, Lin X. Recent advances in computational protocols addressing intrinsically disordered proteins. *Biomolecules*. 2019;9(4). doi:10.3390/biom9040146

60. Robustelli P, Ibanez-De-Opakua A, Campbell-Bezat C, et al. Molecular Basis of Small-Molecule Binding to α-Synuclein. *J Am Chem Soc*. 2022;144(6):2501-2510. doi:10.1021/jacs.1c07591

61. Wang H, Xiong R, Lai L. Rational drug design targeting intrinsically disordered proteins. *Wiley Interdiscip Rev Comput Mol Sci*. 2023;13(6). doi:10.1002/wcms.1685

62. Robustelli P, Piana S, Shaw DE. Developing a molecular dynamics force field for both folded and disordered protein states. *Proc Natl Acad Sci U S A*. 2018;115(21):E4758-E4766. doi:10.1073/pnas.1800690115

63. Heller GT, Shukla VK, Figueiredo AM, Hansen DF. Picosecond Dynamics of a Small Molecule in Its Bound State with an Intrinsically Disordered Protein. *J Am Chem Soc*. 2024;146(4):2319-2324. doi:10.1021/jacs.3c11614

64. Scott DE, Spry C, Abell C. Differential Scanning Fluorimetry as Part of a Biophysical Screening Cascade. In: ; 2016:139-172. doi:10.1002/9783527683604.ch07

65. Bruce D, Cardew E, Freitag-Pohl S, Pohl E. How to Stabilize Protein: Stability Screens for Thermal Shift Assays and Nano Differential Scanning Fluorimetry in the Virus-X Project. *J Vis Exp JoVE*. 2019;(144). doi:10.3791/58666

66. Hofmann L, Gulati S, Sears A, Stewart PL, Palczewski K. An effective thiol-reactive probe for differential scanning fluorimetry with a standard real-time polymerase chain reaction device. *Anal Biochem*. 2016;499:63-65. doi:10.1016/j.ab.2016.01.016

67. Lea WA, Simeonov A. Differential scanning fluorometry signatures as indicators of enzyme inhibitor mode of action: Case study of glutathione s-transferase. *PLoS ONE*. 2012;7(4). doi:10.1371/journal.pone.0036219

68. Gao K, Oerlemans R, Groves MR. Theory and applications of differential scanning fluorimetry in early-stage drug discovery. *Biophys Rev*. 2020;12(1):85-104. doi:10.1007/s12551-020-00619-2

69. Shao H, Oltion K, Wu T, Gestwicki JE. Differential scanning fluorimetry (DSF) screen to identify inhibitors of Hsp60 protein-protein interactions. *Org Biomol Chem*. 2020;18(22):4157-4163. doi:10.1039/d0ob00928h

70. Niesen FH, Berglund H, Vedadi M. The use of differential scanning fluorimetry to detect ligand interactions that promote protein stability. *Nat Protoc*. 2007;2(9):2212-2221. doi:10.1038/nprot.2007.321

Chapter 2 Targeting Loop Dynamics in the Search for Modulators for CBP KIX

2.1 Abstract

CBP KIX is validated therapeutic target for cMyb-dependent cancers yet due to its conformational dynamics, the discovery of drug-like inhibitors has been challenging. There are few screening and characterization techniques appropriate for dynamic proteins and dynamic protein complexes despite the prevalence of dynamic proteins in the proteome. Here we assess the thermostability method differential scanning fluorimetry (DSF) for the characterization and targeting of the dynamic coactivator motif CBP KIX. Through a comprehensive buffer screen, DSF conditions for KIX and KIX-transcription factor complexes were identified that provided robust and reproducible readouts of binding. Further assessment in a multiwell screening format produced an assay with a Z' of 0.66. suitable for high-throughput applications. The subsequent DSF screen of 2,846 compounds led to 1.4% hit rate. 29 validated modulators were assessed by protein-observed NMR, which defined ~60% of the modulators as having significant engagement in the α_1/α_2 loop region. Dual function assessment via fluorescence polarization identified the small molecule oxyclozanide as orthosteric/allosteric inhibitor of CBP KIX. The key interactions of this synthetically tractable molecule seen in docking studies confirm that it holds significant potential for therapeutic development.

2.2 Introduction

The kinase-inducible domain interacting domain (KIX) of CBP is one of the most well-studied activator-binding domains (ABDs).[1–17] This dynamic domain within CBP binds to numerous transcriptional activators via two binding sites.[2,6] As commonly seen in protein-protein interactions (PPIs), these binding sites are large (>900 Å^2) and lack topography. CBP KIX occupies a wide distribution of conformational micro-states that are individually sparsely populated, and each individual binding partner has its own set of KIX micro-states that it preferentially engages. [18] Conventional drug- or probe-discovery methods are designed for protein targets that have less conformational mobility, and, as a result, the development of selective and potent small molecule inhibitors is especially challenging. Nonetheless, disordered regions within coactivators and their substructures are often essential for conformational exchange and allosteric communication,[12,19] so focusing on the modulation of these regions has substantial potential for therapeutic development.

Several biophysical studies support a model in which that the flexible loop connecting the α_1 and α_2 helices of the CBP KIX domain is a key allosteric regulatory site.[18] Small molecules that engage this loop often act as effective orthosteric/allosteric modulators. However, there is no systematic method for the discovery of such modulators. Instead, the inhibitors that tune loop dynamics have been discovered serendipitously or through modification of the domain. For example, Mapp Lab studies with CBP KIX discovered the natural product garcinolic acid unexpectedly through a fluorescence polarization (FP) counter-screen and found that it inhibits KIX PPIs by engaging a non-canonical site comprising the α_1/α_2 loop.[1] In another example, site-directed mutagenesis was performed on CBP KIX to discover compound 1-10, a small

molecule inhibitor that covalently tethers to the MLL binding site and effectively inhibits its PPIs by impacting the loop dynamics.[8] And while site-directed approaches can address this methods gap, they are not generalizable since they require installation of a specifically positioned nucleophilic residue.[20–22] Thus, a more generally applicable method is necessary for the identification of modulators for dynamic protein domains.

We hypothesize that biophysical methods that measure protein stability would be effective approaches for identifying small molecules that affect the conformation of a dynamic protein such as KIX. Consistent with this hypothesis, inhibitors that engage the α_1/α_2 loop, including 1-10 and garcinolic acid, considerably increase the thermal stability of CBP KIX.[1,8] For that reason differential scanning fluorimetry (DSF) is a method of interest for the identification of such modulators, as it monitors protein thermostability.[23,24] Changes in a protein's free energy of unfolding (ΔG_U) during a binding event alters its thermal stability and by association, apparent melting temperature (T_M). Traditionally, DSF has been used to confirm target engagement of well-structured proteins and screen compounds against dynamic domains with high melting temperatures.[25–27] In the case of many dynamic domains, a low melting temperatures can present a challenge in the application of DSF as a primary screening method.[28–30] Here we demonstrate that CBP KIX can be targeted using a DSF-led approach for the discovery of ligands that modulate its loop dynamics. Further assessment of the ligands by other biophysical and computational methods reveals modulator binding to the α_1/α_2 loop region and leads to the discovery of a mixed mechanism, small molecule inhibitor that exhibits significant promise for therapeutic development.

2.3 Results and Discussion

2.3.1 Buffering conditions facilitate the thermostability evaluation of the CBP KIX domain

Binding-induced conformational changes of ABDs have been studied using biophysical methods such as NMR spectroscopy and transient and steady-state kinetic measurements.[13,16,31,32] However, such methods are rarely applicable to high throughput screening. In contrast, DSF has been widely used in both high throughput ligand screening and protein characterization, albeit with more structured, thermostable proteins. Preliminary data with the ABD Med25 AcID indicates that assessment of conformationally dynamic ABDs and their binding events is possible. (Figure B.1 and unpublished data from Dr. Julie Garlick) CBP KIX has a relatively low thermostability ($T_M \cong 55°C$) and upon performing an initial screen with CBP KIX, the resulting melting curves produced high intrinsic fluorescence overlapping with the melting transition. (Figure B.2A) The significant variance in the T_M for the triplicate measurement of CBP KIX derived from a single protein-dye solution suggests a lack of homogeneity and examining SYPRO Orange in the absence of protein reveals that buffer-dye interactions are a major contributor. (Figure B.2B) For this reason, assay conditions that would limit intrinsic fluorescence became the initial focus of the work.

We carried out a standard buffer screen[35–37] to identify optimal combinations of pH and salt. More specifically, eighty different buffer combinations were screened and led to the identification of four viable conditions. (Figure 2.1A) The melt curves of CBP KIX under these conditions exhibited a consistent sigmoidal shape with some intrinsic

fluorescence, which is likely due to some dye binding at ambient temperature. Others have shown that the addition of detergent to the buffer can alleviate high background fluorescence.[34,35] Accordingly, the four previous conditions screened with varying detergent conditions led to the discovery of three conditions that reduces the intrinsic fluorescence signal. (Figure 2.1B)

Next, we determined if the newly identified DSF conditions could detect the binding of native transcriptional activation domains (TADs) to CBP KIX. This required the incorporation of a reducing agent into the DSF conditions to minimize TAD aggregation and oligomerization. The three previously identified conditions were tested with the reducing agent dithiothreitol (DTT), leading to the discovery of the Triton-containing buffering condition as the best candidate for CBP KIX DSF screening. (Figure 2.1C) However, when TAD affinity was examined in the new condition via fluorescence polarization, there was a decrease by five orders of magnitude in native ligand binding (Figure B.3) that mirrored the relative increase of sodium phosphate concentration. Consequently, the buffer and salt concentration were reduced to decrease the negative impacts on binding (Figure 2.1D), which had a minimal effect on CBP KIX thermal stability. Therefore, new buffering condition of 25 mM sodium phosphate, 125 mM sodium chloride, 0.001% Triton X-100 at pH 7.8 was carried forward for further assay evaluation.

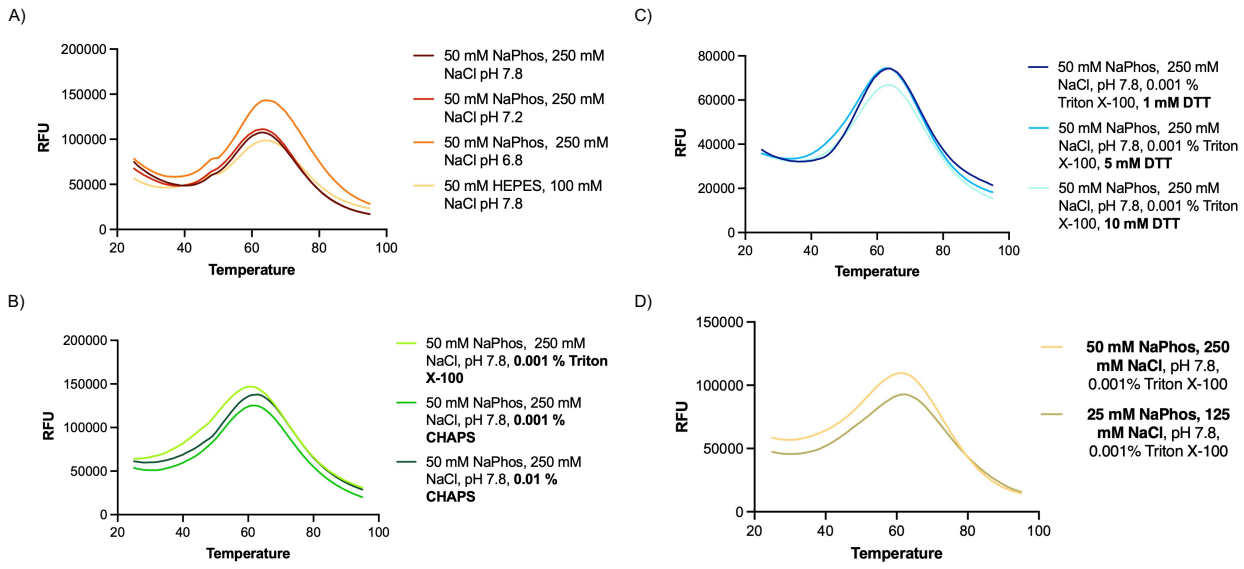


Figure 2.1 CBP KIX buffer composition screening. A) Buffer-salt-pH combinations screening yielded four promising buffers that were subsequently screened with B) varying detergent conditions led to the discovery of three buffers. C) DTT screening identified the hit buffer, which subsequently subjected to D) concentration reduction screening to minimize buffer impact on CBP KIX interactions.

Upon improving the conditions to monitor the domain, the DSF assay was suited for examining CBP KIX binding events.[18] (Figure 2.2A) When thermal stability screening was executed in the presence of the TADs for native activator binding partners Myb and MLL, there is an appreciable alteration in the CBP KIX thermostability when in complex with MLL alone and both Myb and MLL, (Figure 2.2B). This suggests that the differential conformational stabilization that CBP KIX experiences upon binding produces corresponding changes in protein unfolding temperatures. This also serves as a proof-of-concept for the usage of DSF as primary screen for conformationally dynamic ABDs like CBP KIX.

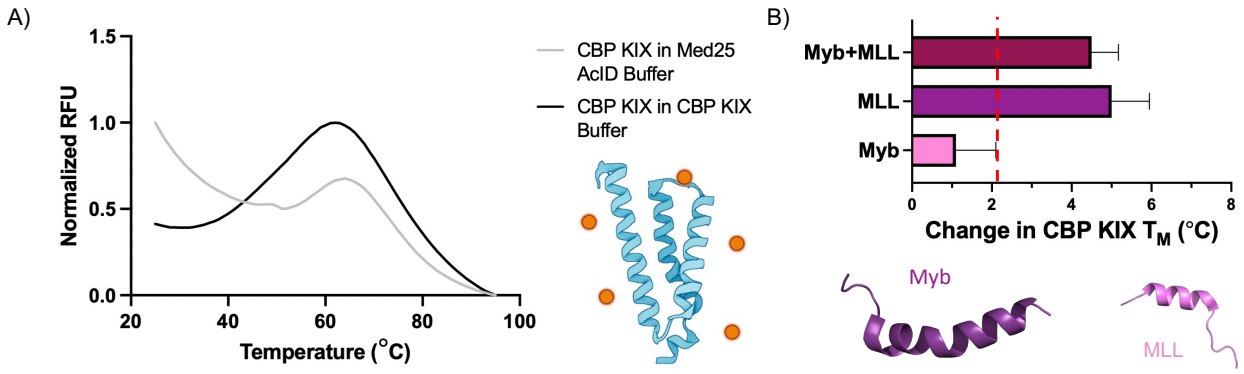


Figure 2.2 The optimized buffer conditions enable the examination of CBP KIX binding events via DSF. A) Adjustment of the buffer conditions resulted in decreased intrinsic fluorescnece for the CBP KIX melting curve. B) The native ligand, MLL, caused a statistically significant change in CBP KIX's melting temperature on its own and in complex with Myb. The red dashed line represents the threshold for significance for thermal stabilization of CBP KIX, which is a three standard deviation change in mean T_M. All experiments were performed in triplicate and the error bars represent the standard deviation from the mean.

2.3.2 High-throughput conformational stability assessment of CBP KIX in the presence of a diverse chemical library

With optimized conditions for DSF in hand, assessing the conditions in a high throughput screening format became the next step. High-throughput screening (HTS) require positive and negative controls that act as thresholds for assay efficacy. MybLLtide, a picomolar inhibitor of CBP KIX that links TADs of Myb and MLL, was chosen as the positive control as it significantly stabilizes the domain.[14] (Figure 2.3A) what was the negative control. The quality of the assay for HTS was subsequently assessed in control experiments to calculate coefficient of variance (CV), signal-to-background ratio(S:B), and the statistical parameter Z'. (Figure 2.3B) For this assay, acceptable values for each parameter were achieved, so the pilot screen was initiated.

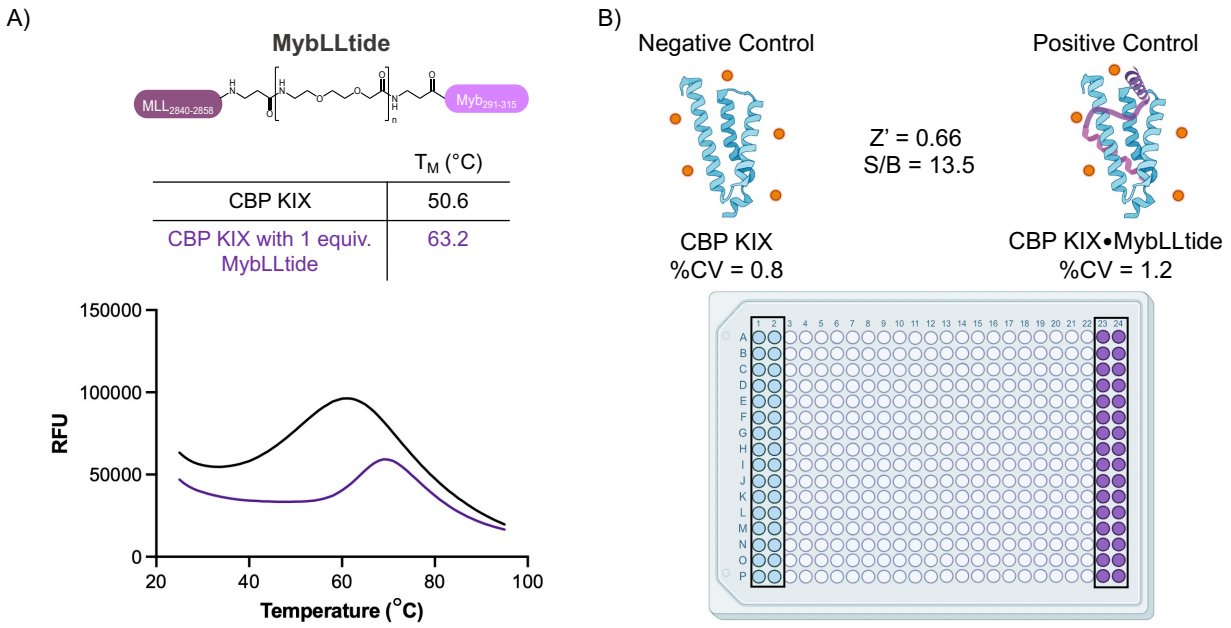


Figure 2.3 Dual-site inhibitor MybLLtide serve as the optimal positive control effector for HTS. A) Single concentration DSF screen of CBP KIX in the presence and absence of an equivalent of MybLLtide. Initial experiments were performed in triplicate. B) A representation of the preparation for HT-DSF screening and validating parameters to proceed in said screening. Each control was run with 192 replicates.

A diverse library of compounds increased the likelihood for discovering ligands with distinct conformational impacts. The NIH Clinical Collection and MicroSource 2400 compound libraries within the Center for Chemical Genomics are composed of known bioactive molecules and FDA-approved drugs with diverse structures. A DSF screen of these libraries identified 323 preliminary hits that alter CBP KIX's T_M in a statistically significant (-3 SD < CBP KIX T_M > 3 SD). About two-thirds of the modulators evoked positive shifts and the other third caused negative thermal shifts, which was likely due to binding a less stable conformer of the protein. (Figure 2.4A) Afterwards, to confirm target engagement and eliminate false positives from the screen, CBP KIX thermostability was measured in a dose-response follow up with all the preliminary hits.

(Figure 2.4B) This led to 41 hits being validated and identified as having a concentration-dependent effect on CBP KIX T_M.

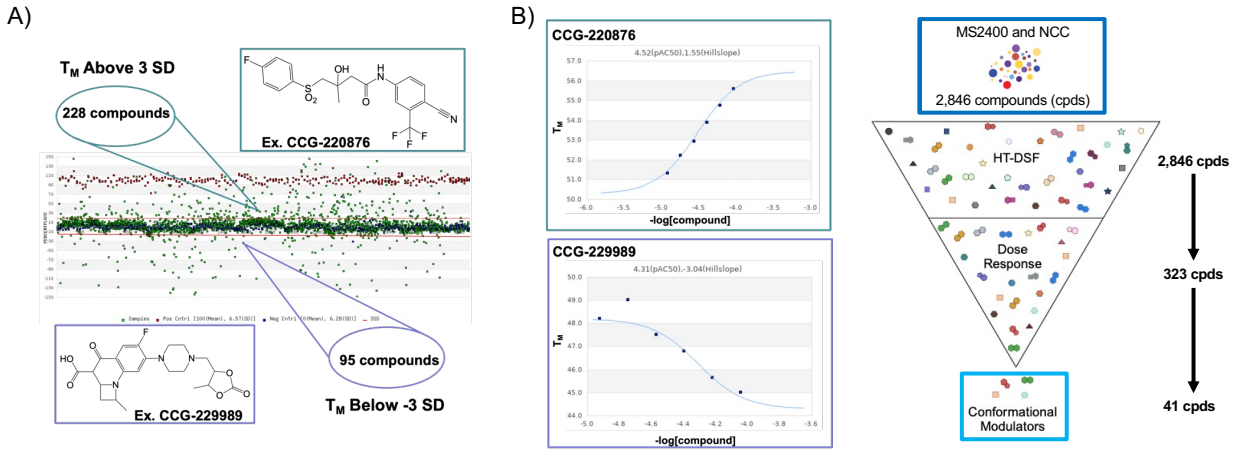


Figure 2.4 The single point DSF screening of a diverse library against CBP KIX. A) The pilot screen with CBP KIX yielded compounds that caused positive and negative thermal shifts with two examples on display. B) Follow-up dose-response DSF screening discovered 41 modulators that had a sigmoid-like transition with increasing compound concentrations. The dose-response DSF experiments were performed with mid to low micromolar compound concentrations and in duplicate.

2.3.3 A dual approach to examine modulator effects on the CBP KIX domain and its PPIs

The next step was to map the molecules' effects on the CBP KIX domain and survey their impact on the CBP KIX PPI network, which done via nuclear magnetic resonance (NMR) spectrometry and fluorescence polarization (FP).[4,5,38–40] Of the 41 hit compounds, 29 modulators were commercially available and thus purchased. To identify molecules that initiated significant shifts in the CBP KIX domain, $^{1}H,^{15}N$-HSQC NMR spectroscopy was performed and the chemical shift perturbations of the residues in the protein backbone upon stabilizer introduction were recorded. 17 of the ligands caused statistically significant chemical shifts in CBP KIX backbone residues, (Figure 2.5A) indicating environmental changes due to binding. When examining those ligands,

7 compounds exhibited widespread impacts with shifts in all three helices of the CBP KIX domain, while the other 10 compounds displayed localized effects in the modification of residues in one or two helices. (Figure 2.5B) These results reveal the two subsets of modulators (widespread and localized) that induce differential changes in CBP KIX.

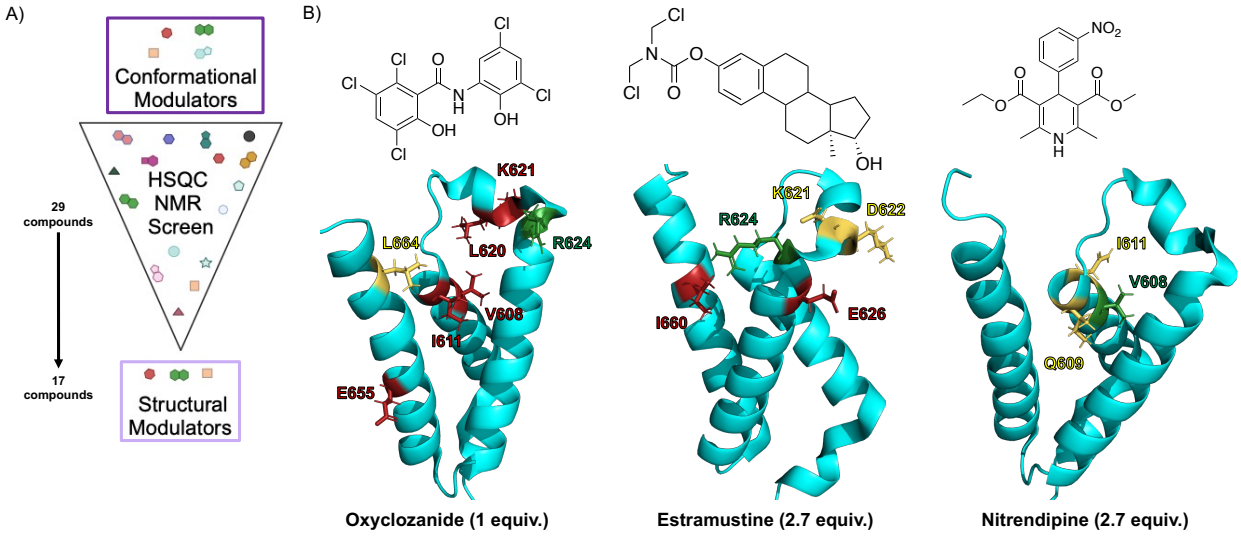
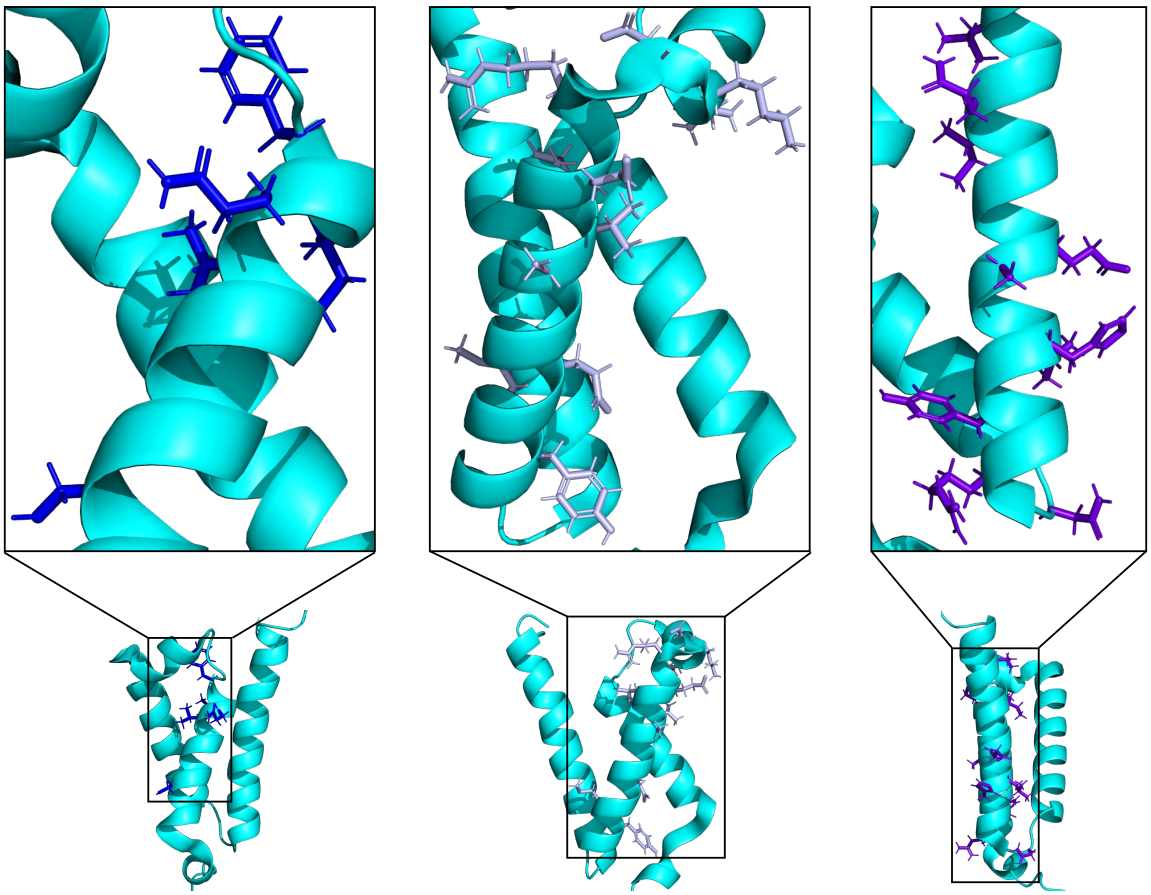


Figure 2.5 Examination of the modulators by HSQC NMR identified those initiated significant shifts in the backbone. A) Seventeen compounds were shown to cause a statistically significant change in residue chemical shift in Hertz as calculated using the equation in the chapter methods. The threshold for compound selection was set as those compound that have one or more residues that experience a chemical shift change of at least three standard deviations for the mean chemical shift. B) Some compounds initiated widespread changes while others caused localized shifts only. The solution structure for CBP KIX (PDB:2AGH) was used to visualize the significant residue perturbations. The residues highlighted in red experienced a chemical shift change between one and two standard deviations in the presence of the indicated ligand. The residues highlighted in yellow experienced a chemical shift change between two and three standard deviations in the presence of the indicated ligand. The residues highlighted in green experienced a chemical shift change of more than three standard deviations in the presence of the indicated ligand.

Chemical shift perturbations indicated that all 17 ligands engage the CBP KIX domain adjacent to the dynamic loop between the α_1 and α_2 helices. The chemical shifts above one standard deviation for all 17 compounds were assessed to pinpoint the key regions perturbed by modulators engagement. (Appendix Figure B.4) Almost all

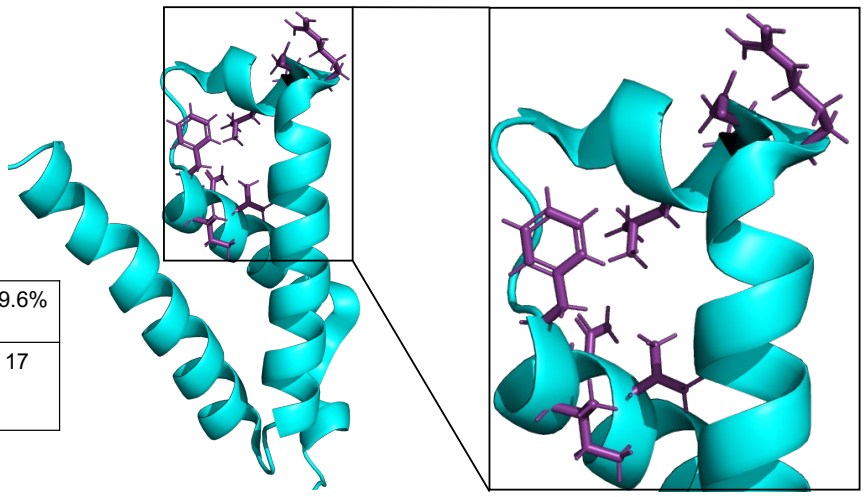
compounds perturb residues in the α_2 helix and approximately 50% of the total chemical shifts occur within this helix, implicating the importance of the α_2 helix in stabilization. Of the remaining total shifts, about 25% of them are dispersed across the α_3 helix; however, the other 25% of chemical shifts are confined to few residues in the α_1 helix, suggesting potencially significant ligand contacts with the α_1 helix. (Figure 2.6A) Given these results and the contextual importance of the α_1/α_2 in stability, chemical shifts from Val608 to Arg624 were examined to reveal that more than half of all the chemical shifts occur in this region and all 17 compounds invoke significant shifts around this loop, (Figure 2.6B) suggesting that they all directly induce effects on the IDR between the α_1 and α_2 helices.

A)



	1	2	3
Shifts in α helix	23.7%	51.7%	24.6%
Compounds with shifts in α helix	12	16	11

B)



Shifts around the α_1/α_2 loop	59.6%
Compounds with shifts around the α_1/α_2 loop	17

Figure 2.6 Visualization of the key residues perturbed by modulator binding. A) A breakdown of the notable chemical shifts of one standard deviation or more seen with all seventeen significant modulators show that most of the compound interact with helix-2 and many compounds interact with few residues in

helix-1. B) Focusing on the residues around the loop revealed that all compounds cause notable chemical shifts in that region. The solution structure for CBP KIX (PDB:2AGH) was used to visualize the significant perturbations.

Next, we assessed the impact of each of the modulators on the CBP KIX PPI network. Since CBP KIX can simultaneously bind two partners via its two binding sites, we developed an FP assay to simultaneously monitor changes at both sites.[41–43] To do this, interactions of CBP KIX with the fluorescently labeled versions of the standard MLL construct and an extended Myb construct (Myb32)[10] were first profiled to define the suitability of the dual competitive assay, (Figure 2.7A) which confirmed that MLL binding to the domain does not impact Myb32 binding and vice versa. Then, garcinolic acid, the natural product reported to inhibit the binding of both MLL and c-Myb TADs with similar IC_{50} values,[1] was assessed, and its effect on MLL and Myb binding was recapitulated in the dual assay format, (Figure2.7B) demonstrating the assay's effectiveness in reporting changes at both binding sites.

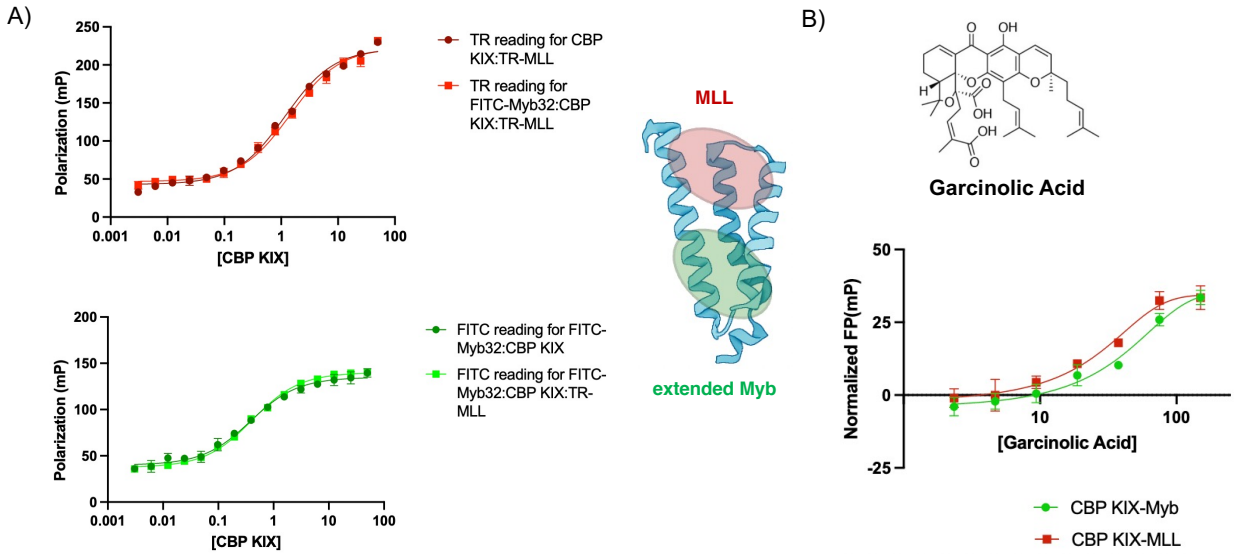


Figure 2.7 Establishment of the dual fluorescence polarization assay for CBP KIX. A) The binary and ternary complexes in the CBP KIX FP assay do not display visible differences. The direct binding FP assay was performed with mid to low micromolar CBP KIX concentrations. PDB ID: 4D7X. B) The dual FP assay can reproduce the inhibitory activity seen with a single probe approach. The competitive FP assay was performed with mid to low micromolar compound concentrations. All experiments were performed in triplicate and the error bars represent the standard deviation from the mean.

The 29 hits from the HTS were subsequently evaluated in the competitive dual FP assay in a dose-response format. (Figure 2.8A) From this, one compound, oxyclozanide, was found to inhibit binding at both of CBP KIX's canonical binding sites, (Figure 2.8B) making it a so-called "global" inhibitor of the domain. It is important to note that oxyclozanide also appeared as a hit in the NMR assessment amongst the ligands that initiated widespread structural shifts in CBP KIX. This signifies the inherent value of this conformational modulator as it impacts the PPIs and consequently, function of the domain.

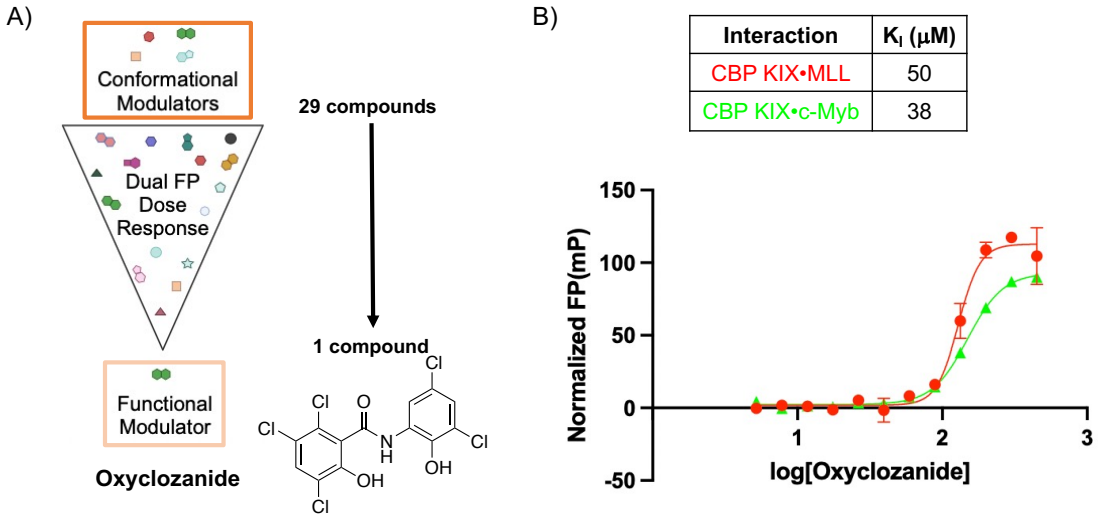


Figure 2.8 Discovery of a mixed mechanism inhibitor in oxyclozanide. A) The dual FP assay yielded a singular hit in oxyclozanide. B) This compound displayed moderate inhibition at both sites. The FP assay was performed with high to low micromolar compound concentrations and in triplicate. The error bars represent the standard deviation from the mean.

2.3.4 Investigation of the oxyclozanide scaffold and its key interactions

Oxyclozanide is a synthetically accessible small molecule, making structure-activity relationship (SAR) studies straightforward. First, to examine the relative

importance of functionalization on each aromatic ring and begin the investigation of scaffold modification, analogs lacking functional groups on either aromatic ring were produced by collaborator Dr. Amol Mhetre. (Figure 2.9A) In the study of these analogs, the concentration-dependent change in melting temperature seen with oxyclozanide is not observed with either analog. (Figure 2.9B). In addition, although the analogs seem to have a minor impact on MLL binding, neither of them inhibits Myb binding. (Figure 2.9C) This illustrates that functionalization on each aromatic ring is pivotal for oxyclozanide's ability to modulate CBP KIX.

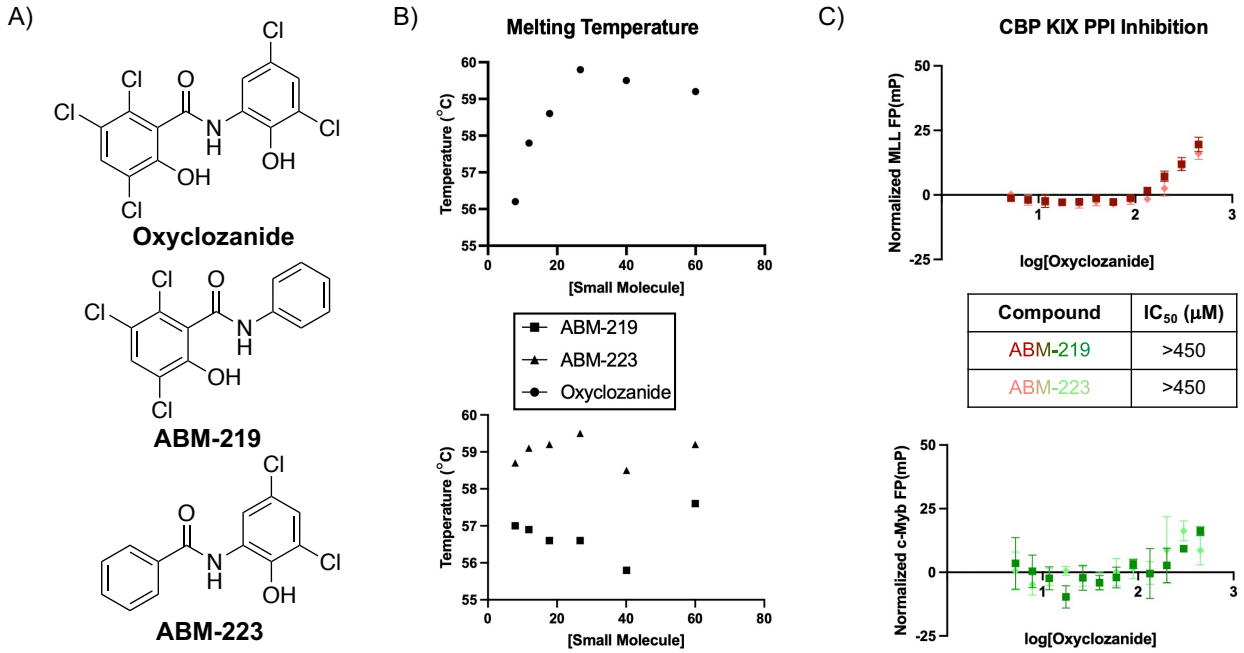


Figure 2.9 Assessment of the oxyclozanide analogs. A) Analogs of oxyclozanide lacking ring substitutions were synthesized and tested alongside the resynthesized commercial compound. Compounds were synthesized by Dr. Amol Mhetre. B) When examining the compounds' ability to shift the thermostability of CBP KIX in a dose-dependent manner, neither analog exhibited a dose-response relationship. The DSF experiments were performed with mid to low micromolar compound concentrations. C) Also, neither analog inhibited CBP KIX PPIs at either site. The FP assays were performed with high to low micromolar compound concentrations. All experiments were performed in triplicate and the error bars represent the standard deviation from the mean.

Further modification of the oxyclozanide scaffold requires guidance to improve upon its modular affinity and physicochemical properties. Docking studies serve as great guides for SAR.[44,45] A combination of experimental and computational structural information enabled the mapping of the modulator binding mode and visualization of the key interactions between CBP KIX and oxyclozanide. Blessing Oloyede performed the NMR-guided docking to discover the most like ligand pose and investigate the essential interactions. (Figure 2.10) Oxyclozanide forms many proximal hydrophobic interactions, most notably Leu664 and Ile 611 interact with the amine aromatic ring and its associated chlorine functional groups. The carbonyl aromatic ring of the small molecule makes numerous contacts with Arg624. This residue forms weak polar interactions at the chlorine on C6 and a weak H-bond with chlorine on C5. In addition, it was determined that Arg624 acts as a hydrogen bond donor and cation in π-coordination interactions with the carbonyl aromatic ring. These results set the precedent for future SAR studies and optimization of the scaffold for translation down the drug discovery pipeline.

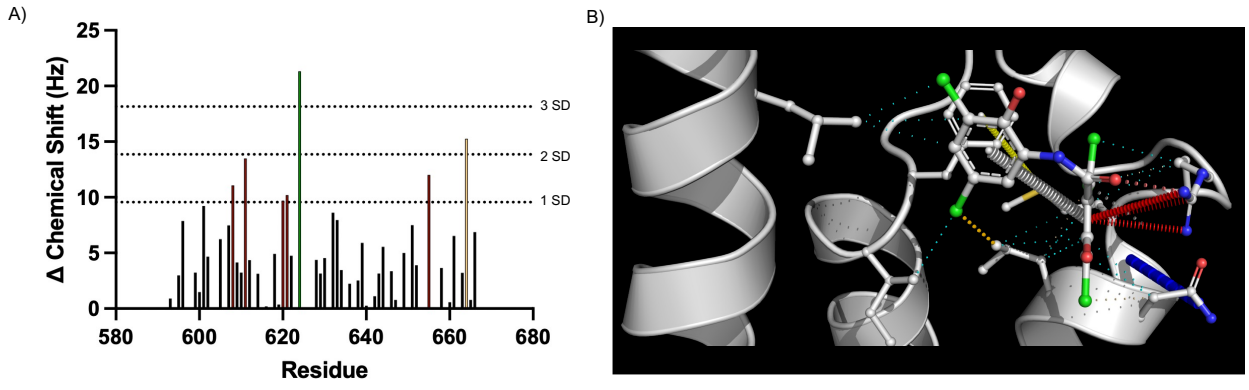


Figure 2.10 Mapping the key interactions between oxyclozanide and CBP KIX. A) The HSQC NMR performed with one equivalent of oxyclozanide led to statistically significant chemical shifts as calculated using the equation in the chapter methods. B) In studies carried out by Blessing Oloyede, the NMR-guided docking led to the identification of a most likely binding pose. The cyan dashes indicate proximal

hydrophobic interactions, and the orange dash indicates a weak hydrogen bond. The thick red dashes indicate π-coordination interactions and the thick white dashes indicates π-π interactions.

2.4 Conclusions

Mixed mechanism inhibitors are extremely valuable tools in targeting proteins that participate in transient interactions. In this work, DSF proves to be effective at identifying modulators that invoke change in protein stability regardless of binding site for even a relatively low-melting ABD. Pilot screening of a diverse library against complex target CBP KIX identified a suite of small molecules that stabilized the dynamic domain. Further examination of these modulators using NMR unveiled a significant number of them engaged the flexible loop in the domain, validating the value of DSF at the helm of conformational stabilizer identification. In addition, functional assessment via FP identified a small molecule scaffold that inhibits the PPIs of CBP KIX at both of its canonical binding sites, most likely due to a mixed mechanism. Finally, this small molecule, oxyclozanide, is synthetically tractable for further optimization in the development of a more potent allosteric/orthosteric inhibitor.

2.5 Materials and Methods

Protein expression and purification

The Med25 expression plasmid, referred to as pAcID(394-543)-His6, was generously provided by Prof. Patrick Cramer.[46] Med25 AcID and CBP KIX (586-672) were expressed and purified from heat-shock competent BL21-AI *E. coli*, in Terrific Broth (TB) containing 0.1 mg/mL ampicillin and 0.05 mg/mL tetracycline, using previously described conditions.[32,46] 15N-labeled CBP KIX was similarly expressed. Plasmid was transformed via heat-shock into competent E. coli BL21 (DE3) cells. The

cells were then plated on LB agar plates with selection antibiotic. A 50 mL overnight culture was prepared from plated colonies in LB, and it was used on inoculate a 1L culture of M9 minimal media supplemented with 0.1 mg/mL of ampicillin, 1 g/L $^{15}NH_4Cl$, 2 g/L D-glucose, and 0.5% 15N-labeled Bioexpress media (all labeled components were purchased from Cambridge Isotopes). Before inoculation, the overnight culture was pelleted, and media exchanged into the same M9 minimal media. All cells were grown at 37 °C to an optical density (OD600nm) of 0.8.

Temperature was subsequently reduced to 18°C and protein expression was induced upon addition of IPTG to a final concentration of 0.25 mM. Cells were pelleted via centrifugation at 6000 xg for 20 mins at 4°C. Cell pellets were stored at -80°C prior to purification. The harvested pellets (2) were thawed on ice and resuspended in 35 mL of lysis buffer/HisTrap Buffer A (50 mM sodium phosphate, 300 mM sodium chloride, 10 mM imidazole, pH 7.2) containing 2-mercaptoethanol and one cOmplete protease inhibitor (Roche, 11873580001). Cells were then lysed by sonication on ice and cellular lysates were cleared by centrifugation at 9500 rpm for 20 min at 4°C. The Hisx6 tagged protein was affinity purified using immobilized metal ion affinity chromatography (IMAC) on a HisTrap HP Ni Sepharose column (GE Healthcare). Elution was conducted using an imidazole gradient with HisTrap Buffer B (50 mM sodium phosphate, 300 mM sodium chloride, 600 mM imidazole, pH 7.2). The elution fractions were pooled and diluted 1:2 with Source S Buffer A (50 mM sodium phosphate pH 7.2) then another cOmplete protease inhibitor tablet was added. The eluent was subsequently purified by cation exchange FPLC (Source 15S, GE Healthcare) using a gradient of Source S Buffer B (50 mM sodium phosphate, 1 M sodium chloride, pH 7.2).

The FPLC purified protein was then dialyzed into storage buffer (Unlabeled protein: 10 mM sodium phosphate, 150 mM NaCl, 10% v/v glycerol, 0.001% v/v NP-40, 1 mM DTT pH 6.8)(15N-labeled protein: 20 mM sodium phosphate buffer, pH 6.5, 150 mM NaCl, 3 mM DTT) overnight, concentrated, aliquoted, and stored at -80°C. Final protein was greater than 90% pure as determined by Coomassie stained polyacrylamide gel. Protein concentration was determined by UV-Vis spectroscopy using an extinction coefficient, ε = 12,950 M^{-1} cm^{-1}.

Synthesis and isolation of transcriptional activation domain peptides

Activator peptides were synthesized using rink amide resin (CEM) using standard Fmoc solid-phase peptide synthesis protocols as previously described.

Fluorophore Coupling and Acetylation: For Texas-Red coupling, an excess (2 equivalents) of Texas-Red (TR) was dissolved in anhydrous dimethylformamide (DMF) with 10% (vol/vol) anhydrous diisopropylethylamine (DIPEA) and added to the thoroughly dried peptide on resin. N-terminal coupling of fluoresceine isothiocyanate (FITC) fluorophore was conducted by adding 2 equivalents of FITC in 25% (vol/vol) diisopropylethylamine in dimethylformamide. For acetyl capping, 1.5 mL of DMF was added to the peptide on resin and then 50 molar equivalents of acetic anhydride followed by 50 molar equivalents of DIPEA were added. The fluorophore coupling and acetylation was performed for 18 hours at RT.

Peptides were deprotected and cleaved from the resin for 4 hours in 90% trifluoroacetic acid (TFA), 5% thioanisole, 3% ethanedithiol (EDT) and 2% anisole. Crude peptides were filtered to remove resin and transferred to a 15 mL falcon tube,

dried under nitrogen stream, and precipitated from cold ether. Peptide suspensions were then centrifuged at 4000xg for 10 minutes at 4°C, and the ether decanted. Crude peptides were resuspended in 20% acetonitrile, purified via HPLC on an Agilent 1260 HPLC using a semi-prep C18 column (Phenomenex). Pure fractions were collected and lyophilized to afford pure peptides. Final purity was determined via analytical HPLC and identity was confirmed using mass spectrometry. Analytical spectra were obtained using an analytical C18 column (Phenomenex) on an Agilent 1260 HPLC. Mass spectra were obtained using an Agilent 6230 LC/TOF and an Agilent 6545 LC/Q-TOF. Sequences, mass spectra, and analytical spectra of all the peptides can be found in Appendix A.

For this chapter, FITC-MLL (2840-2858), TR-MLL (2840-2858), FITC-Myb (291-316), FITC-Myb (284-316)/FITC-Myb32, Ac-MLL (2840-2858), and Ac-Myb (291-316) were synthesized and purified. For all peptides, a gradient of 20-60% acetonitrile over 50 min was used for HPLC purification.

Differential scanning fluorimetry (DSF) with peptides and peptidomimetics

Experiments were conducted in triplicate utilizing 20 µL sample volumes in 8-strip PCR tubes sealed with clear cap strips. CBP KIX was diluted to 15 µM in its new standard buffer (25 mM sodium phosphate, 125 mM sodium chloride, 0.001% Triton X-100, pH 7.8) with dithiothritol (DTT) added to a final concentration of 1 mM. The protein was incubated with the following conditions at RT for 30 minutes: 1 molar equivalent of MLL (2840-2858); 1 molar equivalent of Myb (291-316); 2 molar equivalents combined of MLL (2840-2858) and Myb (291-316); and 1 molar equivalent of MybLLtide (generously provided by Dr. Stephen Joy). After incubation, SYPRO orange dye

(Invitrogen) was added to a final 5X concentration, and an Applied Biosystems StepOnePlus qPCR instrument was utilized to obtain melting curves by exciting at 488 nm and monitoring emission at 602 nm over a temperature gradient of 25-95°C with a 1°C/min ramp. Raw fluorescence data (RFU), also known as the multicomponent data, was imported into the online data analysis program, DSFworld, and T_M was calculated using a sigmoidal fitting model that accounts for a single transition with a high initial, decaying fluorescence. For data visualization, RFU is plotted as a function of temperature using GraphPad Prism software. The maximum of the first derivative is the reported T_M, with T_M of each ligand calculated as the difference between the Tm of the protein and the T_M of the protein + ligand, considering the difference of standard deviations. Significant shifts in T_M were defined by a more three standard deviation (S.D.) change (negative or positive) from the mean of the protein-dye control.

High-throughput DSF screen

To determine the assay efficacy for high-throughput screening, two control plates (MicroAmp Optical 384-well Reaction Plate) were tested. Each plate contained 128 negative control wells, containing the protein dosed with DMSO, and 128 positive control wells, containing the protein-ligand complex mixture. To determine the Z-Score and coefficient of variance (CV), 22.5 μM CBP KIX was plated followed by addition of 1 molar equivalent of MybLLtide. The protein and peptidomimetic were incubated for 30 min at room temperature before SYPRO Orange was added to a final concentration of 12.5X. The plates were spun at 100 rpm for 1 min and the Applied Biosystems QuantStudio 6 Flex Real-Time PCR was utilized to obtain melting curves, replicating

methods of the peptide DSF screen. The multicomponent data was processed using Applied Biosystems Protein Thermal Shift software to determine the Boltzmann-fitted T_M for each control well. The assay demonstrated excellent performance, denoted by the Z' and CV in the main text of this chapter.

The pilot screen of 2,846 compounds was completed in the Center for Chemical Genomics. CBP KIX (22.5 μM final concentration) were plated in 384-well format and treated with 90 μM (final concentration) of each library compound. The plates incubated for 30 min at room temperature and the SYPRO Orange was added (12.5X final concentration) before spinning and thermostability measurements using the QuantStudio 6 Flex Real-Time PCR. Each plate contained 32 negative control wells and 32 positive control wells. Using an initial activity threshold of a $T_M \geq 3$ S.D. above the average signal of that of the negative controls and a $T_M \leq 3$ S.D. below the average signal of that of the negative controls, 584 molecules (20.5%) were identified. After the elimination of hits that were identified as pan-assay inhibitors (PAINS), reactive, and promiscuous as well as those that display autofluorescent properties, 323 compounds (11.3%) were identified as preliminary CBP KIX hits.

For the dose response follow-up, each of the 323 compounds were assessed in duplicate at six concentrations (90, 60, 40, 26.7, 17.8, and 11.9 μM). The compounds were incubated with 22.5 μM of CBP KIX for 30 min, 12.5X SYPRO Orange was added, and the plate was spun. Subsequent QuantStudio 6 Flex Real-Time PCR thermal melts yielded 41 hits (1.4%), which were defined as those compounds that produced a concentration-dependent change in melting temperature.

Heteronuclear single quantum coherence (HSQC) NMR

NMR assignments of CBP KIX (586-672) was determined from previous studies using 13C,15N-labeled protein. [Pomerantz, Henley, Joy, Breen] Constant time 1H,15N-HSQC experiments were performed using 75 μM 15N-labeled CBP KIX in NMR buffer (20 mM sodium phosphate pH 6.5, 150 mM NaCl, 3 mM DTT, 10% D2O, and 2% DMSO) on a Bruker 600 MHz instrument equipped with a cryoprobe. Data processing was performed and analyzed using Mestrenova. Ligand-protein complexes were assessed at either 1 or 2.7 equivalents of compound, relative to protein concentration. A control spectrum was obtained with CBP KIX and DMSO only. Chemical shift perturbations (∆δ) were calculated from the proton (∆δH) and nitrogen (∆δN) chemical shifts by:

$$Chemical\ shift\ (Hz)\ =\ \sqrt{((\Delta\delta 15N)^2 + (\Delta\delta 1H)^2)}$$

Of the assigned residues, the average chemical shift amongst the dataset and thresholds for 1, 2, and 3 standard deviations from the mean chemical shift were determined. Those compounds that caused at least one 3 S.D. chemical shift in the protein were selected as hits.

Fluorescence Polarization (FP) Direct Binding

Direct binding experiments were performed using fluorescence polarization as previously described.[32] Low volume, non-binding, black 384-well plates (Corning) were used, and fluorescence polarization was measured using a PHERAStar plate reader. In triplicate, the protein is serially diluted (2x dilutions) in the plate and a constant

concentration of tracer (concentration of 20 nM) was added to make a final volume of 20 µL. For the dual FP direct binding, two separate modules were used one at a time to accommodate the detection of both FITC and TR. For all direct binding experiments, a binding isotherm accounting for ligand depletion (assuming a 1:1 binding model) was fit to the obtained polarization values as a function of protein concentration to obtain the equilibrium dissociation constant, K_d:

$$y = c + (b - c) \times \frac{(K_d + a + x) - \sqrt{(K_d + a + x)^2 - 4ax}}{2a}$$

“a” and “x” are the total concentrations of fluorescent peptide and protein, respectively, “y” is the observed anisotropy at a given protein concentration, “b” is the maximum observed anisotropy value, and “c” is the minimum observed anisotropy value. Each data point is an average of three independent wells with the indicated error bars representing the standard deviation from the mean. Data was analyzed and visualized using GraphPad Prism.

Dual FP screen

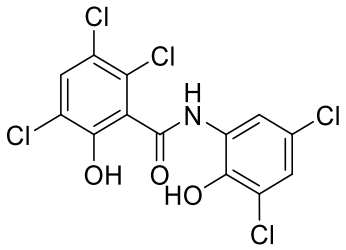
Assays were performed in a final volume of 20 µL in black, 384-well Corning plates. CBP KIX (0.8 µM final concentration) was pre-incubated with TR-MLL (20 nM final concentration) and FITC-Myb32 (20 nM final concentration) for 1 hour. Of the 41 hit compounds, 29 compounds were purchased from the commercial supplier Molport and tested. These compounds were assessed in triplicate at twelve concentrations (1.5X dilutions starting at 450 µM final concentration). The diluted compounds were then plated, and the protein-tracer mix was added. The plates were incubated for 2 hours at

room temperature before fluorescence polarization measurements in the fluorescein and Texas Red channels were made using the PheraStar plate reader. Percent inhibition for each compound was determined at the highest concentration using wells containing protein treated with DMSO as a negative control and wells containing fluorophore-tagged peptides alone as a positive control. The final hit was selected based upon a more than 50% inhibition of both tracers. The IC_{50} value was converted to K_I values using the apparent K_d value calculated from the direct binding experiments of each coactivator ABD•FITC-TAD complex using a K_I calculator.87 Reported K_I value is the average of three independent wells with the indicated error representing the standard deviation of the triplicates.

Analog Production

The commercially available product oxyclozanide was synthesized under the name **ABM-217** by Dr. Amol Mhetre, a post-doctoral fellow in the Nikolovska-Coleska Lab at the University of Michigan. Afterwards, Dr. Mhetre synthesized the analogs lacking substitutions on the amine and carboxyl connected rings **ABM-219** and **ABM-223**, respectively. Note: **ABM-220** is an intermediate that was also synthesized, however, solubility in assay buffer prevented testing. Following is the synthesis and characterization data for the production of ABM-217, 219, 220 and 223.

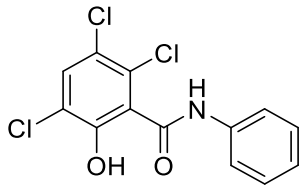
ABM-217



47 2,3,5-trichloro-*N*-(3,5-dichloro-2-hydroxyphenyl)-6-hydroxybenzamide

A mixture of 2,3,5-trichloro-6-hydroxybenzoic acid (0.1 g, 0.414 mmol), 2-amino-4,6-dichlorophenol (73.7 mg, 0.414 mmol) and Thionyl Chloride ($SOCl_2$, 1.0 eq.) in 6 mL of Toluene was refluxed at 110 °C. for 16 h. The progress was monitored by thin-layer chromatography (TLC). Upon complete consumption of the starting materials, the reaction mixture was gradually cooled to room temperature. The remaining solvent was concentrated, and the resulting solid residue was diluted in Hexane and transferred into a 15 mL Falcon tube. The mixture was centrifuged at 4000 rpm for 5 min, the supernatant was decanted, and the solid pellet was washed twice with 10% ethanol in water and centrifuged. The solid pellet was then resuspended in CH_2Cl_2, transferred into a 20 mL clean glass vial, and the CH_2Cl_2 was evaporated. The residue was dried under high vacuum to afford the desired product **ABM-217** (70 mg, 42%) as a brown solid. **^{1}H NMR** (500 MHz, DMSO-d_6) δ 10.60 (s, 1H), 10.34 (s, 1H), 9.99 (s, 1H), 8.08 (d, J = 2.6 Hz, 1H), 7.83 (s, 1H), 7.34 (d, J = 2.5 Hz, 1H); **LCMS**: m/z for $C_{13}H_7Cl_5NO_3$ (M + H) 402.10; **Purity**: 98.77%.

ABM-219



1,2 2,3,5-trichloro-6-hydroxy-*N*-phenylbenzamide

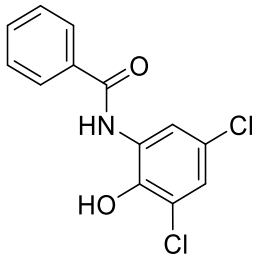
The synthesis of **ABM-219** followed the same procedure as **ABM-217**, starting from 2,3,5-trichloro-6-hydroxybenzoic acid (150 mg, 0.621 mmol) and aniline (58 mg, 0.621 mmol). The reaction yielded the desired product, **ABM-219** (85 mg, 43% yield).**^{1}H NMR** (500 MHz, DMSO-d_6) δ 10.60 (s, 1H), 7.85 (s, 1H), 7.70 – 7.65 (m, 2H), 7.35 (t, *J* = 7.8 Hz, 2H), 7.11 (tt, *J* = 7.5, 1.1 Hz, 1H); **LCMS:** m/z for $C_{13}H_9Cl_3NO_2$ (M + H) 315.90; **Purity**: 99.99%

ABM-220[18]

To a solution of 2-amino-4,6-dichlorophenol (100 mg, 0.562 mmol) in dry THF (5 mL), DIPEA (196 µL, 1.12 mmol) was added, and the reaction mixture was cooled to 0 °C. Benzoyl chloride (158 mg, 1.12 mmol) was added dropwise, and the reaction mixture was stirred at room temperature for 12 hours. The progress was monitored by thin-layer chromatography (TLC). Upon complete consumption of the starting material, the reaction mixture was diluted with water (15 mL) and extracted with ethyl acetate (3 × 10 mL). The combined organic layers were washed with brine, dried over Na_2SO_4, and concentrated under reduced pressure to afford a brown solid. The solid was washed with Et_2O (2 × 15 mL), filtered, and dried under vacuum to yield the desired product **ABM-220** (190 mg, 88%). **^{1}H NMR** (500 MHz, DMSO-d_6) δ 10.35 (s, 1H), 8.14 (d, *J* = 7.7 Hz, 2H), 7.90 (d, *J* = 2.5 Hz, 1H), 7.78 (d, *J* = 7.7 Hz, 2H), 7.76 – 7.69 (m, 2H), 7.56

(dt, *J* = 23.8, 7.5 Hz, 3H), 7.44 (t, *J* = 7.6 Hz, 2H); **LCMS:** m/z for $C_{20}H_{12}Cl_2NO_3$ (M - H) 384.1; **Purity**: 99%.

ABM-223



[4,5,38] *N*-(3,5-dichloro-2-hydroxyphenyl)benzamide

To a solution of **ABM-220** (189 mg, 0.561 mmol) in THF-MeOH-water (1:1:1, 5 mL), $LiOH \cdot H_2O$ (236 mg, 5.62 mmol) was added, and the reaction mixture was stirred at room temperature for 12 hours. The reaction mixture was concentrated and diluted with water (10 mL), then acidified with 1N HCl to pH 4. The aqueous layer was extracted with ethyl acetate (3 × 25 mL). The combined organic layers were washed with brine, dried over Na_2SO_4, and concentrated under reduced pressure to afford the desired product ABM-223 (103 mg, 65 %). **^{1}H NMR** (500 MHz, DMSO-d_6) δ 10.99 (s, 1H), 8.17 (s, 2H), 8.08 (s, 1H), 7.73 – 7.60 (m, 2H), 7.49 (td, *J* = 7.7, 1.6 Hz, 1H), 7.42 (td, *J* = 7.8, 1.7 Hz, 1H); **LCMS:** m/z for $C_{13}H_8Cl_2NO$ (M - H) 280.0; **Purity**: >95 %.

Ligand Docking

Oxyclozanide was docked to the CBP KIX domain (PDB ID: 2AGH) using the Rigid CDOCKER protocol, a CHARMM-based molecular dynamics simulated annealing method. The receptor structure was first retrieved from the Protein Data Bank and

prepared by removing water molecules and ligands, adding hydrogens, assigning protonation states, and performing energy minimization to relieve steric clashes. The ligand, Oxyclozanide, was either drawn or obtained from a chemical database. It was converted to a 3D structure, protonated appropriately, and energy minimized. The binding site on the CBP KIX domain was defined either by known interaction hotspots based on HSQC-NMR chemical shifts of the protein, and a docking region was specified around this site. CDOCKER was then used to perform the docking, where multiple ligand poses were generated through simulated annealing and scored using interaction energy metrics. The resulting poses were evaluated, and the top-ranked conformations were examined for hydrogen bonding, hydrophobic contacts, and compatibility with known structural features of the binding site. Following docking, the best-scoring pose was selected for further analysis. Docking was performed by Blessing Oloyede.

2.6 References

1. Breen ME, Joy ST, Baruti OJ, et al. Garcinolic acid distinguishes between GACKIX domains and modulates interaction networks. *ChemBioChem*. Published online August 2023. doi:10.1002/cbic.202300439

2. Brüschweiler S, Konrat R, Tollinger M. Allosteric communication in the KIX domain proceeds through dynamic repacking of the hydrophobic core. *ACS Chem Biol*. 2013;8(7):1600-1610. doi:10.1021/cb4002188

3. Chatterjee S, Angelakos CC, Bahl E, et al. The CBP KIX domain regulates long-term memory and circadian activity. *BMC Biol*. 2020;18(1). doi:10.1186/s12915-020-00886-1

4. Gee CT, Arntson KE, Koleski EJ, Staebell RL, Pomerantz WCK. Dual Labeling of the CBP/p300 KIX Domain for 19F NMR Leads to Identification of a New Small-Molecule Binding Site. *ChemBioChem*. 2018;19(9):963-969. doi:10.1002/cbic.201700686

5. Gee CT, Koleski EJ, Pomerantz WCK. Fragment screening and druggability assessment for the CBP/p300 KIX domain through protein-observed 19F NMR

spectroscopy. *Angew Chem - Int Ed*. 2015;54(12):3735-3739. doi:10.1002/anie.201411658

6. Law SM, Gagnon JK, Mapp AK, Brooks CL. Prepaying the entropic cost for allosteric regulation in KIX. *Proc Natl Acad Sci U S A*. 2014;111(33):12067-12072. doi:10.1073/pnas.1405831111

7. Lee CW, Arai M, Martinez-Yamout MA, Dyson HJ, Wright PE. Mapping the interactions of the p53 transactivation domain with the KIX domain of CBP. *Biochemistry*. 2009;48(10):2115-2124. doi:10.1021/bi802055v

8. Wang N, Majmudar CY, Pomerantz WC, et al. Ordering a dynamic protein Via a small-molecule stabilizer. *J Am Chem Soc*. 2013;135(9):3363-3366. doi:10.1021/ja3122334

9. Yang K, Stanfield RL, Martinez-Yamout MA, Dyson HJ, Wilson IA, Wright PE. Structural basis for cooperative regulation of KIXmediated transcription pathways by the HTLV-1 HBZ activation domain. *Proc Natl Acad Sci U S A*. 2018;115(40):10040-10045. doi:10.1073/pnas.1810397115

10. Sato N, Suetaka S, Hayashi Y, Arai M. Rational peptide design for inhibition of the KIX–MLL interaction. *Sci Rep*. 2023;13(1). doi:10.1038/s41598-023-32848-2

11. Odoux A, Jindal D, Tamas TC, Lim BWH, Pollard D, Xu W. Experimental and molecular dynamics studies showed that CBP KIX mutation affects the stability of CBP:c-Myb complex. *Comput Biol Chem*. 2016;62:47-59. doi:10.1016/j.compbiolchem.2016.03.004

12. Palazzesi F, Barducci A, Tollinger M, Parrinello M. The allosteric communication pathways in KIX domain of CBP. *Proc Natl Acad Sci U S A*. 2013;110(35):14237-14242. doi:10.1073/pnas.1313548110

13. Zor T, De Guzman RN, Dyson HJ, Wright PE. Solution Structure of the KIX Domain of CBP Bound to the Transactivation Domain of c-Myb. *J Mol Biol*. 2004;337(3):521-534. doi:10.1016/j.jmb.2004.01.038

14. Joy ST, Henley MJ, De Salle SN, et al. A Dual-Site Inhibitor of CBP/p300 KIX is a Selective and Effective Modulator of Myb. *J Am Chem Soc*. 2021;143(37):15056-15062. doi:10.1021/jacs.1c04432

15. Uttarkar S, Dukare S, Bopp B, Goblirsch M, Jose J, Klempnauer KH. Naphthol AS-E phosphate inhibits the activity of the transcription factor Myb by blocking the interaction with the KIX domain of the coactivator p300. *Mol Cancer Ther*. 2015;14(6):1276-1285. doi:10.1158/1535-7163.MCT-14-0662

16. Radhakrishnan I, Pérez-Alvarado GC, Parker D, Dyson HJ, Montminy MR, Wright PE. Solution Structure of the KIX Domain of CBP Bound to the Transactivation

Domain of CREB: A Model for Activator:Coactivator Interactions. *Cell*. 1997;91:741-752.

17. Liu Y, Joy ST, Henley MJ, et al. Inhibition of CREB Binding and Function with a Dual-Targeting Ligand. *Biochemistry*. 2024;63(1):1-8. doi:10.1021/acs.biochem.3c00469

18. Peiffer AL, Garlick JM, Joy ST, Mapp AK, Brooks CL. Allostery in the dynamic coactivator domain KIX occurs through minor conformational micro-states. *PLoS Comput Biol*. 2022;18(4 April). doi:10.1371/journal.pcbi.1009977

19. Leander M, Yuan Y, Meger A, Cui Q, Raman S. Functional plasticity and evolutionary adaptation of allosteric regulation. *Proc Natl Acad Sci U S A*. 2020;117(41):25445-25454. doi:10.1073/pnas.2002613117/-/DCSupplemental

20. Kathman SG, Statsyuk AV. Covalent tethering of fragments for covalent probe discovery. *MedChemComm*. 2016;7(4):576-585. doi:10.1039/c5md00518c

21. Lodge JM, Justin Rettenmaier T, Wells JA, Pomerantz WC, Mapp AK. FP tethering: A screening technique to rapidly identify compounds that disrupt protein-protein interactions. *MedChemComm*. 2014;5(3):370-375. doi:10.1039/c3md00356f

22. Sijbesma E, Somsen BA, Miley GP, et al. Fluorescence Anisotropy-Based Tethering for Discovery of Protein-Protein Interaction Stabilizers. *ACS Chem Biol*. 2020;15(12):3143-3148. doi:10.1021/acschembio.0c00646

23. Shao H, Oltion K, Wu T, Gestwicki JE. Differential scanning fluorimetry (DSF) screen to identify inhibitors of Hsp60 protein-protein interactions. *Org Biomol Chem*. 2020;18(22):4157-4163. doi:10.1039/d0ob00928h

24. Makley LN, McMenimen KA, DeVree BT, et al. Pharmacological chaperone for α-crystallin partially restores transparency in cataract models. *Science*. 2015;350(6261):674-677. doi:10.1126/science.aac9145

25. Bergsdorf C, Wright SK. A Guide to Run Affinity Screens Using Differential Scanning Fluorimetry and Surface Plasmon Resonance Assays. In: *Methods in Enzymology*. Vol 610. Academic Press Inc.; 2018:135-165. doi:10.1016/bs.mie.2018.09.015

26. Scott DE, Spry C, Abell C. Differential Scanning Fluorimetry as Part of a Biophysical Screening Cascade. In: ; 2016:139-172. doi:10.1002/9783527683604.ch07

27. Lea WA, Simeonov A. Differential scanning fluorometry signatures as indicators of enzyme inhibitor mode of action: Case study of glutathione s-transferase. *PLoS ONE*. 2012;7(4). doi:10.1371/journal.pone.0036219

28. Makley LN, Gestwicki JE. Expanding the Number of “Druggable” Targets: Non-Enzymes and Protein-Protein Interactions. *Chem Biol Drug Des*. 2013;81(1):22-32. doi:10.1111/cbdd.12066

29. Chen J, Liu X, Chen J. Targeting intrinsically disordered proteins through dynamic interactions. *Biomolecules*. 2020;10(5). doi:10.3390/biom10050743

30. Liu J, Perumal NB, Oldfield CJ, Su EW, Uversky VN, Dunker AK. Intrinsic disorder in transcription factors. *Biochemistry*. 2006;45(22):6873-6888. doi:10.1021/bi0602718

31. Henley MJ, Linhares BM, Morgan BS, Cierpicki T, Fierke E □ CA, Mapp AK. Unexpected specificity within dynamic transcriptional protein-protein complexes. *Proc Natl Acad Sci U S A*. 2020;117(44):27346-27353. doi:10.1073/pnas.2013244117/-/DCSupplemental

32. Henderson AR, Henley MJ, Foster NJ, et al. Conservation of coactivator engagement mechanism enables small-molecule allosteric modulators. *Proc Natl Acad Sci U S A*. 2018;115(36):8960-8965. doi:10.1073/pnas.1806202115

33. Deller MC, Kong L, Rupp B. Protein stability: A crystallographer's perspective. *Acta Crystallogr Sect Struct Biol Commun*. 2016;72:72-95. doi:10.1107/S2053230X15024619

34. Reinhard L, Mayerhofer H, Geerlof A, Mueller-Dieckmann J, Weiss MS. Optimization of protein buffer cocktails using Thermofluor. *Acta Crystallograph Sect F Struct Biol Cryst Commun*. 2013;69(2):209-214. doi:10.1107/S1744309112051858

35. Brudar S, Hribar-Lee B. Effect of buffer on protein stability in aqueous solutions: A simple protein aggregation model. *J Phys Chem B*. 2021;125(10):2504-2512. doi:10.1021/acs.jpcb.0c10339

36. Bruce D, Cardew E, Freitag-Pohl S, Pohl E. How to Stabilize Protein: Stability Screens for Thermal Shift Assays and Nano Differential Scanning Fluorimetry in the Virus-X Project. *J Vis Exp JoVE*. 2019;(144). doi:10.3791/58666

37. Wu T, Yu J, Gale-Day Z, et al. Three essential resources to improve Differential Scanning Fluorimetry (DSF) experiments. *bioRxiv*. Published online 2020. doi:10.1101/2020.03.22.002543

38. Egner JM, Jensen DR, Olp MD, et al. Development and Validation of 2D Difference Intensity Analysis for Chemical Library Screening by Protein-Detected NMR Spectroscopy. *ChemBioChem*. 2018;19(5):448-458. doi:10.1002/cbic.201700386

39. Li K, Jadhav P, Wen Y, Tan H, Wang J. Development of a Fluorescence Polarization Assay for the SARS-CoV-2 Papain-like Protease. *ACS Pharmacol Transl Sci*. 2025;8(3):774-784. doi:10.1021/acsptsci.4c00642

40. Marlowe T, Alvarado C, Rivera A, et al. Development of a High-Throughput Fluorescence Polarization Assay to Detect Inhibitors of the FAK–Paxillin Interaction. *SLAS Discov*. 2020;25(1):21-32. doi:10.1177/2472555219874313

41. Du Y, Nikolovska-Coleska Z, Qui M, et al. A Dual-Readout F^2 Assay That Combines Fluorescence Resonance Energy Transfer and Fluorescence Polarization for Monitoring Bimolecular Interactions. *ASSAY Drug Dev Technol*. 2011;9(4):382-393. doi:10.1089/adt.2010.0292

42. Nikolovska-Coleska Z, Wang R, Fang X, et al. Development and optimization of a binding assay for the XIAP BIR3 domain using fluorescence polarization. *Anal Biochem*. 2004;332(2):261-273. doi:10.1016/j.ab.2004.05.055

43. Xiao X, Zhen S. Recent advances in fluorescence anisotropy/polarization signal amplification. *RSC Adv*. 2022;12(11):6364-6376. doi:10.1039/D2RA00058J

44. Bhattacharya S, Lin X. Recent advances in computational protocols addressing intrinsically disordered proteins. *Biomolecules*. 2019;9(4). doi:10.3390/biom9040146

45. Kump KJ, Miao L, Mady ASA, et al. Discovery and Characterization of 2,5-Substituted Benzoic Acid Dual Inhibitors of the Anti-apoptotic Mcl-1 and Bfl-1 Proteins. *J Med Chem*. 2020;63(5):2489-2510. doi:10.1021/acs.jmedchem.9b01442

46. Vojnic E, Mourão A, Seizl M, et al. Structure and VP16 binding of the Mediator Med25 activator interaction domain. *Nat Struct Mol Biol*. 2011;18(4):404-410. doi:10.1038/nsmb.1997

Chapter 3 Setting the Stage for Targeting and Investigating the MED15 KIX Motifs

3.1 Abstract

Outside of CBP and p300, the KIX domain can be found in the Mediator subunit MED15 across many species. The human ARC105/MED15 is linked to diabetes and hypertension, and the yeast *C. glabrata* GAL11/MED15 (cgMed15 KIX) is associated with multi-drug resistance. Despite the structural and sequential conservation within the KIX motifs, there are currently no good inhibitors for Arc105 and cgMed15 KIX, and there has been no investigation of conservation of their conformational dynamics. In this chapter, a similar workflow as developed in Chapter 2 was implemented to define ligands of the lesser studied Arc105 and cgMed15 KIX. Upon assay optimization, the 29 CBP KIX modulators were screening via DSF against both KIX motifs to discover modulators for each. Shared amongst the CBP, Arc105, and cgMed15 KIX modulators was oxyclozanide, which, upon functional assessment, was also found to be a pan-inhibitor for the KIX domains, suggesting some similarities in conformal selection. Thus, computational dynamics were performed and Arc105 KIX's TAD ligand pool was increased to set the stage for mechanistic studies of these motifs.

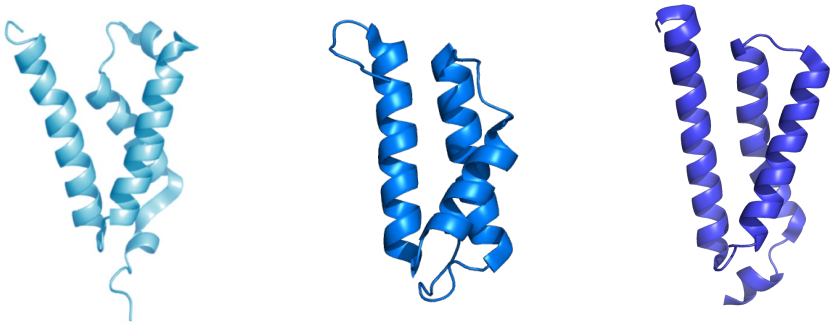
3.2 Introduction

The kinase-inducible domain interaction (KIX) fold was first identified in the master coactivator CBP in 1996 as a binding partner for the transcription factor CREB.[1] It was subsequently found that this approximately 90 residue motif is the binding partner for >15 distinct transcription factors, including MLL, c-Myb, FOXO1, BRCA1, p53, and

cJun. As described in more detail in Chapter 1, CBP KIX uses only two binding sites to form binary and ternary complexes with transcription factor binding partners. The residues Pro-617–Lys-621 (of the α_1/α_2 loop) as well as the α_1, and α_3 helices of the CBP KIX domain form a groove that serves as the TAD interface for MLL, cJun, and other TFs. On the opposite face of the bundle is a hydrophobic groove formed by the α_1 and α_3 helices that binds c-Myb, BRCA1, and CREB, among others. Prior work by us and others has demonstrated that distinct conformational microstates engage each of the transcription factor binding partners.[2–5] In other words, the conformational dynamics of the domain are integral to CBP KIX's role as a hub domain.

Since the discovery of CBP KIX, KIX motifs have been identified in a number of coactivators. This includes the CBP paralog p300, and the p300 KIX motif is nearly identical (90% sequence identity) to that of CBP KIX.[1] Consistent with the structural similarity, p300 KIX shares many of the same transcription factor binding partners. KIX motifs are also found in the coactivators ARC105/MED15, *S. cerevisiae* GAL11/MED15, and *C. glabrata* GAL11/MED15. The Arc105/MED15 subunit KIX motif is found only in metazoans displays a high structural similarity in the α_1 and α_2 helices as compared to CBP KIX. The Med15/GAL11 KIX motifs in the yeast species *Saccharomyces cerevisiae* and *Candida glabrata* display significant sequence similarity with each other, and these constructs have significant structural similarity with human Arc105 KIX.[1] (Figure 3.1) While it is assumed that the ARC105/MED15, *S. cerevisiae* GAL11/MED15, and *C. glabrata* GAL11/MED15 KIX domains play a similar hub function in transcription initiation, there is far less known about the suite of transcription factor

binding partners as compared to CBP and p300.




```
CBP KIX       GWHEHVTQDLRSHLVHKLVQAIFPTPDPAALKDRRMENLVAYAKKVEGDMYESANSRDEYYHLLAEKIYKIQKELEEKRRSRL
Arc105 KIX    DWRS---TAFRQKLVSQIEDAMRKAG----------VAHSKSSKDMESHVFLKAKTRDEYLSLVARLIIHFRDIHNKKSQAS
cgMed15 KIX   QDKDTLSNAERERKNVNGLLQVLMDINTLNGGSSDTADKIRIHAKNFEAA-FAKSSSKKEYMDSMNEKVAVMRNTYNTRKNAVTA
```

Figure 3.1 An illustration of the sequence and structural similarities within the KIX motifs. The PDB files for CBP KIX (2AGH), ARC105 KIX (2GUT), and cgMED15 KIX (4D7X) were utilized to model the structural similarities. The light grey highlighting indicates the helices for each of the KIX motifs. The bold red letters are exact residue matches amongst the KIX motifs and the bolded black letters are aligned residues with similar properties. The PDB files for CBP KIX (2AGH), ARC105 KIX (2GUT), and cgMED15 KIX (4D7X) were utilized to model the structural similarities.

The transcription factor PPIs formed by all of the KIX domains discussed above are of high value for drug discovery as they are dysregulated in disease. ARC105 KIX acts as a key regulator of SREBP-dependent gene regulation, which is commonly dysregulated in obesity, type 2 diabetes and hypertension. *C. glabrata* and *S. cerevisiae* GAL11/MED15 KIX mediates the interactions with Pdr1, a zinc cluster transcription factor (TF) responsible for multidrug resistance in invasive fungal infections. The yeast TF Oaf-1, which shares several attributes with vertebrate protein PPARα that is also linked to obesity and diabetes, is activated by select fatty acids to bind GAL11/MED15 KIX in the regulation of peroxisomal β-oxidation.[7–14] However, there are no good inhibitors for any of the MED15s and limited data regarding binding mechanism.

In Chapter 2 we demonstrated that differential scanning fluorimetry (DSF) is an effective technique for identifying inhibitors of the CBP KIX domain. We hypothesized that, given the structural similarities among the KIX family, including conformational dynamics, an analogous screening strategy would be effective for identifying modulators and inhibitors of cgMED15 KIX and ARC105/MED15 KIX. Here we set forth conditions for a DSF-led approach for the discovery of modulators of the lesser-studied motifs. Screening of the 29 CBP KIX modulators from Chapter 2 identified a diverse set of modulators for each motif and suggests oxyclozanide as a pan-inhibitor/modulator for KIX domains. Furthermore, we confirmed the conformational fluidity of ARC105 KIX and Pdr-1 as alternative ligand for the investigation of that fluidity. Together, these results set stage for the dissection of the KIX motif as a family and the discovery of more potent inhibitors for ARC105 and cgMED15 KIX.

3.3 Results and Discussion

3.3.1 Optimization of assay conditions for cgMED15 and ARC105/MED15 KIX motifs

Under the standard SYPRO Orange dye and the CBP KIX buffering conditions developed in Chapter 2 for DSF, *C. glabrata* Med15 (cgMed15) KIX displays a low melting temperature (T_M = 35.8±0.4°C) with a high intrinsic fluorescence, (Figure C.1A) which is not suitable for screening nor characterization. There were thus two issues to address, the high background fluorescence and the low melting temperature. First, we tested the Med25 AcID buffer (10 mM sodium phosphate, 100 mM sodium chloride, 0.001% NP-40, pH 6.8), which led to no change despite the one-unit pH difference and

different detergent. (Figure C.1B) This result suggests that the high background fluorescence and low T_M observed with SYPRO Orange likely stemmed from dye-induced unfolding of cgMED15 KIX.

Thus, to discover a condition with reduced intrinsic fluorescence and a relatively higher T_M, we examined the alternative solvatochromic dye bis-ANS. Using bis-ANS as the dye, cgMed15 KIX buffer condition screening was performed to further optimize cgMed15 KIX conditions for DSF-based screening and characterization with increased dynamic range. (Figure 3.2A) Previous work performed by rotation student Miguel Nieves Santiago (Figure C.2) determined that low pH buffers (pH 6.5-6.8) optimize the fluorescence output of bis-ANS when monitoring the unfolding of Med25 AcID, and that MES and MOPS buffers with lower concentrations of salt (50 mM sodium chloride) resulted in an increased dynamic range as compared to other buffers. Consequently, these conditions were used alongside the Med25 AcID and CBP KIX (25 sodium phosphate, 125 mM sodium chloride, 0.001% Triton X-100, pH 7.8) conditions in cgMed15 KIX buffer screening, which led to the selection of the MOPS buffer with the pH of 6.8 that was subsequently subjected to detergent screening. This screen resulted in the discovery of the cgMed15 KIX DSF condition, (Figure 3.2B) which yielded a T_M of 38.5$\pm$0.8°C with a lower intrinsic fluorescence signal. The established condition for cgMed15 KIX produced an improved dynamic range, which encouraged further DSF examination of this KIX motif.

In contrast to cgMED15 KIX, DSF of ARC105 KIX using the conditions established for CBP KIX readily led to the production of a sigmoidal curve, indicating that the buffering conditions established for CBP KIX are appropriate for ARC105 KIX (Figure

3.2C). As a final step before carrying out DSF screening on both KIX domains, positive controls for each domain were identified. For cgMED15 KIX, the transcriptional activation domain from the native transcription factor binding partner Pdr1 (residues 1051-1068) was assessed. As shown in Figure D, Pdr-1, having a K_D of 2 μM, produced a statistically significant change in cgMED15 KIX with 4 equivalents of peptide. For ARC105 KIX, residues 18-42 of the native binding partner SREBP-1a were used. Consistent with the K_D of SREBP-1a for ARC105 KIX (3 μM), approximately 4 °C melting temperature change in ARC105 KIX was observed with 4 equivalents of peptide (Figure 3.2D). Significant alteration of protein thermostability upon partner binding solidified the value of DSF-defined protein stability assessment across KIX motifs.

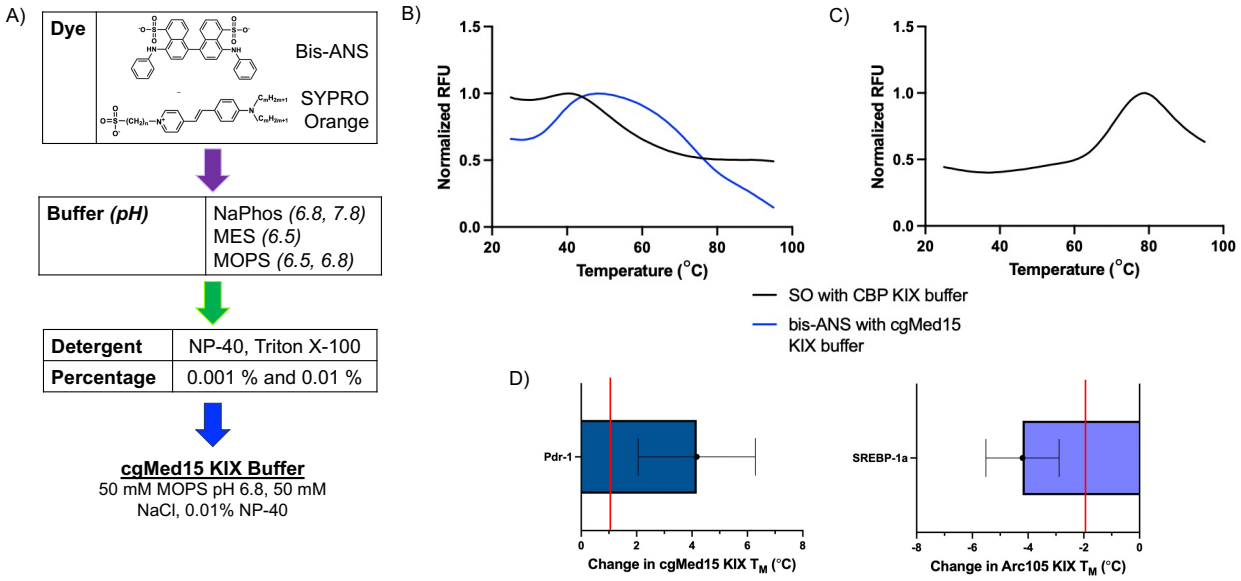


Figure 3.2 Assay optimization steps and the proof-of-concept for DSF application against MED15 KIX motifs. A) A brief summary of the dye and buffer screening performed in DSF to optimize the experimental conditions for cgMED15 KIX DSF screening. B) Adjustment of the dye and buffer conditions resulted in a different melting curve character for cgMED15 KIX as well as a slightly increased melting temperature. C) The previously established conditions for CBP KIX were amenable for the thermostable ARC105 KIX. D) The cognate ligands for cgMED15 and ARC105 KIX caused statistically significant change in their respective partner's melting temperature. The red line represents the threshold for significance for thermal stabilization of ARC105 KIX, which is a three standard deviation change in T_M. All experiments were performed in triplicate and the error bars represent the standard deviation from the mean.

3.3.2 Identification of diverse modulators for cgMed15 KIX and Arc105 KIX and exploration of oxyclozanide's inhibition of alpha helical domains

The 29 CBP KIX modulators discovered by DSF (Chapter 2) provide the perfect starting point for investigating potential probes. Small DSF screens against cgMed15 KIX and Arc105 KIX produced 5 and 12 preliminary hits, respectively, which were identified as causing a 3 standard deviation change in T_M (Figure 3.3A). Of the 5 preliminary cgMed15 KIX hits, 4 of them intersected with the 12 preliminary Arc105 KIX hits. Oxyclozanide, being one of the intersecting hits, contains 3 rotatable bonds that allows the compound to shift conformations and consequently shift the T_M of cgMed15 KIX (ΔT_M = -3°C) and Arc105 KIX (ΔT_M = -4°C). This CBP KIX functional modulator oxyclozanide is thus implicated as a pan-KIX modulator. Subsequent dose-response assays led to the discovery of 2 additional hits with distinct structures and properties for each of the two KIX motifs as well as the confirmation of oxyclozanide as a pan-modulator. (Figure 3.3B and 3.3C) This result suggests that oxyclozanide could be a good starting point for the development of modulators of the KIX domains.

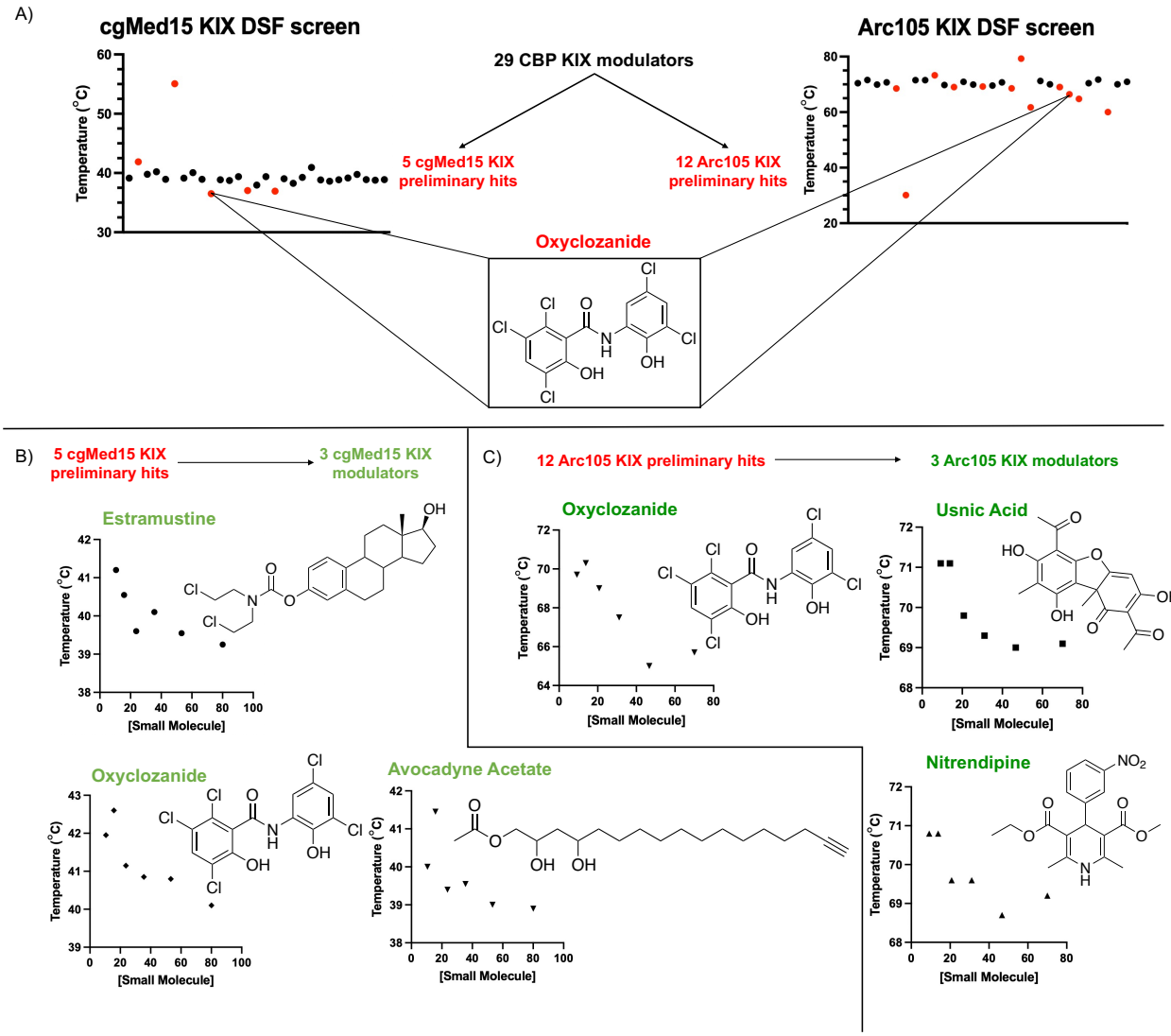


Figure 3.3 Use of the 29 CBP KIX modulators in DSF screening for MED15 KIX motifs. A) Single concentration DSF screening the validated CBP KIX modulators yielded a suite of preliminary hits for both ARC105 and cgMED15 KIX with oxyclozanide as a potential common linkage between the KIX motifs. B) Dose response DSF narrowed down the hit pool for both KIX motifs and validated 3 modulators for each. In addition, oxyclozanide was a confirmed common linkage amongst the KIX motifs. The DSF experiments were performed with mid to low micromolar compound concentrations. All experiments were performed in triplicate.

Due to its status as an inhibitor of CBP KIX PPIs and pan-modulator of KIX motifs, oxyclozanide was tested as a competitive inhibitor for the cgMED15-PDR-1 and ARC105-SREBB-1a complexes. (Figure 3.4A) This revealed modest inhibition of these interactions, which was not improved with the oxyclozanide analogs. (Figure 3.4B) So,

oxyclozanide presents as a pan-inhibitor and modulator for KIX motifs and serves a good starting point for the development of more potent inhibitors for cgMed15 KIX and Arc105 KIX.

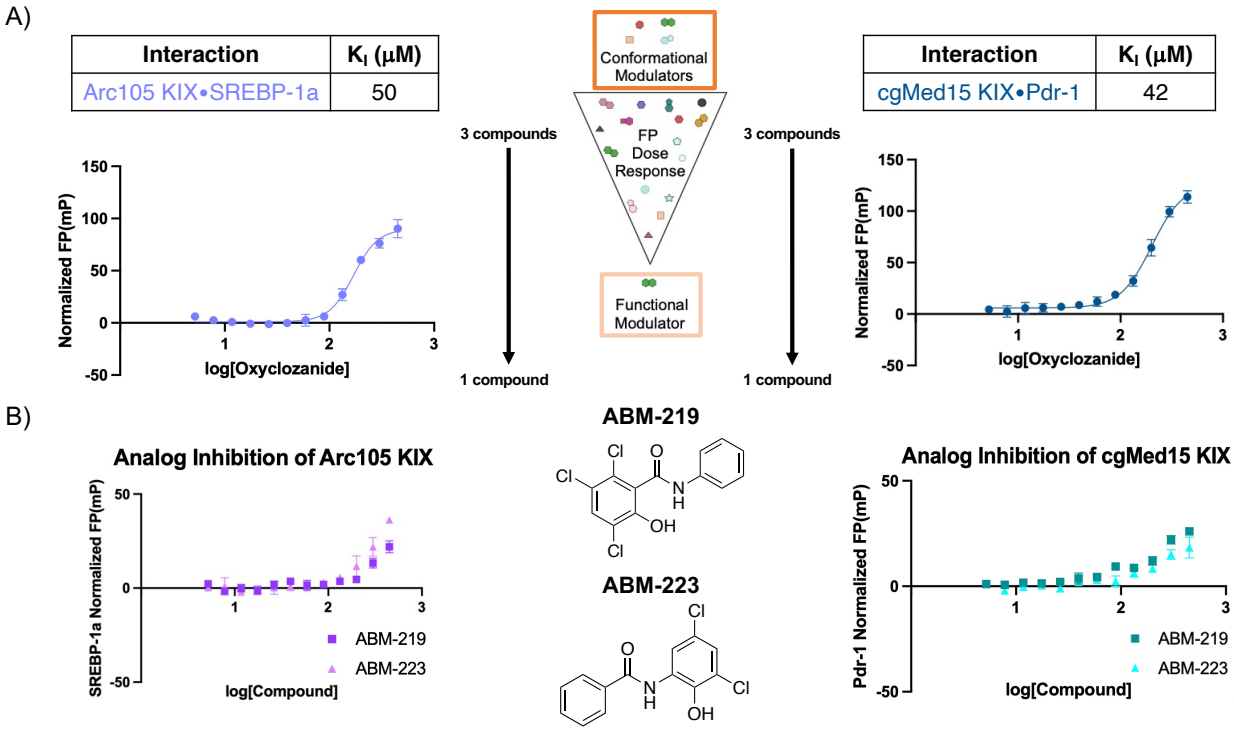


Figure 3.4 Recognition of oxyclozanide a pan-inhibitor for KIX motifs. A) The modulators for both KIX motifs were tested via FP for their inhibitory affinity, which identified oxyclozanide as the sole modulator that also inhibits ARC105 and cgMED15 KIX PPIs. B) With the identification of oxyclozanide as a pan-inhibitor, its analogs were also tested for inhibition, which was fruitless. The FP assays were performed with high to low micromolar compound concentrations. All experiments were performed in triplicate and the error bars represent the standard deviation from the mean.

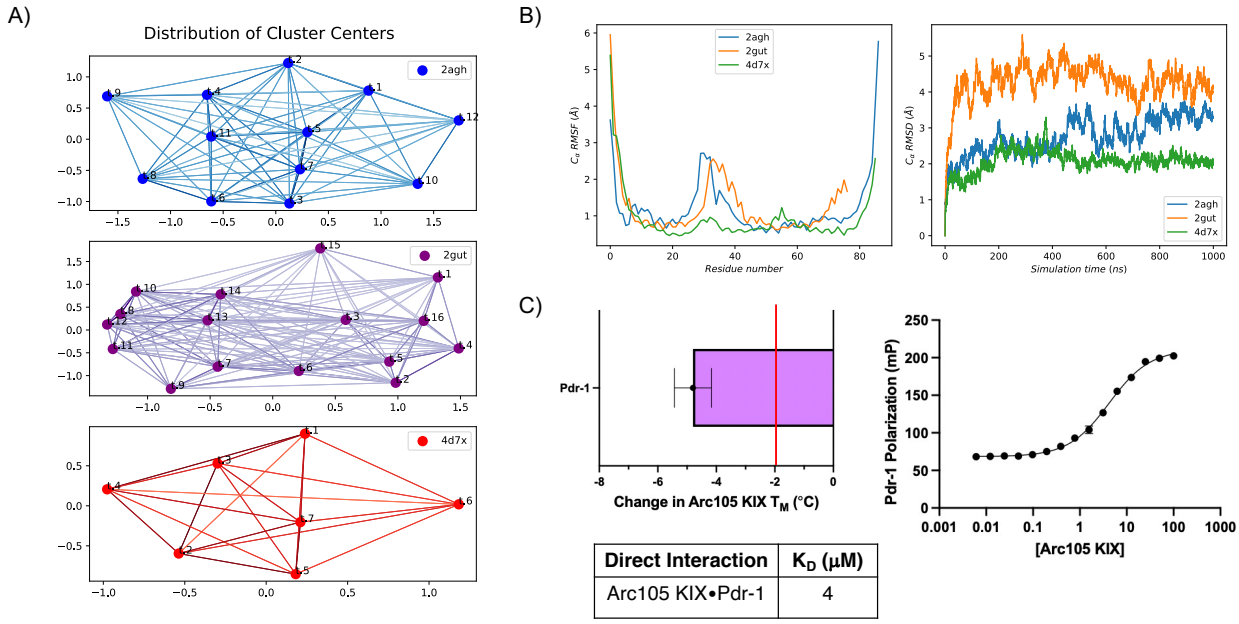
The inherent promiscuity of oxyclozanide as a pan-KIX inhibitor requires an evaluation of compound selectivity. Thus, examination of the compound and its analogs was performed against other key transcription coactivator domains with differing structural characteristics. The IBiD motif, a domain also found in CBP, has a compact helical structure, while the AcID domain within Mediator subunit Med25 has a core β-barrel surrounded by three α-helices; so, these two domains were utilized as models to

determine the degree of oxyclozanide promiscuity. The interaction between the transcription factor ACTR and the coactivator domain IBiD was inhibited by oxyclozanide to a similar degree as the KIX motifs, (Figure C.3B) however, Med25 AcID's PPIs were negligibly affected by the compound. (Figure C.4B) This indicates oxyclozanide's affinity for α-helical bundles and the need for domain-specific compound modifications for each ABD with which oxyclozanide interacts.

3.3.3 Examination of the conformational and ligand landscape of ARC105 KIX

Previous Mapp Lab studies of TAD conformational selection for CBP KIX and Med25 AcID have provided valuable insights into each domain's mechanism of molecular recognition. While cgMed15 KIX has more than one established TAD for these studies, Arc105 KIX only has one partner, which limits the information that can be gained through mechanistic studies. A closer look at the relative conformational dynamics of the KIX motifs is paramount to defining additional ligands for the lesser-studied Arc105 KIX, thus molecular dynamics simulations were performed by Emily Campbell. When looking at the number of spatial clusters as a measure of the "size" of the conformational landscape for each protein sampled computationally, CBP KIX, represented by the PDB 2AGH, and Arc105 KIX (2GUT) are more conformationally flexible as they occupy more conformational clusters than cgMed15 KIX (4D7X). (Figure 3.5A) The former two show larger fluctuations, particularly near the loop regions between the α_1 and α_2 helices. (Figure 3.5B) This analysis supports the inference that Arc105 KIX displays a conformational fluidity that enables binding to versatile sets of ligands.

The TAD binding partners of other KIX motifs serve as the optimal tools for discovering alternative partners for Arc105 KIX binding mechanism. Due to the hydrophobic core similarities of the yeast and human Med15 KIX domain and previous evidence of binding, Pdr1 was first assessed for its ability to significantly modulate Arc105 KIX. (Figure 3.5C) The resulting modulation led to the functional exploration of the TAD constructs of CBP and cgMed15 KIX. Thus, direct binding experiments were performed with MLL, Pdr1, and Oaf1. (Figure3.5C and Figure C.3) Of these ligands, only Pdr-1 displayed significant affinity for Arc105 KIX comparable to the direct interactions of established ABDs and their native TADs. When contrasting the peptide sequences of native ligand SREBP1a and Pdr1, Pdr1 contains aromatic amino acids, which are not present in SREBP1a, and a higher overall percentage of amino acids with hydrophobic side chains. (Figure C.3) Although Pdr1 is not known to be expressed in *homo sapiens*, these results implicate the potential for Arc105 KIX to interact with a homologous sequence/structure in its native network and defines a TAD sequence to be used in examining ARC105 KIX conformational selection.



Direct Interaction	K_D (μM)
Arc105 KIX•Pdr-1	4

Figure 3.5 Expanding the conformational landscape and ligandibility of ARC105 KIX. Molecular dynamics simulations were performed with the ligand subtracted version of CBP KIX (PDB:2AGH), ARC105 KIX (PDB:2GUT), and cgMED15 KIX (PDB:4D7X). This data was utilized to A) determine the approximate amount of conformational clusters for each apo protein selects as well as B) track the apparent structural dynamics of each apo protein. Computational experiments were performed by Emily Campbell. C) DSF and FP were performed with Pdr-1 to determine the peptide's effect on Arc105 KIX thermostability and establish the dissociation constant for the interaction. The FP assay was performed with high to sub micromolar ARC105 KIX concentrations. The red line represents the threshold for significance for thermal stabilization of ARC105 KIX, which is a three standard deviation change. Biochemical experiments were performed in triplicate and the error bars represent the standard deviation from the mean.

3.4 Conclusions

KIX is a highly conserved domain across species; however, the extent of this conservation is variable. Leveraging current knowledge and tools pays huge dividends in the examination of the lesser studied motifs. Implementing a similar workflow as established for CBP KIX, structurally diverse conformational modulators were identified for both Arc105 and cgMed15 KIX. In addition, oxyclozanide was found to act as a functional modulator across compact alpha helical ABDs, indicating the opportunity in and necessity for domain-specific structural modification to transform this compound scaffold and develop more potent and selective inhibitors for the KIX motifs. Finally, to

facilitate the investigation of the lesser studied dynamic domain, the relative conformational dynamics of the KIX motifs were examined and a new binding partner for Arc105 KIX was discovered. Together, this work sets the stage for further investigation of and drug development for the lesser studied KIX motifs.

3.5 Materials and Methods

Protein expression and purification

Proteins were expressed and purified as described in the "Protein expression…" section of Chapter 2 with minor modifications. ARC105 KIX (5-78) was transformed via heat-shock into competent E. coli BL21 (DE3) cells. This construct was prepared from plasmid pET-15B His6-ARC105(1-78) using the Q5® Site-Directed Mutagenesis Kit (New England Biolabs) with the primers listed below. Plasmid sequence identity was confirmed via standard Sanger sequencing methods through Eurofins Genomics. Protein concentration was determined by UV-Vis spectroscopy using an extinction coefficient, ε = 6,990 M^{-1} cm^{-1}.

Primer	Sequence (5'-3')
Arc105 Forward	CTATGgggcaagagaccgactggc
Arc105 Reverse	CCCCgcgcggcaccaggcc

cgMed15 KIX(6-90) was expressed as previously described with minor modifications. Plasmid was transformed via heat-shock into competent E. coli BL21 (DE3) cells. Cell pellets (2) were lysed via sonication in lysis buffer (10 mM sodium

phosphate, 300 mM sodium chloride, 10 mM imidazole, pH 7.2) containing 2-mercaptoethanol and two cOmplete protease inhibitor tablets. For the second round of purification, two cOmplete protease inhibitor tablets were added to the diluted eluent. Protein concentration was determined by UV-Vis spectroscopy using an extinction coefficient, ε = 2,980 M^{-1} cm^{-1}.

Synthesis and isolation of transcriptional activation domain peptides

The peptides FITC-Pdr-1(1051-1068), FITC-SREBP-1a(18-42), FITC-Oaf-1 (1028-1047), Ac-Pdr-1(1051-1068), and Ac-SREBP-1a(18-42) were synthesized as described in the previous chapter. For all peptides except the Pdr-1 peptides, a gradient of 20-60% acetonitrile over 60 min was used for HPLC purification. For the Pdr-1 peptides, a gradient of 20-40% acetonitrile over 40 min was used for HPLC purification.

DSF with compounds and TAD

Experiments were performed as previously described in the “DSF with peptides…” section of Chapter 2 with some modifications. DTT was added to the respective buffer for a final concentration of 1 mM for the TAD conditions only. Arc105 KIX was diluted to 17.5 μM in the CBP KIX standard buffer (25 mM sodium phosphate, 125 mM sodium chloride, 0.001% Triton X-100, pH 7.8). The protein was incubated with each of the compounds and TADs (final concentration 70 uM) at RT for 30 minutes. After incubation, SYPRO orange dye (Invitrogen) was added to a final 7.5X concentration, and an Applied Biosystems StepOnePlus qPCR instrument was utilized to obtain melting curves by exciting at 488 nm and monitoring emission at 602 nm over

a temperature gradient of 25-95°C with a 1°C/min ramp. cgMed15 KIX was diluted to 20 μM in the new cgMed15 DSF buffer (50 mM MOPS, 50 mM sodium chloride, 0.01% NP-40 pH 6.8). The protein was incubated with the each of the compounds and TAD (final concentration 80 μM) at RT for 30 minutes. After incubation, bis-ANS dye (Fisher) was added to a final 10 μM concentration, and an Applied Biosystems StepOnePlus qPCR instrument was utilized to obtain melting curves by exciting at 493 nm and monitoring emission at 517 nm over a temperature gradient of 25-95°C with a 1°C/min ramp.

Dose response was performed in a similar manner as that which was described in "High-throughput DSF…" section of Chapter 2. The initial compounds for each protein were assessed in duplicate at six concentrations (1.5X dilutions starting at 4 equivalents of compound relative to protein).

Molecular Dynamics Simulations

Molecular Dynamics was performed using the NMR structures indicated in the main text. All molecular dynamics simulations were performed using GPUs through the CHARMM compatible OpenMM interface. The fluctuations of the Cα atoms and the number of spatial clusters were used as a measure of the "size" of the conformational landscape each protein sampled. Simulations were performed by Emily Campbell.

FP Direct Binding and Competition

The direct binding experiments mimic those modeled in the section "Fluorescence Polarization (FP) Direct…" of Chapter 2. The significance of TAD peptide affinity was determined by the relative abundance of data points on either side of the

sigmoidal binding transition. The competition experiments mirror the “Dual FP…” section in Chapter 2. Arc105 KIX (final concentration of 12.5 μM) was pre-incubated with FITC-SREBP-1a and FITC-Pdr-1 (final concentration 20 nM) separately for 30 min. cgMed15 KIX was also pre-incubated with FITC-Pdr-1 (final concentration 20 nM) for 30 min.

3.6 References

1. Thakur JK, Yadav A, Yadav G. Molecular recognition by the KIX domain and its role in gene regulation. *Nucleic Acids Res*. 2014;42(4):2112-2125. doi:10.1093/nar/gkt1147

2. Peiffer AL, Garlick JM, Joy ST, Mapp AK, Brooks CL. Allostery in the dynamic coactivator domain KIX occurs through minor conformational micro-states. *PLoS Comput Biol*. 2022;18(4 April). doi:10.1371/journal.pcbi.1009977

3. Law SM, Gagnon JK, Mapp AK, Brooks CL. Prepaying the entropic cost for allosteric regulation in KIX. *Proc Natl Acad Sci U S A*. 2014;111(33):12067-12072. doi:10.1073/pnas.1405831111

4. Wang N, Lodge JM, Fierke CA, Mapp AK. Dissecting allosteric effects of activator-coactivator complexes using a covalent small molecule ligand. *Proc Natl Acad Sci U S A*. 2014;111(33):12061-12066. doi:10.1073/pnas.1406033111

5. Wang N, Majmudar CY, Pomerantz WC, et al. Ordering a dynamic protein Via a small-molecule stabilizer. *J Am Chem Soc*. 2013;135(9):3363-3366. doi:10.1021/ja3122334

6. Breen ME, Mapp AK. Modulating the masters: chemical tools to dissect CBP and p300 function. *Curr Opin Chem Biol*. 2018;45:195-203. doi:10.1016/j.cbpa.2018.06.005

7. Yang F, Vought BW, Satterlee JS, et al. An ARC/Mediator subunit required for SREBP control of cholesterol and lipid homeostasis. *Nature*. 2006;442(7103):700-704. doi:10.1038/nature04942

8. Thakur JK, Arthanari H, Yang F, Chau KH, Wagner G, Näär AM. Mediator subunit Gal11p/MED15 is required for fatty acid-dependent gene activation by yeast transcription Factor Oaf1p. *J Biol Chem*. 2009;284(7):4422-4428. doi:10.1074/jbc.M808263200

9. Borah S, Shivarathri R, Srivastava VK, Ferrari S, Sanglard D, Kaur R. Pivotal role for a tail subunit of the RNA II mediator complex CgMED2 in azole tolerance and

adherence in Candida glabrata. *Antimicrob Agents Chemother*. 2014;58(10):5976-5986. doi:10.1128/AAC.02786-14

10. Waseem M, Das S, Mondal D, Jain M, Thakur JK, Subbarao N. Identification of novel inhibitors against Med15a KIX domain of Candida glabrata. *Int J Biol Macromol*. 2023;253. doi:10.1016/j.ijbiomac.2023.126720

11. Nishikawa JL, Boeszoermenyi A, Vale-Silva LA, et al. Inhibiting fungal multidrug resistance by disrupting an activator-Mediator interaction. *Nature*. 2016;530(7591):485-489. doi:10.1038/nature16963

12. Hidalgo P, Ansari AZ, Schmidt P, et al. Recruitment of the transcriptional machinery through GAL11P: Structure and interactions of the GAL4 dimerization domain. *Genes Dev*. 2001;15(8):1007-1020. doi:10.1101/gad.873901

13. Zhao X, Xiaoli, Zong H, et al. Inhibition of SREBP transcriptional activity by a boron-containing compound improves lipid homeostasis in diet-induced obesity. *Diabetes*. 2014;63(7):2464-2473. doi:10.2337/db13-0835

14. Näär AM, Beaurang PA, Robinson KM, et al. Chromatin, TAFs, and a novel multiprotein coactivator are required for synergistic activation by Sp1 and SREBP-1a in vitro. *Genes Dev*. 1998;(12):3020-3031.

Chapter 4 Uncovering Colorimetric Dye Sensors that Engage Conformationally Dynamic ABDs and Detect Their Binding Events

4.1 Abstract

Colorimetric dyes provide a cheap and accessible alternative to current methods that look at conformational change, and the colorimetric array is leveraged to narrow down the sensors of interest. RGB analysis and the single point analysis of absorbance change reduce the spectral variables to discover three candidate dye sensors that show concentration-dependent changes in the presence of the model ABDs. Follow-up assessment via spectral and principal component analysis confirmed each of the candidate's ability to differentiate CBP KIX and Med25 AcID as well as revealed the broad colorimetric capabilities of erythrosin B. As a colorimetric sensor that can engage both model ABDs, erythrosin B's sensitivity to significant ABD ligand engagement was assessed using known mixed mechanism inhibitors for Med25 AcID and CBP KIX, garcinolic acid and norstictic acid, respectively. Erythrosin B data exhibited clustering patterns consistent with the thermostability data for each ligand for erythrosin B, suggesting the sensor's ability to conformational stabilization. Thus, with further studies, colorimetric dyes such as erythrosin B may serve as an even more affordable and accessible means to screen against conformationally fluid proteins.

4.2 Introduction

Protein function has historically been viewed as dependent on a well-defined three-dimensional structure.[1] As a result, most of the drug discovery approaches have

been best suited to highly ordered proteins. However, more than 50% of the eukaryotic proteome contains intrinsically disordered regions (IDRs) or is intrinsically disordered.[2] It is now well established that IDRs actively participate in many cellular signaling processes like transcriptional regulation,[3,4] and their prevalence in pathology motivates the search for ligands to modulate them.[5,6] For this reason, there is a strong need for new methods to discover and characterize ligands for dynamic proteins.

The most commonly used characterization and screening strategies for dynamic proteins utilize NMR-active nuclei or fluorescent dyes/tags to examine significant changes in dynamics.[7–14] An advantage of protein NMR spectroscopy for detection of ligand binding is that it can provide more detailed information about binding-induced conformational changes and binding site location through changes in chemical shifts of NMR-active nuclei (for example: ^{1}H, ^{14}C, ^{15}N). While powerful, these experiments typically require high field NMR spectrometers, expensive reagents for production of labeled proteins, and considerable specialized expertise for experimental design and analysis.[15] In differential scanning fluorimetry (DSF), a fluorescent dye that interacts preferentially with unfolded regions of a protein is monitored as a protein or protein-ligand complex is subjected to increased temperature. In this way, a change in stability induced by ligand binding can be readily detected. An advantage of DSF is that it is suitable for high throughput screening (HTS) as it can be done with low volumes in microplate formats; in addition, a structural model of the protein of interest is not a pre-requisite for DSF, simplifying assay development. Nonetheless, DSF does require specialized equipment and, often, costly dye reagents.[16–18] For all these reasons, these two strategies may be inaccessible to for application in less resourced environments.

Missing from the dynamic protein screening canon is an assay that utilizes inexpensive reagents and can be accomplished with readily available laboratory equipment. In applications ranging from explosives detection to distinguishing small-molecule analytes, colorimetric dyes have proven to be highly effective components in low-cost, rapid, sensitive assays.[19–21] A wealth of information can be gained from reading the absorbance spectra of colorimetric dyes such that they are very commonly used in forensics and the food/drink industry.[19] In forensics, they are often used to detect chemical-biological-explosive (CBE) threats, and in the food/drink industry, these dyes are employed in quality control checks. For example, TNT was identified in an 8-component colorimetric sensor array using a device that identifies changes in color and fluorescent signal. However, colorimetric dyes are seldomly studied in biochemical screening, despite many having biomedical applications.

Colorimetry-based biochemical screening has significant potential as a number of colorimetric dyes share similar core structures and even overlap with the fluorescent dyes and tags widely used for fluorescence polarization (FP) and DSF.[22] (Figure 1.1) Colorimetric array screening is a valuable technique that could be carried out to identify valuable dyes. Generally, a variety of dyes are screened for their ability to bind some site(s) on the analyte to yield a change in absorbance. Previous studies with the colorimetric array for protein identification used sensors that were known to cause conformational changes in the proteins of interests. Thus, colorimetric screening could provide a more accessible alternative to the more commonly used fluorescence-based techniques and be a broadly useful system to investigate conformationally dynamic proteins and their interactions.

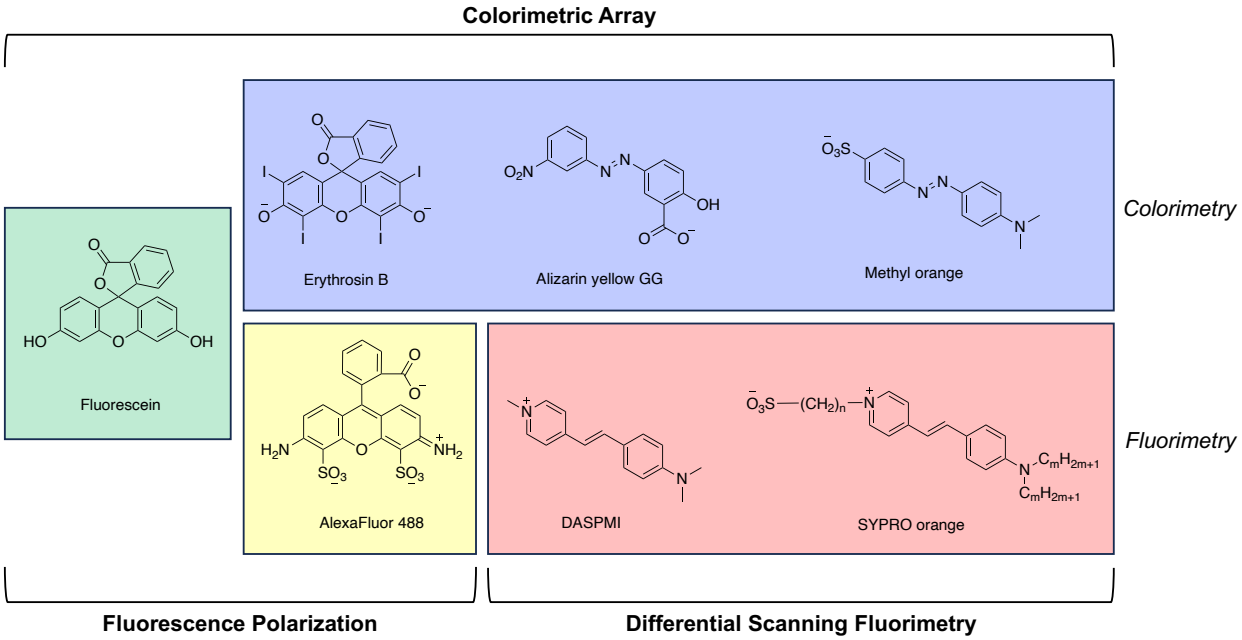


Figure 4.1 Examples of dyes and tags found in colorimetry and fluorimetry

To identify colorimetric dyes that could be used for screening and characterization of dynamic proteins, we used the activator-binding domains (ABDs) Med25 AcID and CBP KIX as the test cases. As described in Chapters 1 and 2, AcID and KIX each use distinct conformations to engage a range of transcriptional activators to form binary and ternary complexes.[23–26] Both domains are high value drug targets and there is a need for screening strategies to characterize known ligands as well as discover novel synthetic modulators. Here we use an array of colorimetric dyes to identify sensors as tools for screening dynamic ABDs Med25 AcID and CBP KIX. Further investigation of colorimetric response led to the identification of versatile sensor erythrosin B as an effective sensor for ABD binding and the accompanying conformational changes.

4.3 Results and Discussion

An essential feature of a robust biochemical screening tool is its capacity to illuminate distinct responses across varying conditions. For example, SYPRO Orange used in DSF produces different fluorescence signatures for Med25 AcID and CBP KIX; additionally, the dynamic range of that fluorescence signature is dictated by the protein concentration. For a colorimetric dye to be a useful screening and/or characterization tool, target differentiation and concentration-dependent spectral changes would be similarly desirable characteristics. Much like the typical drug discovery flowthrough, the colorimetric sensor discovery workflow utilizes a top-down approach is taken in the discovery of directed and broad colorimetric screening tools for Med25 AcID and CBP KIX by examining target differentiation and concentration-response on multiple scales and in different contexts.

4.3.1 Identifying colorimetric tools for two conformationally dynamic coactivator domains Med25 AcID and CBP KIX

The array format is ideal for examining a diverse set of colorimetric sensors for the ABDs Med25 AcID and CBP KIX. In many contexts, colorimetric arrays utilize specific sensors that interact with a class of molecules to characterize and quantify an analyte; however, changes in color pattern and absorbance can perform similar functions to simplify the identification of potential screening tools for the structurally dissimilar ABDs. Red, green, and blue (RGB) color analysis reduces sensor spectra to one of the three variables to evaluate target-dependent color changes.[27,28] Examining single wavelength absorbance changes with varying analyte concentrations at a hones

in on one variable in the sensor spectrum to determine the presence of a concentration-response relationship. Together, RGB and single wavelength analysis can effectively analyze the suite of colorimetric dyes and distinguish preliminary candidates that meaningfully interact with the ABDs.

RGB analysis enables the discovery of some sensors that differentiate Med25 AcID and CBP KIX. In work carried out by Dr. Christopher Azaldegui, an array of colorimetric dyes was treated with increasing concentrations of either CBP KIX or Med25 AcID. Visible spectra (350-700 nm) were collected, converted to RGB representatives, and normalized to a negative control for each individual dye. (Figure 4.2A) Although most dyes did not exhibit selectively significant spectral changes in the presence of CBP KIX, dye #8, Bromothymol Blue, experiences a concentration-dependent colorimetric response. On the other hand, dye #9, Fast Green FCF, is the only dye in the set to display similar changes with Med25 AcID. This indicates each dye's level of specificity for its respective domain, suggesting that bromothymol blue and fast green FCF hold potential as directed screening probes.

To identify dyes that exhibit quantitative concentration-dependence, the array of 23 colorimetric dyes were once again screened in the presence of varied concentrations of Med25 AcID in triplicate (performed by Dr. Christopher Azaldegui). The absorbance spectra were collected and the values for each wavelength were averaged, after which the difference between each to the control was determined and used in linear regression analysis. (Figure 4.2B) Dye #17, Erythrosin B, was identified to experience a max absorbance change at 550 nm that was two standard deviations above the mean for the maximum changes of all 23 dyes. With a concentration-dependent change in

absorbance that is statistically significant, this presents erythrosin B as another candidate for colorimetry-based screening practices.

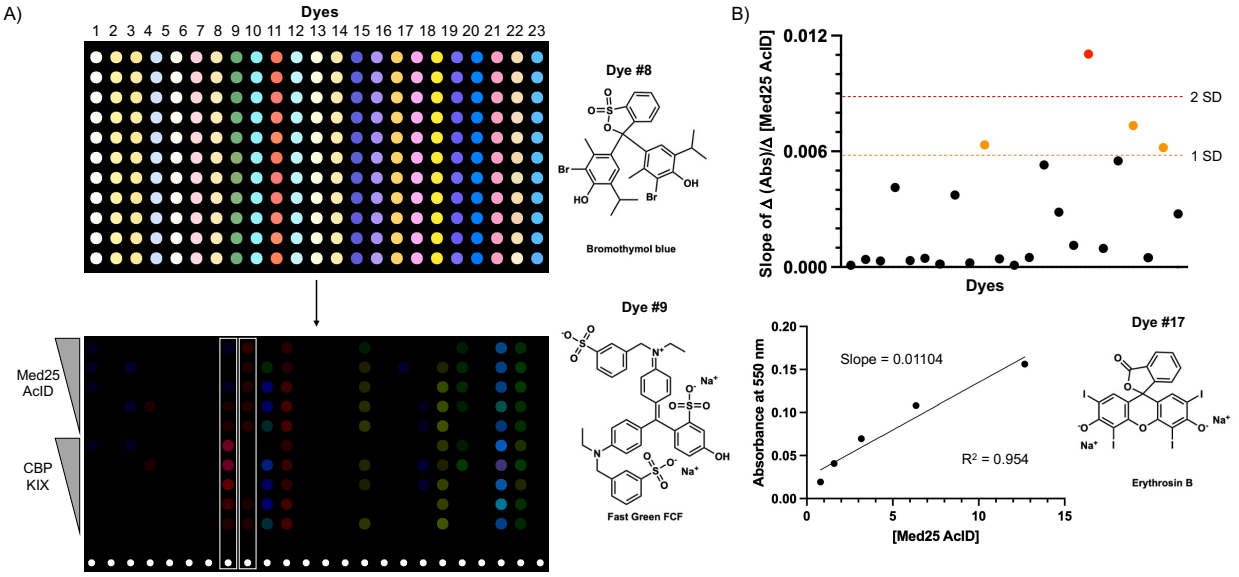


Figure 4.2 Three dye candidates were identified from the colorimetric array as potential tools. A) The RGB analysis performed with the 23 colorimetric dyes to discover two dyes that preferentially interact with each ABD. B) Single point analysis of absorbance changes across Med25 AcID concentrations defined one dye as having more than a two standard deviation (SD) change. All experiments and analyses were performed by Dr. Christopher Azaldegui.

Secondary analysis of the dye confirms and expands upon the results of primary analysis modes. The entire dye absorbance spectra contains significant information that can be gained by expanding the analysis variables. Bromothymol blue exhibits absorbance shifts in the entire curve when either protein is introduced. (Figure 4.3A) Fast green FCF, on the other hand, only exhibits shifts on the perimeter of the absorbance peak. (Figure 4.3B) With erythrosin B, more anomalous behavior is seen, as the presence of CBP KIX causes shift in the λ_{max} and the presence of Med25 AcID results in changes throughout the spectrum. (Figure 4.3C) Taken together, this data shows that all three dyes' unique engagement with Med25 AcID and CBP KIX can be seen throughout the absorption spectra.

Principal component analysis (PCA) translates the many variables of spectral data to a quantitative output for a more robust secondary analysis of dye candidates. [19,29–31] Assessment of the same spectra that illustrated the distinct engagement of each dye with Med25 AcID and CBP KIX using PCA recapitulated the spectral shifts for each dye through distinct clustering patterns. For bromothymol blue, the absorbance spectra separation with a small dynamic range is apparent due to the data clusters of dye only samples being readily distinguished from that of the protein-containing samples, which display some overlap. (Figure D.2A) A similar phenomenon is seen with fast green FCF. Although this dye's spectrum has a much larger dynamic range, the significant absorbance peak overlaps lead to overlaps in the dye clusters that can primarily be discerned by the more extensive variance seen with CBP KIX over Med25 AcID. (Figure D.2B) For erythrosin B, there are no overlaps amongst any of the data clusters, which is in alignment with the visible absorbance spectra shifts; however the clustering patterns for dye only and CBP KIX-containing samples mirror one another, most likely the result of significant spectral baseline overlaps. (Figure D.2C) Therefore, principal component analysis of the dye spectra demonstrates all three candidates' ability to distinguish the dynamic domains and highlights erythrosin B as having significant potential in screening.

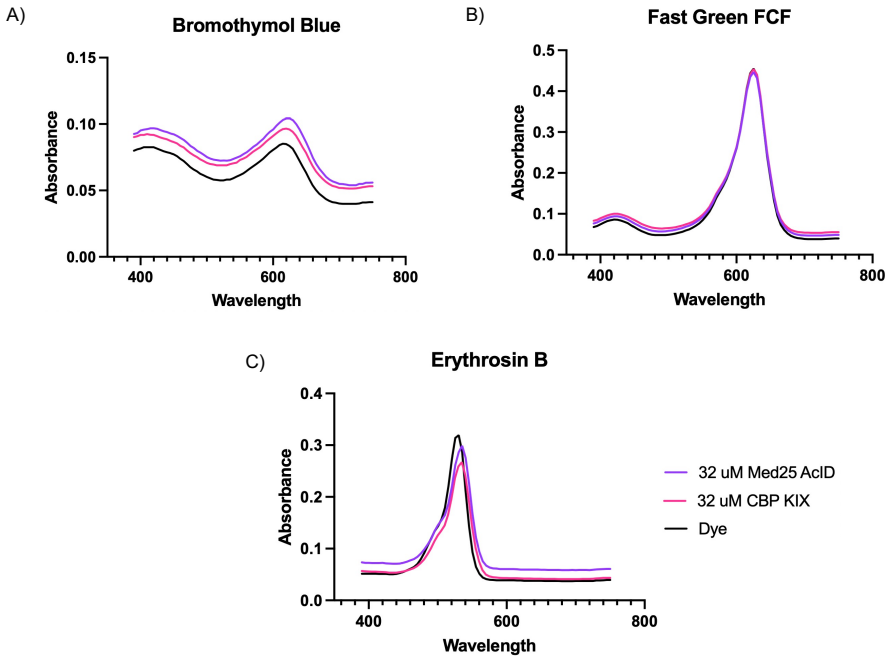


Figure 4.3 Absorbance spectra for the three candidates in the presence and absence of each ABD. The spectra for A) bromothymol blue, B) fast green FCF, and C) erythrosin B was measured from 350 to 750 nm and plotted in GraphPad Prism. These spectra are representatives of triplicate spectra.

Concentration-dependent spectral shifts serve as a great metric for probe sensitivity. In each protein's respective standard buffer, a varied concentration of protein was combined with 10 μM dye and screened in quadruplicate. For fast green FCF, increasing concentrations of Med25 AcID invokes an increase in variance and a shift in the clustering pattern. (Figure 4.4A) On the other hand, erythrosin B with Med25 AcID does not capture the majority (>90%) of the variability in the data and exhibits no clear clustering pattern. (Figure 4.4C) Bromothymol blue experiences inconsistent clustering associated with CBP KIX concentrations. (Figure 4.4B) However, erythrosin B has a diminishing clustering trend associated with its distinct and separable clusters with CBP KIX. (Figure 4.4D) Thus, the PCA results are indicative of fast green FCF as the better

probe for Med25 AcID and erythrosin B as the optimal tool for CBP KIX under their current conditions.

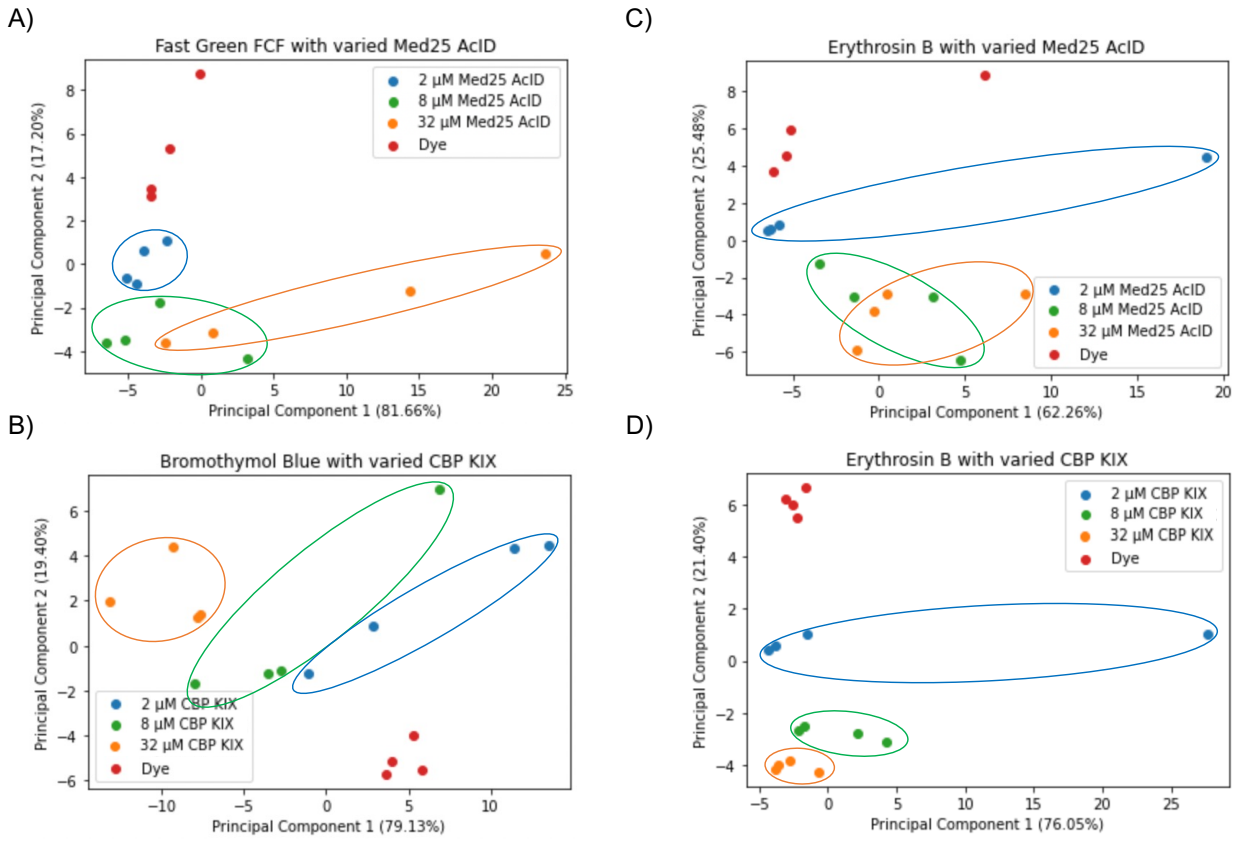


Figure 4.4 PCA plots of the dye sensors in the presence of varied concentrations of ABD. The clustering patterns for A) fast green FCF are comparatively more distinct than those for C) erythrosin B, indicating the former dye's sensitivity to Med25 AcID. For CBP KIX, D) erythrosin B displays a greater sensitivity than B) bromothymol blue.

Secondary assessments that scrutinize the many variables of the absorbance data confirmed the value of these three dyes and revealed new insights about one particular dye. Examination of spectral shifts and analysis by PCA revealed all the dyes' abilities to distinguish the two dynamic transcriptional domains. Concentration-dependence was investigated next, which determined fast green FCF and erythrosin B

were best sensors for Med25 AcID and CBP KIX, respectively. Additionally, these data indicate that erythrosin B is suitable to investigate both ABDs.

4.3.2 Examination of significant ABD conformational stabilization with the colorimetric dye Erythrosin B

Next, we assessed the application of erythrosin B to detect binding of small molecule inhibitors of CBP KIX and of Med25 AcID. We recently reported the discovery of the natural products norstictic acid as the first inhibitor of the Med25 and ETV/PEA3 PPI network and garcinolic acid as the most potent inhibitor of CBP KIX PPIs.[32,33] (Figure 4.5A) Each of these modulators inhibit their respective domain by a mixed allosteric and orthosteric mechanism by binding flexible loop regions. Thus, they serve as excellent tests for the sensitivity of erythrosin B to significant binding events.

The stabilization invoked by these natural products are reflected by the erythrosin B dye response. Dose-response DSF assessment was performed with norstictic and garcinolic acid with their respective targets, and the results showed that both ligands significantly modulate the thermostability of their ABD with as little as one equivalent of inhibitor. (Figure 4.5B and 4.5C) These conditions were then translated to the colorimetric platform, and the absorbance spectra were analyzed by PCA. Each equivalent of ligand created very distinct and separable clusters with the associated ABD, (Figure 4.5D and 4.5E) suggesting that the ligand engagement and substantial stabilization of each ABD is reflected by the colorimetric dye erythrosin B.

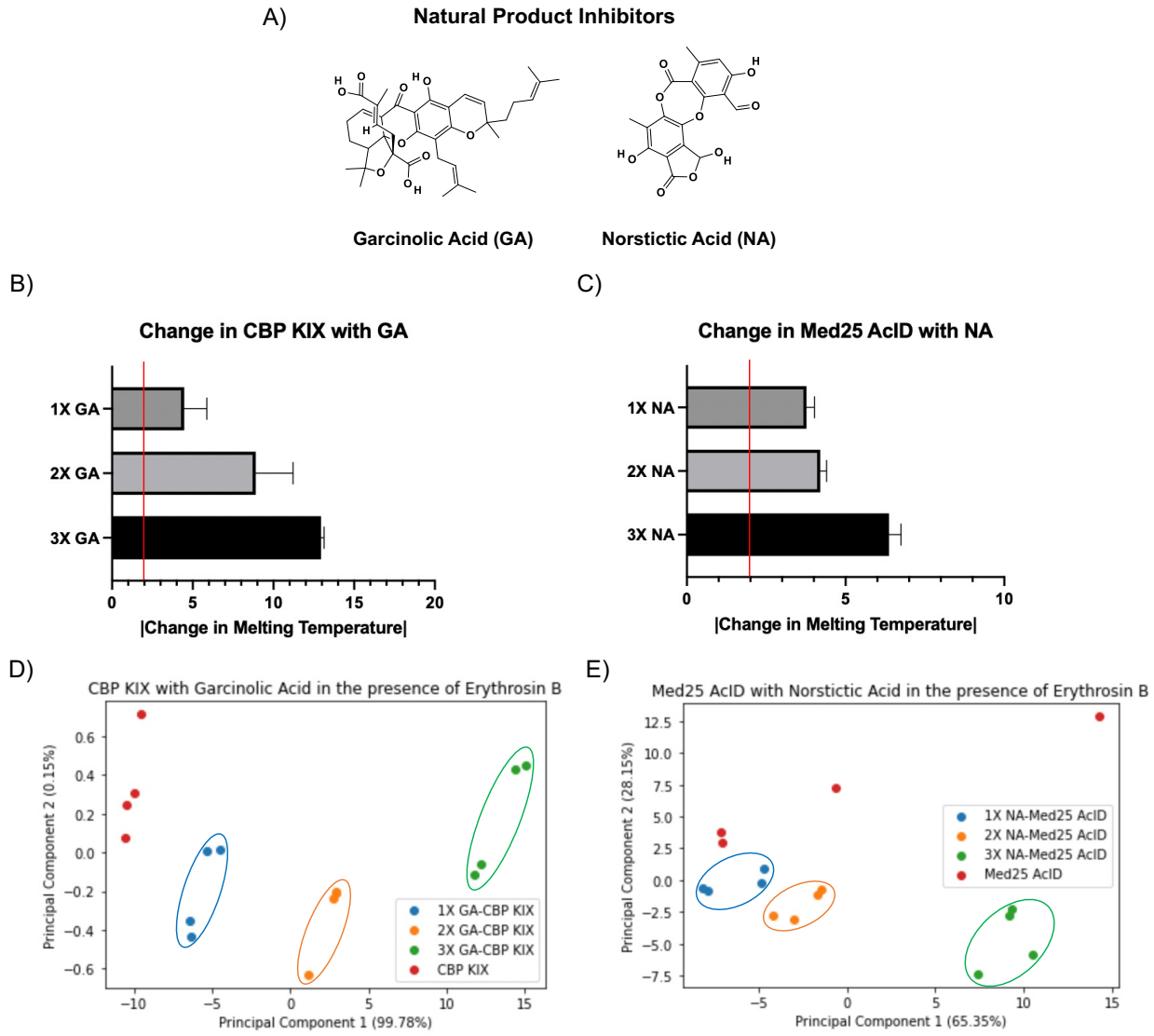


Figure 4.5 A comparative assessment of significant ABD binding events. A) Garcinolic acid and norstictic acid are established micromolar inhibitors for CBP KIX and Med25 AcID, respectively. As measured by differential scanning fluorimetry, B) GA significantly stabilizes CBP KIX and C) NA significantly stabilized Med25 AcID. The red line indicates the threshold of significance. The clustering patterns for the erythrosin B absorbance data with D) CBP KIX:NA and E) Med25 AcID:GA mimic that stabilization data. All experiments were performed in triplicate and the error bars represent the standard deviation from the mean.

4.4 Conclusions

Using data derived from absorbance spectra, colorimetric dyes were set forth as tools for the ABDs Med25 AcID and CBP KIX. Of the 23 colorimetry dyes in the array,

three candidates were selected by RGB and single point wavelength analysis. The screening tool potential of the candidates bromothymol blue, fast green FCF, and erythrosin B was further evaluated via more expansive analysis. One particular dye, erythrosin B, displayed versatility amongst the and the ability to detect considerable ligand-induced stabilization in these domains. Overall, colorimetric dyes hold significant potential for studying dynamic proteins, and the screening and analysis processes for examining these tools is suitable even in the context of teaching novices of biochemistry.

4.5 Materials and Methods

Protein expression and purification

Proteins were expressed and purified as described in Chapter 2.

Dye sensor array screening

Working stocks of dyes were made by first dissolving in DMSO and then further diluting the concentration in a standard PBS solution with pH of 7.4. The initial dye screening array was set up by first adding Med25 AcID and/or CBP KIX into a clear 384-well plate. Subsequently, dye solutions were mixed with the protein to concentrations indicated in Appendix Figure D.4. The 384-well plate was kept in the dark at room temperature for 20-30 min before collecting absorbance spectra. Absorbance spectra from 390-700 nm at 5 nm intervals were collected using a BioTek plate reader. Experiments were performed by Dr. Christopher Azaldegui.

Dye sensor array data analysis

The RGB analysis was completed utilizing Python in which the spectral data from each well is converted into an RGB value. The no-protein control wells are arranged in the array format that matches the protein-containing wells and set as the initial RGB values. Corresponding differences are found (RGB_Final – RGB_Initial) to create a difference map with colors generated from the difference values. For the analysis of change in wavelength absorbance, the triplicate protein-dye absorbance data at each recorded wavelength was averaged and the absorbance for the corresponding control was subtracted. For each wavelength, a simple linear regression was carried out with the background-subtracted absorbance values of the various concentrations of protein. The change in wavelength absorbance was then defined as the maximum linear slope. Analysis was performed by Dr. Christopher Azaldegui.

Dye sensor absorbance assays

Proteins were diluted to 32 μM and then incubated with 10 μM dye for all subsequent assays in the standard Med25 buffer (10 mM sodium phosphate buffer pH 6.8, 100 mM NaCl, 0.001 % NP-40, 10% glycerol,1 mM DTT) or the standard CBP KIX buffer (25 mM sodium phosphate buffer pH 7.8, 125 mM NaCl, 0.001 % Triton X-100, 1 mM DTT) in a clear low-volume 384 well plate (Greiner Bio-One 784101). Samples were incubated at room temperature for 30 minutes, then the plate was spun for 1 minute, and the absorbance was read from 390-750 nm every 5 nm using a BioTek plate reader.

Dye sensor absorbance assays with natural product inhibitors

Absorbance values for norstictic and garcinolic acid binding were determined using a similar assay format as above. These assays were performed in the assay buffer containing a dye concentration of 10 μM for each dye and a protein concentration of 32 μM Med25 AcID or CBP KIX. The inhibitors were assayed at concentrations of 100, 50, and 25 μM. Samples containing protein and each dye were incubated with the inhibitors at RT for 1 hour in the clear, low-volume 384-well plate, and the plate was spun for 1 minute and read as previously indicated.

Dye sensor absorbance assay data analysis

PCA was performed using Python. The absorbance values for each wavelength were considered as a different input variable and the principal components were generated using a correlation matrix. All absorbance spectra were plotted using Graphpad Prism 10.

DSF screen with natural product inhibitors

Experiments were conducted in triplicate utilizing 20 μL sample volumes in PCR strip tubes sealed with clear cap strips. 8 μM Med25 AcID or 15 μM CBP KIX was incubated with norstictic acid or garcinolic acid at the indicated concentrations at RT for 30 minutes. After incubation, 5X SYPRO orange dye (1:100 dilution of purchased 5000X stock; Invitrogen) was added and an Applied Biosystems StepOnePlus qPCR instrument was utilized to obtain melting curves by exciting at 488 nm and monitoring emission at 602 nm over a temperature gradient of 25-95°C with a 1°C/min ramp. Raw

fluorescence data (RFU) was imported into the online data analysis program, DSFworld, and T_m was calculated using a sigmoidal fitting model that accounts for a single transition with a high initial, decaying fluorescence. For data visualization, RFU is plotted as a function of temperature using GraphPad Prism software. The maximum of the first derivative is the reported T_m, with T_m of each ligand calculated as the difference between the T_m of the protein and the T_m of the protein + ligand, considering the difference of standard deviations.

4.6 References

1. Hanson J, Litfin T, Paliwal K, Zhou Y. Identifying molecular recognition features in intrinsically disordered regions of proteins by transfer learning. *Bioinformatics*. 2020;36(4):1107-1112. doi:10.1093/bioinformatics/btz691

2. Metallo SJ. Intrinsically disordered proteins are potential drug targets. *Curr Opin Chem Biol*. 2010;14(4):481-488. doi:10.1016/j.cbpa.2010.06.169

3. Chen J, Liu X, Chen J. Targeting intrinsically disordered proteins through dynamic interactions. *Biomolecules*. 2020;10(5). doi:10.3390/biom10050743

4. Bhagwat AS, Vakoc CR. Targeting Transcription Factors in Cancer. *Trends Cancer*. 2015;1(1):53-65. doi:10.1016/j.trecan.2015.07.001

5. Uversky VN, Oldfield CJ, Dunker AK. Intrinsically disordered proteins in human diseases: Introducing the D 2 concept. *Annu Rev Biophys*. 2008;37:215-246. doi:10.1146/annurev.biophys.37.032807.125924

6. Heller GT, Aprile FA, Michaels TCT, et al. *Small-Molecule Sequestration of Amyloid- as a Drug Discovery Strategy for Alzheimer's Disease*. Vol 6.; 2020. https://www.science.org

7. Egner JM, Jensen DR, Olp MD, et al. Development and Validation of 2D Difference Intensity Analysis for Chemical Library Screening by Protein-Detected NMR Spectroscopy. *ChemBioChem*. 2018;19(5):448-458. doi:10.1002/cbic.201700386

8. Felli IC, Pierattelli R. 13C Direct Detected NMR for Challenging Systems. *Chem Rev*. 2022;122(10):9468-9496. doi:10.1021/acs.chemrev.1c00871

9. Gee CT, Arntson KE, Koleski EJ, Staebell RL, Pomerantz WCK. Dual Labeling of the CBP/p300 KIX Domain for 19F NMR Leads to Identification of a New Small-Molecule Binding Site. *ChemBioChem*. 2018;19(9):963-969. doi:10.1002/cbic.201700686

10. Gee CT, Koleski EJ, Pomerantz WCK. Fragment screening and druggability assessment for the CBP/p300 KIX domain through protein-observed 19F NMR spectroscopy. *Angew Chem - Int Ed*. 2015;54(12):3735-3739. doi:10.1002/anie.201411658

11. Alexandrov AI, Mileni M, Chien EYT, Hanson MA, Stevens RC. Microscale Fluorescent Thermal Stability Assay for Membrane Proteins. *Structure*. 2008;16(3):351-359. doi:10.1016/j.str.2008.02.004

12. Harroun SG, Lauzon D, Ebert MCCJC, Desrosiers A, Wang X, Vallée-Bélisle A. Monitoring protein conformational changes using fluorescent nanoantennas. *Nat Methods*. 2022;19(1):71-80. doi:10.1038/s41592-021-01355-5

13. Du Y, Nikolovska-Coleska Z, Qui M, et al. A Dual-Readout F^2 Assay That Combines Fluorescence Resonance Energy Transfer and Fluorescence Polarization for Monitoring Bimolecular Interactions. *ASSAY Drug Dev Technol*. 2011;9(4):382-393. doi:10.1089/adt.2010.0292

14. Haidekker MA, Theodorakis EA. Molecular rotors - Fluorescent biosensors for viscosity and flow. *Org Biomol Chem*. 2007;5(11):1669-1678. doi:10.1039/b618415d

15. Voehler M, Ashoka MA, Meiler J, Bock PE. Carbon and amide detect backbone assignment methods of a novel repeat protein from the staphylocoagulase in S. aureus. *Biomol NMR Assign*. 2017;11(2):243-249. doi:10.1007/s12104-017-9757-4

16. Hofmann L, Gulati S, Sears A, Stewart PL, Palczewski K. An effective thiol-reactive probe for differential scanning fluorimetry with a standard real-time polymerase chain reaction device. *Anal Biochem*. 2016;499:63-65. doi:10.1016/j.ab.2016.01.016

17. Bergsdorf C, Fiez-Vandal C, Sykes DA, et al. An Alternative Thiol-Reactive Dye to Analyze Ligand Interactions with the Chemokine Receptor CXCR2 Using a New Thermal Shift Assay Format. *J Biomol Screen*. 2016;21(3):243-251. doi:10.1177/1087057115619597

18. Wu T, Hornsby M, Zhu L, Yu JC, Shokat KM, Gestwicki JE. Protocol for performing and optimizing differential scanning fluorimetry experiments. *STAR Protoc*. 2023;4(4). doi:10.1016/j.xpro.2023.102688

19. Kangas MJ, Burks RM, Atwater J, Lukowicz RM, Williams P, Holmes AE. Colorimetric Sensor Arrays for the Detection and Identification of Chemical Weapons and Explosives. *Crit Rev Anal Chem*. 2017;47(2):138-153. doi:10.1080/10408347.2016.1233805

20. Owyeung RE, Panzer MJ, Sonkusale SR. Colorimetric Gas Sensing Washable Threads for Smart Textiles. *Sci Rep*. 2019;9(1). doi:10.1038/s41598-019-42054-8

21. Janzen MC, Ponder JB, Bailey DP, Ingison CK, Suslick KS. Colorimetric sensor arrays for volatile organic compounds. *Anal Chem*. 2006;78(11):3591-3600. doi:10.1021/ac052111s

22. Das AK, Druzhinin SI, Ihmels H, Müller M, Schönherr H. Colorimetric and Fluorimetric DNA Detection with a Hydroxystyryl–Quinolizinium Photoacid and Its Application for Cell Imaging. *Chem - Eur J*. 2019;25(55):12703-12707. doi:10.1002/chem.201903017

23. Vojnic E, Mourão A, Seizl M, et al. Structure and VP16 binding of the Mediator Med25 activator interaction domain. *Nat Struct Mol Biol*. 2011;18(4):404-410. doi:10.1038/nsmb.1997

24. Pattelli ON, Valdivia EM, Beyersdorf MS, et al. A Lipopeptidomimetic of Transcriptional Activation Domains Selectively Disrupts the Coactivator Med25 Protein–Protein Interactions. *Angew Chem - Int Ed*. 2024;63(21). doi:10.1002/anie.202400781

25. Brüschweiler S, Konrat R, Tollinger M. Allosteric communication in the KIX domain proceeds through dynamic repacking of the hydrophobic core. *ACS Chem Biol*. 2013;8(7):1600-1610. doi:10.1021/cb4002188

26. Peiffer AL, Garlick JM, Joy ST, Mapp AK, Brooks CL. Allostery in the dynamic coactivator domain KIX occurs through minor conformational micro-states. *PLoS Comput Biol*. 2022;18(4 April). doi:10.1371/journal.pcbi.1009977

27. Fay CD, Wu L. Critical importance of RGB color space specificity for colorimetric bio/chemical sensing: A comprehensive study. *Talanta*. 2024;266:124957. doi:10.1016/j.talanta.2023.124957

28. Jin Z, Yim W, Retout M, et al. Colorimetric sensing for translational applications: from colorants to mechanisms. *Chem Soc Rev*. 2024;53(15):7681-7741. doi:10.1039/d4cs00328d

29. Kitao A. Principal Component Analysis and Related Methods for Investigating the Dynamics of Biological Macromolecules. *J*. 2022;5(2):298-317. doi:10.3390/j5020021

30. Maisuradze GG, Liwo A, Scheraga HA. Principal Component Analysis for Protein Folding Dynamics. *J Mol Biol*. 2009;385(1):312-329. doi:10.1016/j.jmb.2008.10.018

31. Hou C, Dong J, Zhang G, et al. Colorimetric artificial tongue for protein identification. *Biosens Bioelectron*. 2011;26(10):3981-3986. doi:10.1016/j.bios.2010.11.025

32. Garlick JM, Sturlis SM, Bruno PA, et al. Norstictic Acid Is a Selective Allosteric Transcriptional Regulator. *J Am Chem Soc*. 2021;143(25):9297-9302. doi:10.1021/jacs.1c03258

33. Breen ME, Joy ST, Baruti OJ, et al. Garcinolic acid distinguishes between GACKIX domains and modulates interaction networks. *ChemBioChem*. Published online August 2023. doi:10.1002/cbic.202300439

Chapter 5 Conclusions and Future Directions

5.1 Conclusions

Dynamic protein domains are widely considered to be “undruggable” due to the difficulty associated with defining methods to effectively target them. Those that participate in protein-protein interaction (PPI) networks such as transcriptional protein domains often fall under this misnomer. The underpinning of dynamic domains is their conformational malleability, so a requirement in effectively targeting them is affecting that behavior. This work demonstrates that dye-based drug discovery methods can delineate those probes that modulate dynamic coactivator domains by targeting dynamics.

As seen in Chapter 2, a concerted screening approach that places loop dynamics at the forefront is shown to elucidate modulators that aid in the development of therapeutics and the dissection of conformational dynamics. When thoughtfully applied to dynamic ABDs, DSF proved to be a valuable screening method to define a diverse sect of modulators for CBP KIX. Those modulators that displayed significant chemical shifts upon binding via HSQC NMR were identified as directly interacting with regions adjacent to the α_1/α_2 IDR of CBP KIX. Further investigation of the modulators discovered oxyclozanide, an orthosteric and allosteric inhibitor of CBP KIX . This small molecule scaffold has significant potential for structure-guided modification to generate a drug molecule.

Chapter 3 demonstrates that the sequential and structural conservation of the KIX motifs aid the definition of novel ligands and investigation of dynamics. Application of an analogous strategy as seen in Chapter to the *homo sapien* and *candida glabrata* MED15 KIX motifs led to the discovery of structurally diverse modulators with one being shared amongst all, oxyclozanide. (Figure 5.1) PPI inhibition for both MED15 KIX domains established oxyclozanide as a great starting scaffold for targeting the conserved KIX domain. Further investigating that conservation elucidated the dynamic nature and ligandability of Arc105 KIX, implicating the value of additional library screenings and mechanistic studies for the MED15 KIX domains.

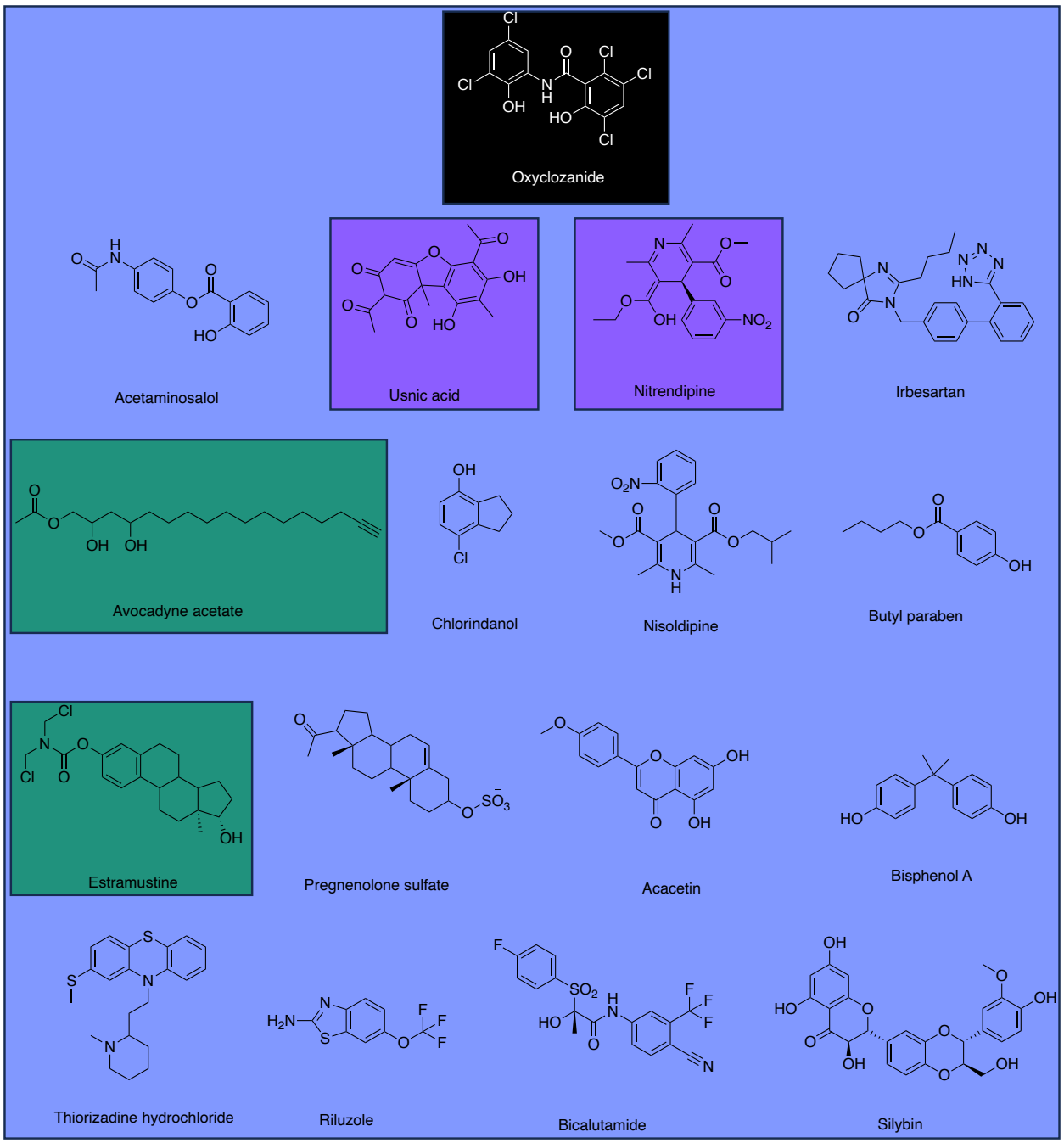


Figure 5.1 The KIX motif modulators identified in this work

Colorimetric dyes are established as valuable tools for investigating dynamic domains in Chapter 4. The colorimetric array is leveraged for the preliminary discovery of three colorimetric sensor candidates. Further assessment of these candidates led to

the classification of bromothymol blue and fast green FCF as protein-specific probes and facilitated the discovery of erythrosin B's ABD versatility. The mirroring of ABD thermostability shifts invoked by mixed mechanism inhibitors exemplify the promise of this dye for future screening efforts.

5.2 Future Directions

5.2.1 Structure-guide development of a more potent mixed mechanism inhibitor

Salicylanilides are a multipurpose class of compounds that have various therapeutics applications;[1] therefore, establishing enhanced potency and selectivity should be a priority. The surface view of the docking developed in Chapter 2 provides valuable insight into the preferred substitution positions for CBP KIX. (Figure 5.2) For example, the chlorine on the C5 position of the amine aromatic ring and the chlorine on the C3 position on the carbonyl aromatic ring may be substituted with extended or larger substituents to facilitate more extensive contacts with CBP KIX. Thus, the development of a library of oxyclozanide analogs would be invaluable. The salicylanilide derivative discovered in this work has significant potential for development into a more potent and selective mixed mechanism inhibitor for CBP KIX.

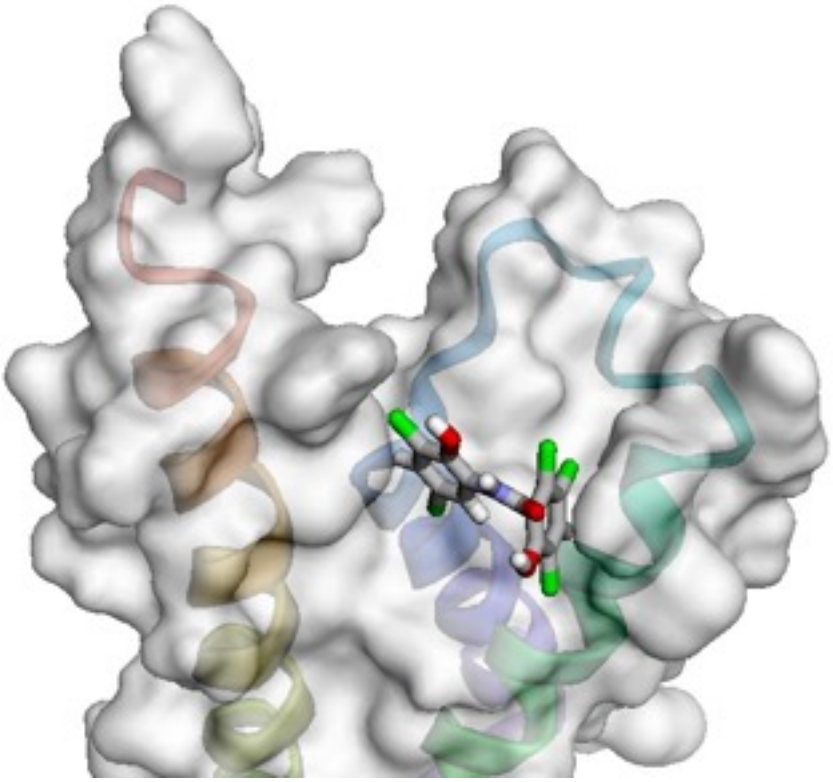


Figure 5.2 The surface view of oxyclozanide docked with CBP KIX

5.2.2 All-around probing of the MED15 KIX motifs

The evidence presented in Chapter 3 of this work provide the basis for screening against and probing Arc105 and cgMed15 KIX. The established screening platform for these domains can be utilized to screen any additional oxyclozanide analogs and larger, diverse compound libraries. Additionally, steady-state kinetics experiments can be utilized to compare the TAD conformational selections of cgMed15 and ARC105 KIX.

5.2.3 Mechanistic insights into the colorimetric dyes

Initial screening by two different modes identified three colorimetric dyes with a multitude of properties that can contribute to their biomolecular interactions. Bromothymol blue is a pH indicator with pK_a of ~7.30. Although the mechanism of action

by which this dye interacts with biomolecules is less studied, due to the structure, this dye exhibits significant hydrophobicity that is implicated as the major contributor to its interactions.[2–4] Fast green FCF historically has been used as a food additive and a protein stain. This dye is reported as a tight yet promiscuous protein binder, interacting with proteins through a myriad of mechanisms such as hydrophobic interactions, salt bridges, and π-π stacking.[5–7] Erythrosin B is traditionally used in the food industry and for histological staining. However, recent reports suggest erythrosin B is an inhibitor for biologically relevant targets, such as the flavivirus NS2B-NS3 protease, where it acts as an orthosteric inhibitor by forming hydrogen bonds, π-π stacking, and π-cation interactions.[8–11] The mechanism by which these dyes interact with Med25 AcID and CBP KIX remains unknown, however, as seen with SYPRO Orange and bis-ANS, screening applicability is not contingent upon insight into the mechanics. On the other hand, further assessment of the dyes' mechanics can be valuable in their establishment as widely-used tools.

Although dye mechanism is not an absolute necessity for usage, some background can be helpful for assay development. As seen in Chapter 2 and previous literature, protein properties and buffer conditions play significant roles in effective assay development. Med25 AcID has a significant number of exposed positively charged and aromatic amino acid residues to participate in salt bridges and π-π stacking. With fast green FCF, it can be implicated that the introduction of Med25 AcID results in a more uniform dye association to protein with a high potential for multiple associations to a single Med25 AcID, and the increased protein concentrations may lead to less dye uniformity and more single associations to Med25 AcID at variable sites. Hydrophobic

dyes like bromothymol blue are known to experience self-association and as defined in Chapter 2, CBP KIX has looser hydrophobic packing that enables dye engagement at ambient temperature. With bromothymol blue, the dye behavior is indicative of inconsistent dye coordination with self at low CBP KIX concentrations, and it shows that the data points gain more uniformity as free dye is diminished at a high CBP KIX concentration. Additionally, similar to Med25 AcID, CBP KIX has multiple positively charged and aromatic amino acid residues on the surface that can take part in π-π stacking and π-cation interactions. The concentration-dependent clustering of CBP KIX with erythrosin B points to a greater environmental variability at low concentration of CBP KIX like that which is seen with bromothymol blue, while the re-clustering with increased CBP KIX concentrations suggests the ordering of dye molecules and the finite association with CBP KIX. For Med25 AcID with erythrosin B, much like glycerol can interfere with SYPRO Orange signal in DSF, this osmolyte in the standard Med25 buffer likely interacts with the erythrosin B via hydrogen bonding, causing higher variability in the dye signal and interference in Med25 AcID interactions. Results of the PCA as well as prior knowledge of dye properties allows one to make inferences about the protein-dye interactions, which can be further substantiated in the development of colorimetric dyes as broad or directed screening tools.

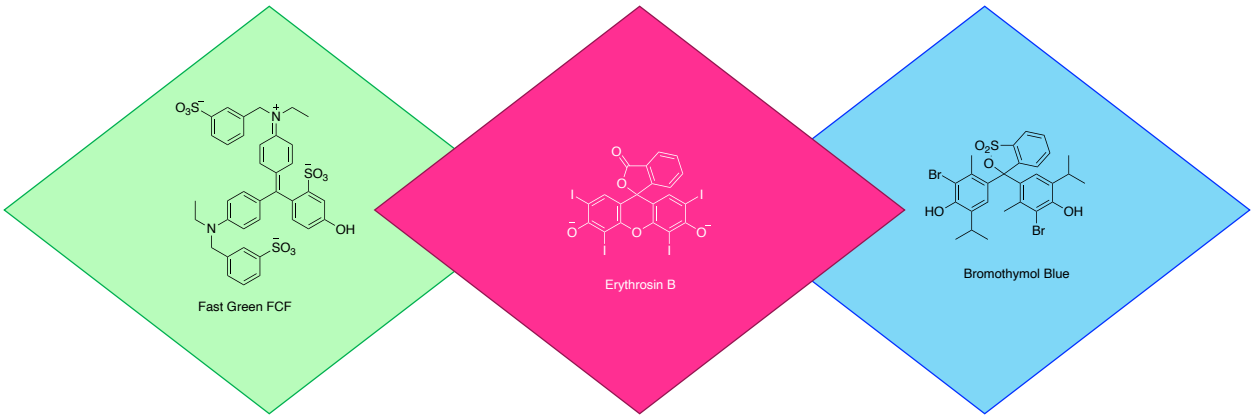


Figure 5.3 The colorimetric dyes identified for model domains Med25 AcID and CBP KIX

5.3 References

1. Lal J, Ramalingam K, Meena R, et al. Design and synthesis of novel halogen rich salicylanilides as potential antileishmanial agents. *Eur J Med Chem*. 2023;246. doi:10.1016/j.ejmech.2022.114996

2. Puschett J, Rao B, Karandikar B, Matyjaszewski K. Indicator characteristics of bromothymol blue derivatives. *Talanta*. 1991;38(3):335-338. doi:10.1016/0039-9140(91)80058-8

3. Khan SA, Ilies MA. Development and Optimization of a Bromothymol Blue-Based PLA2 Assay Involving POPC-Based Self-Assemblies. *Int J Mol Sci*. 2024;25(17):9517. doi:10.3390/ijms25179517

4. Shimada T, Hasegawa T. Determination of equilibrium structures of bromothymol blue revealed by using quantum chemistry with an aid of multivariate analysis of electronic absorption spectra. *Spectrochim Acta A Mol Biomol Spectrosc*. 2017;185:104-110. doi:10.1016/j.saa.2017.05.040

5. Abbas RF, Hassan MJM, Rheima AM. Magnetic solid-phase extraction of Fast Green dye based on magnetic nanoparticles (GO/Co3O4/Fe3O4) prepared by photo-irradiation method. *Green Anal Chem*. 2023;7:100086. doi:10.1016/j.greeac.2023.100086

6. Niimi T, Miyazaki N, Oiki H, et al. Versatile application of fast green FCF as a visible cholangiogram in adult mice to medium-sized mammals. *Sci Rep*. 2025;15(1):1960. doi:10.1038/s41598-024-84355-7

7. Yang J, Liu R, Lu F, et al. Fast Green FCF Attenuates Lipopolysaccharide-Induced Depressive-Like Behavior and Downregulates TLR4/Myd88/NF-κB Signal Pathway

in the Mouse Hippocampus. *Front Pharmacol*. 2019;10:501. doi:10.3389/fphar.2019.00501

8. Elfadil D, Della Pelle F, Compagnone D, Amine A. Green Synthesis of Molecularly Imprinted Polymers for Dispersive Magnetic Solid-Phase Extraction of Erythrosine B Associated with Smartphone Detection in Food Samples. *Materials*. 2022;15(21):7653. doi:10.3390/ma15217653

9. Franke JD, Braverman AL, Cunningham AM, Eberhard EE, Perry GA. Erythrosin B: A Versatile Colorimetric and Fluorescent Vital Dye for Bacteria. *BioTechniques*. 2020;68(1):7-13. doi:10.2144/btn-2019-0066

10. Li Z, Sakamuru S, Huang R, et al. Erythrosin B is a potent and broad-spectrum orthosteric inhibitor of the flavivirus NS2B-NS3 protease. *Antiviral Res*. 2018;150:217-225. doi:10.1016/j.antiviral.2017.12.018

11. Pravinata LC, You Y, Ludescher RD. Erythrosin B Phosphorescence Monitors Molecular Mobility and Dynamic Site Heterogeneity in Amorphous Sucrose. *Biophys J*. 2005;88(5):3551-3561. doi:10.1529/biophysj.104.054825

Appendices

Appendix A: Sequences and Characterization of Synthesized Peptides

Table A.1 Sequences of activator peptides used in this study.

Peptide	Sequence (N → C)
MLL (2840-2858)	FITC-βAla-DSGNILPSDIMDFVLKNTP
MLL (2840-2858)	βAla-DSGNILPSDIMDFVLKNTP
C2841S MLL (2840-2858)	TR-βAla-DSGNILPSDIMDFVLKNTP
Myb (291-316)	FITC-βAla-KEKRIKELELLLMSTENELKGQQVLP
	βAla-KEKRIKELELLLMSTENELKGQQVLP
V314A P316W Myb (284-316)	FITC-βAla-YNDEDPEKEKRIKELELLLMSTENELKGQQALW
Pdr1(1051-1068)	FITC-βAla-GDLEDLYSILWSDVYPDS
	Ac- βAla-GDLEDLYSILWSDVYPDS
SREBP1a (18-42)	FITC-βAla-APCDLDAALLTDIEDMLNLINNQDSD
	Ac-βAla-APCDLDAALLTDIEDMLNLINNQDSD
Oaf1 (1028-1047)	FITC-βAla-GYFGGLDLFDYDFLFGNDFA

Table A.2 Summary of masses of activator peptides used in this study.

Peptide	Exact Mass	Observed Mass
FITC-MLL	2553.09	2552.81
βAla-MLL	2162.04	2163.03 (M+1)
TR-MLL	2735.18	2734.22 (M-1)
FITC-Myb	3527.80	3526.81 (M-1)
βAla-Myb	3126.75	3126.75
FITC-Myb32	4451.10	4450.11 (M-1)
FITC-Pdr-1	2547.05	2548.06 (M+1)
Ac-Pdr-1	2198.01	2200.02 (M+2)
FITC-SREBP-1a	3279.36	3278.36 (M-1)
Ac-SREBP-1a	2930.32	2930.34
FITC-Oaf-1	2754.09	2752.09 (M-2)

High Resolution Mass Spectrometry Data for Activator Peptides

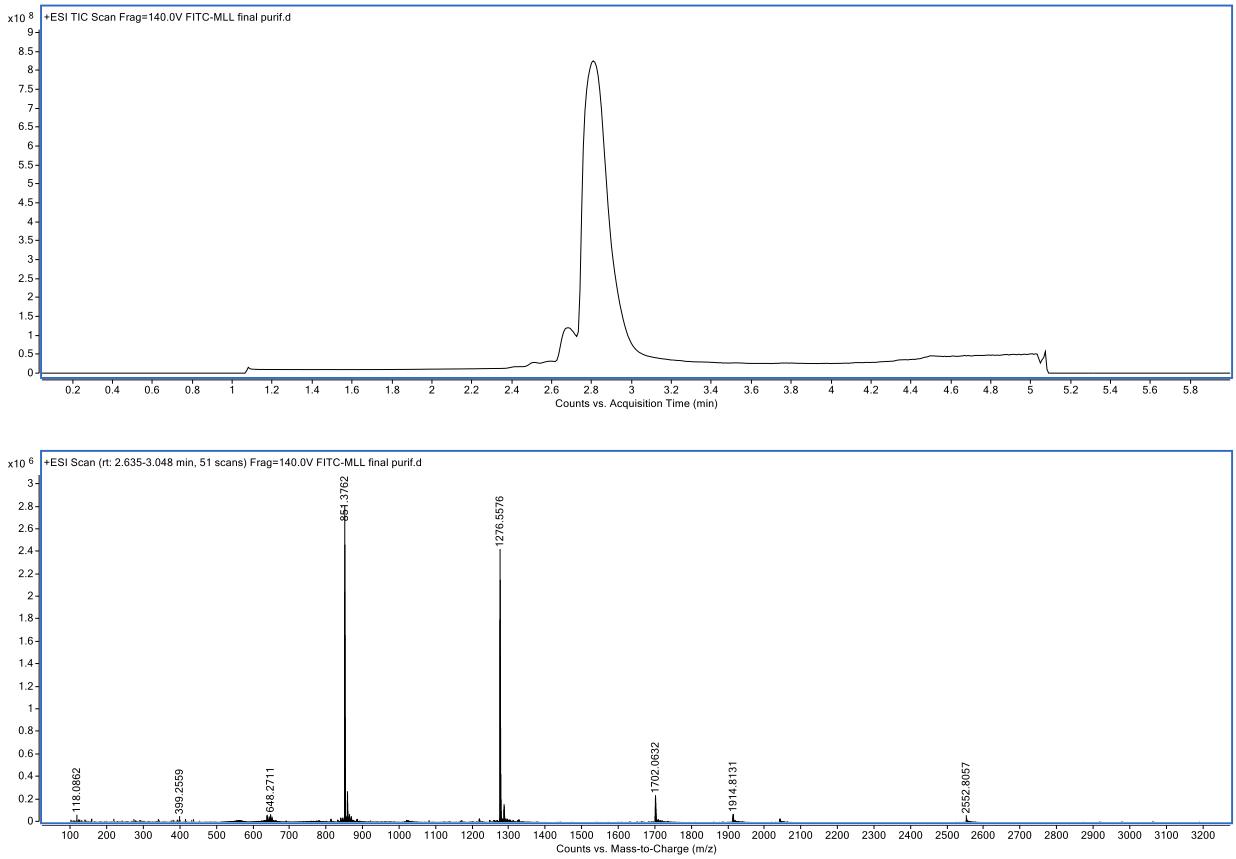


Figure A.1 Chromatogram and MS Spectrum for FITC-MLL

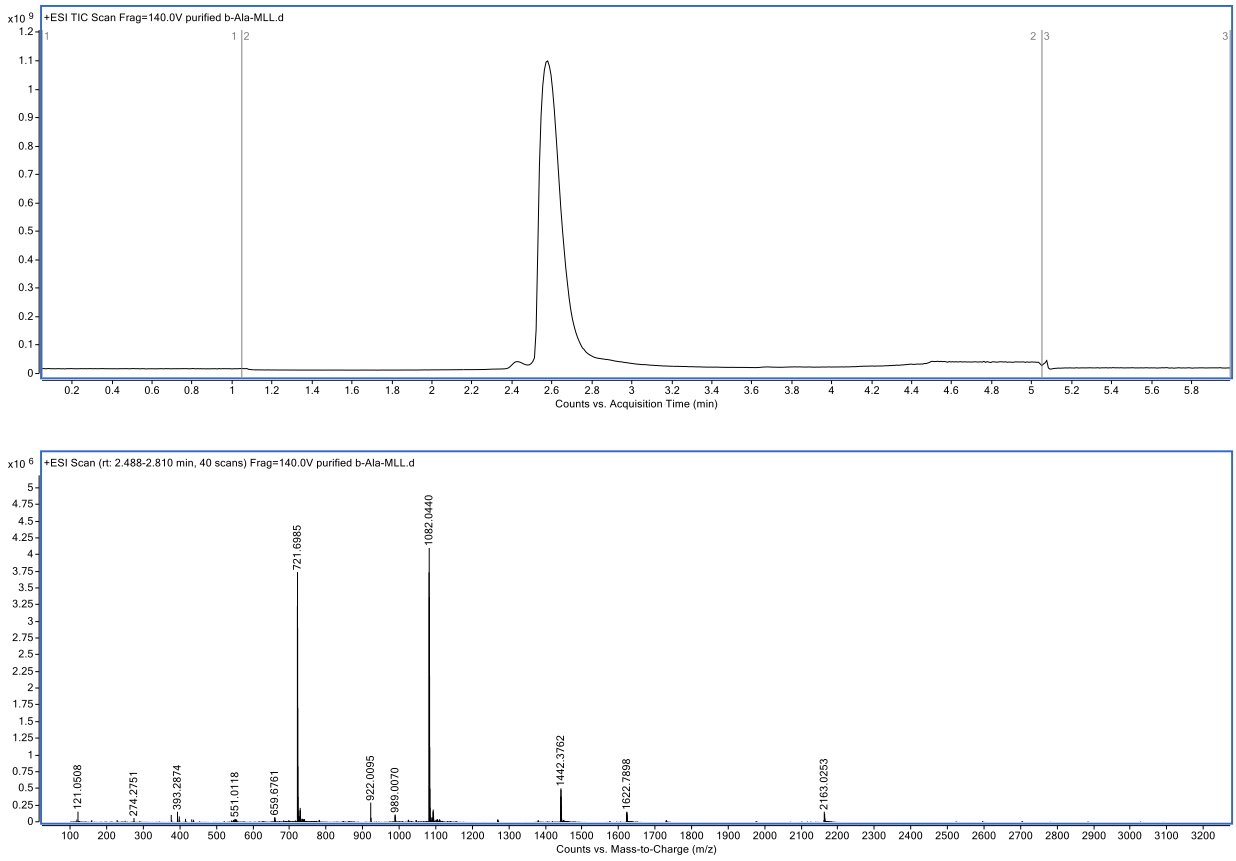


Figure A.2 Chromatogram and MS Spectrum for Unlabeled MLL

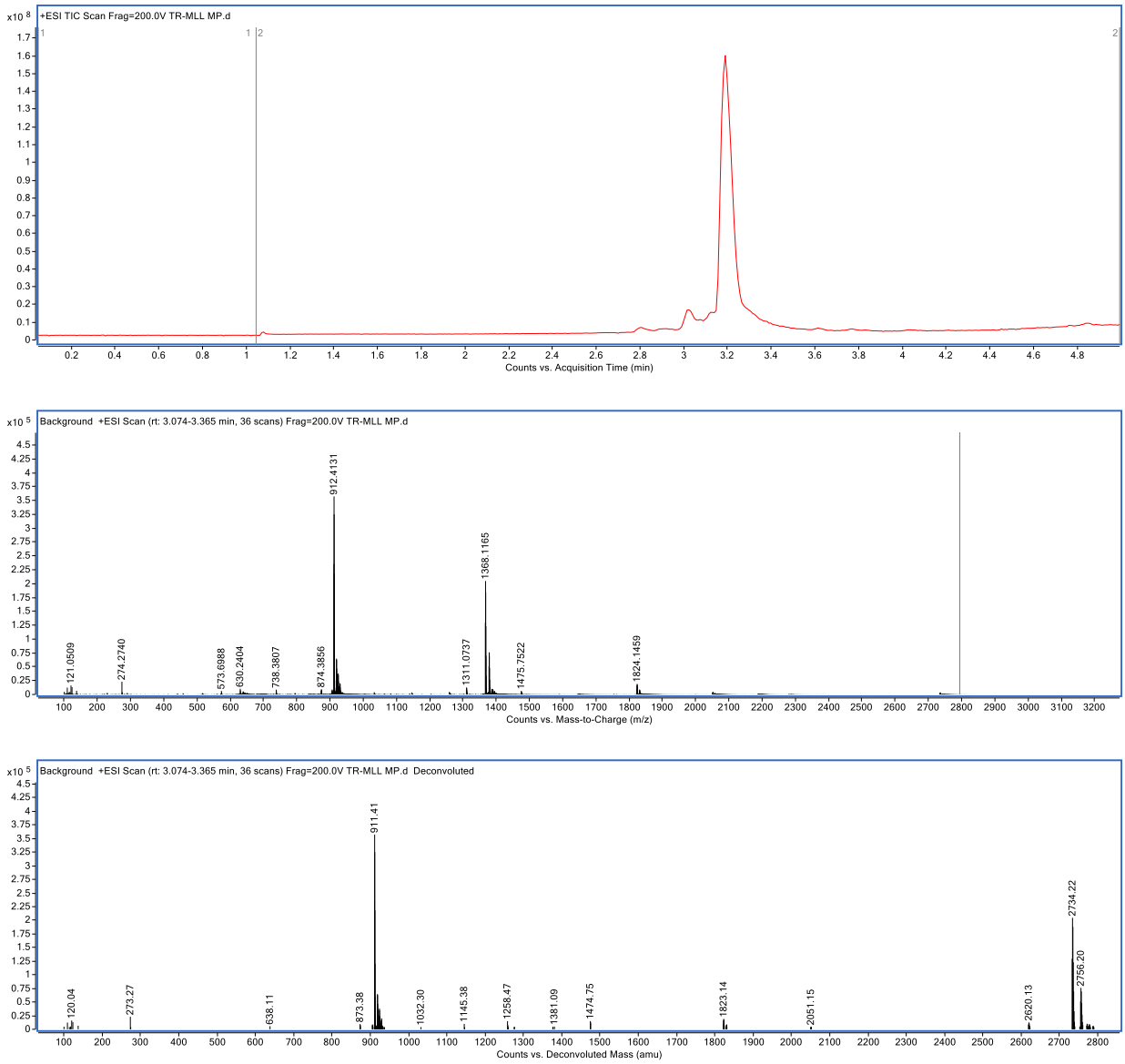


Figure A.3 Chromatogram and MS Spectra for TR-MLL

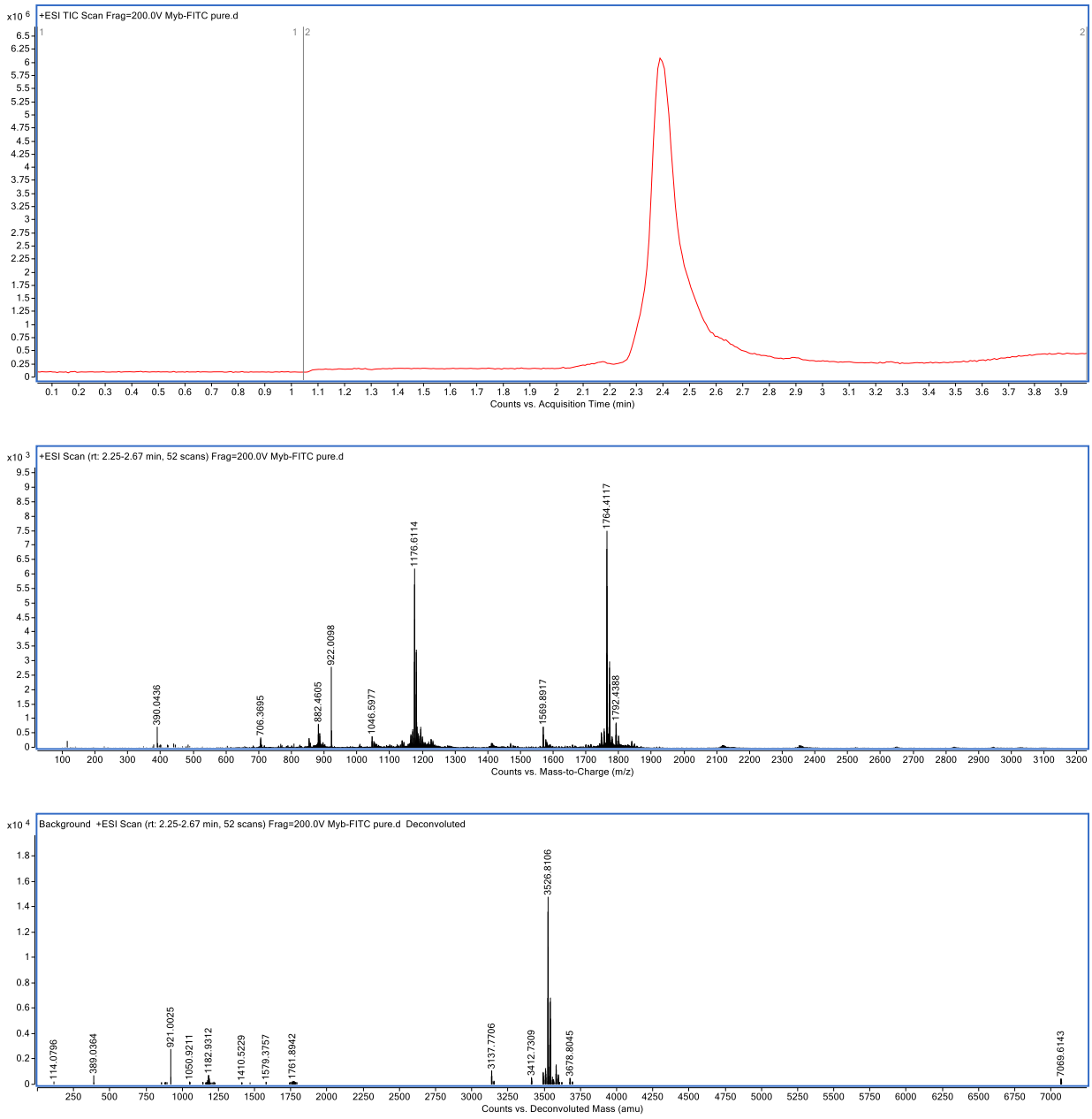


Figure A.4 Chromatogram and MS Spectra for FITC-Myb

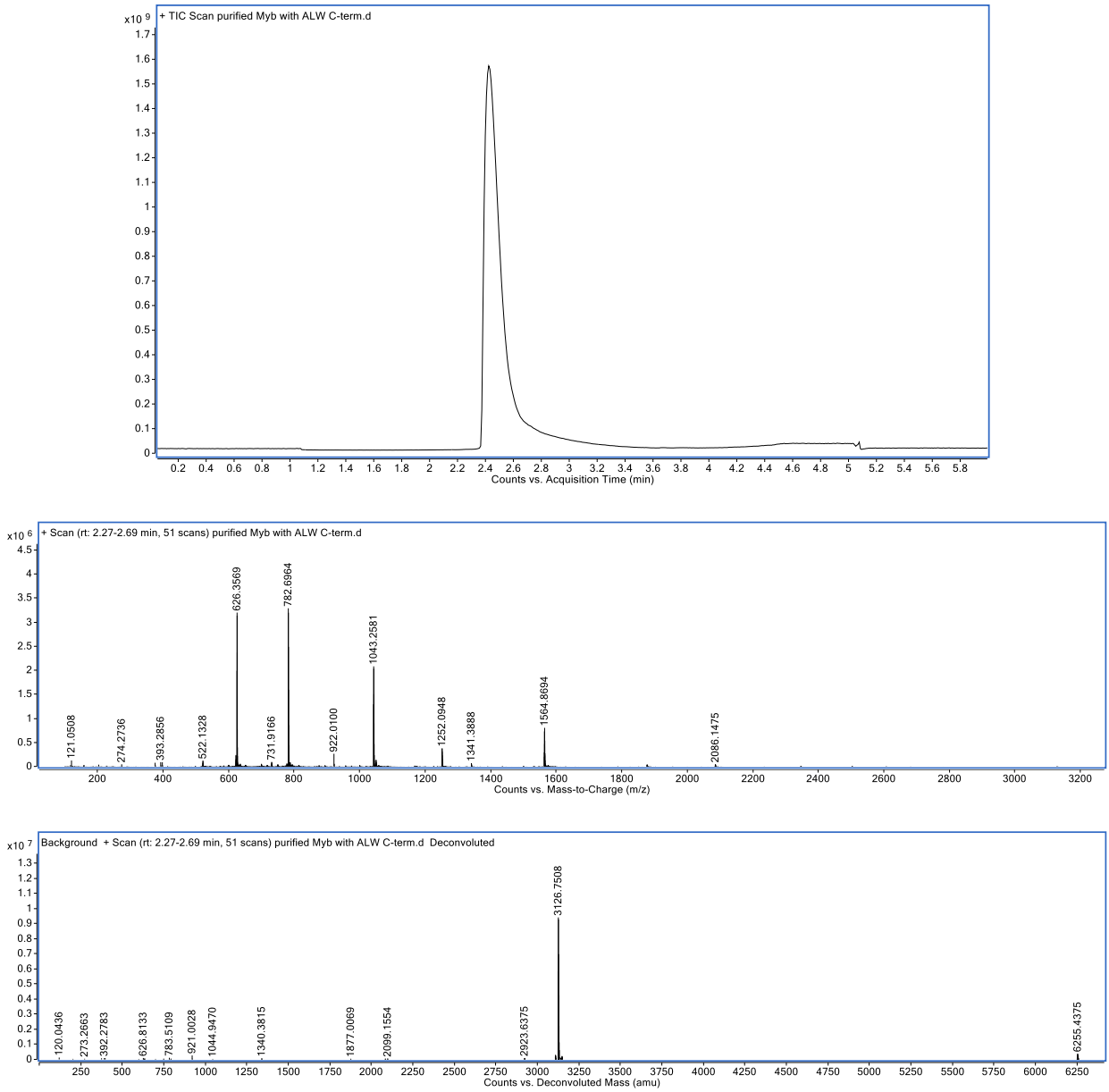


Figure A.5 Chromatogram and MS Spectra for unlabeled Myb

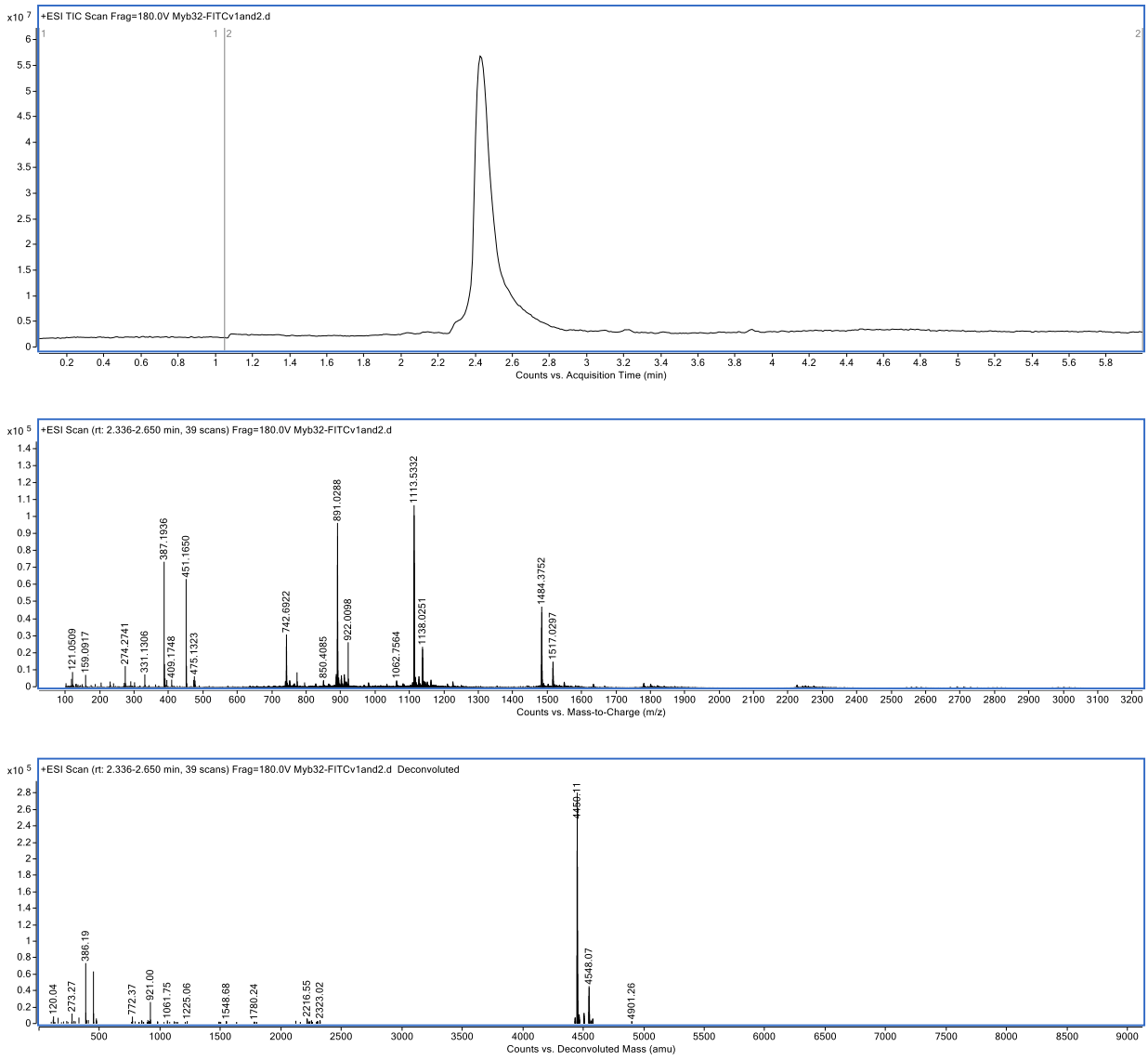


Figure A.6 Chromatogram and MS Spectra for FITC-Myb32

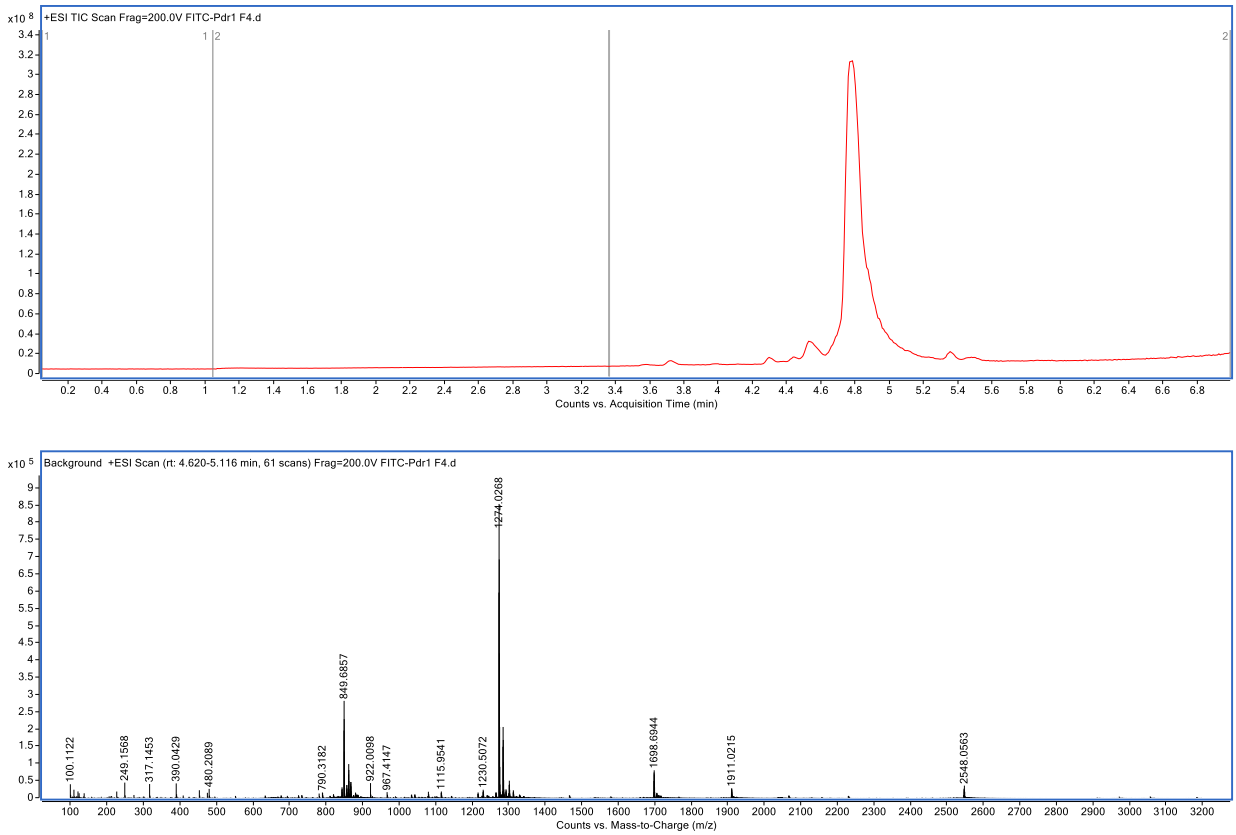


Figure A.7 Chromatogram and MS Spectrum for FITC-Pdr1

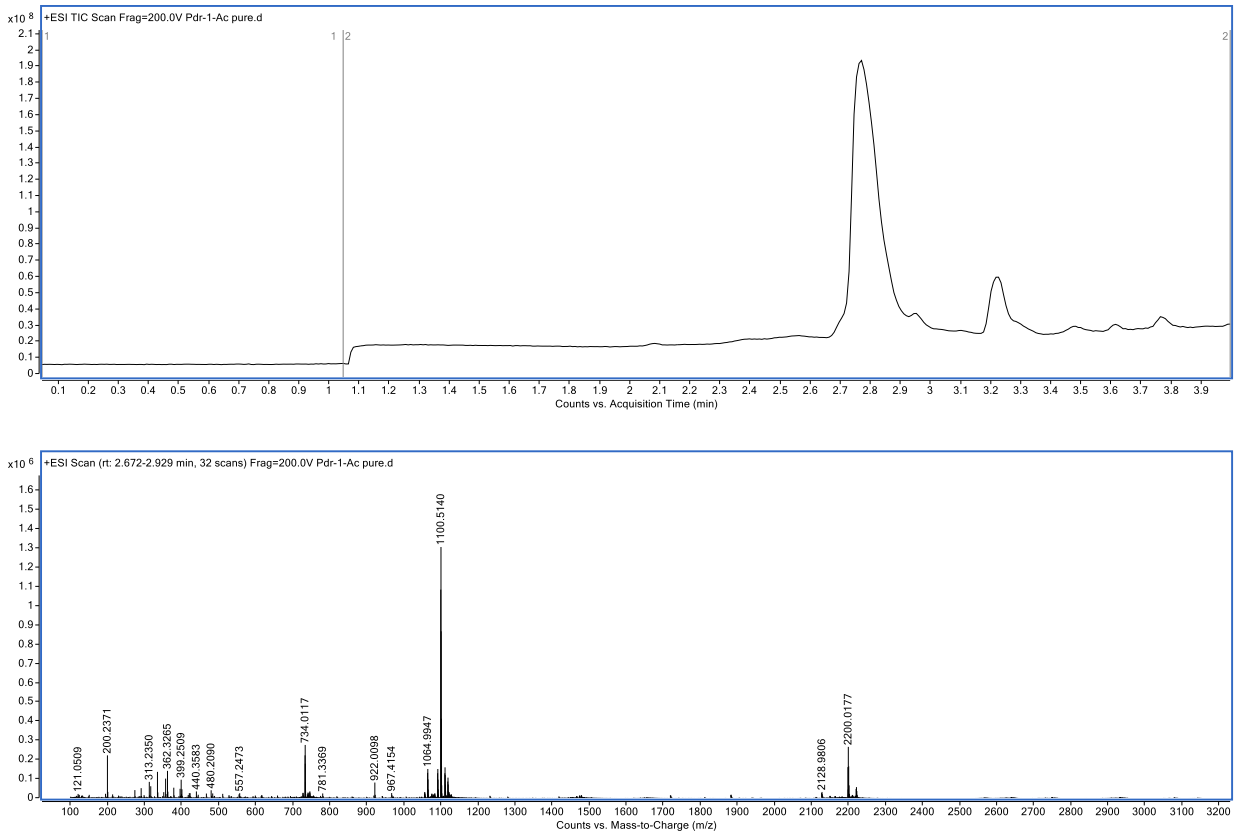
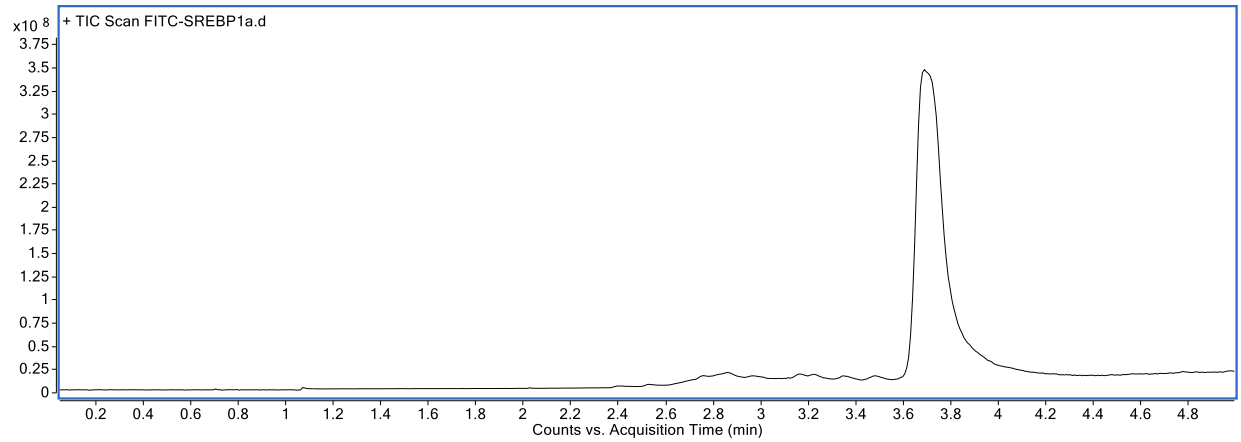
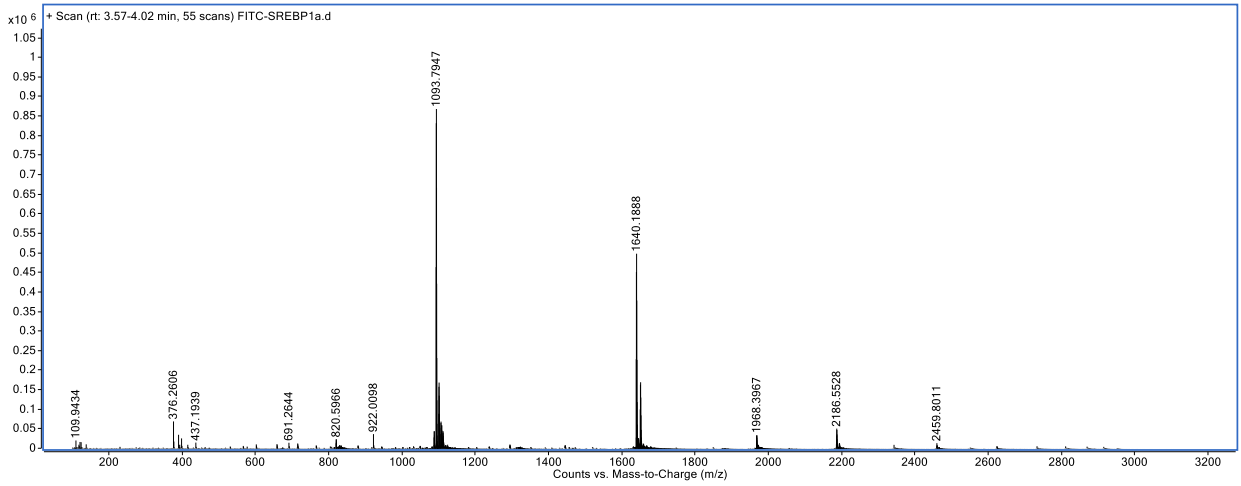


Figure A.8 Chromatogram and MS Spectrum for Ac-Pdr1





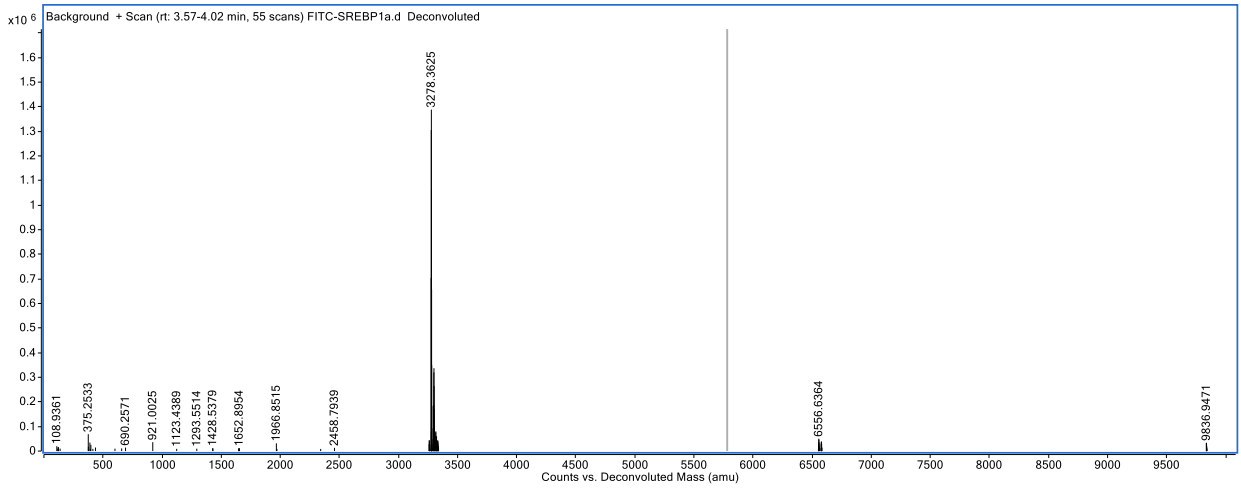


Figure A.9 Chromatogram and MS Spectra for FITC-SREBP1a

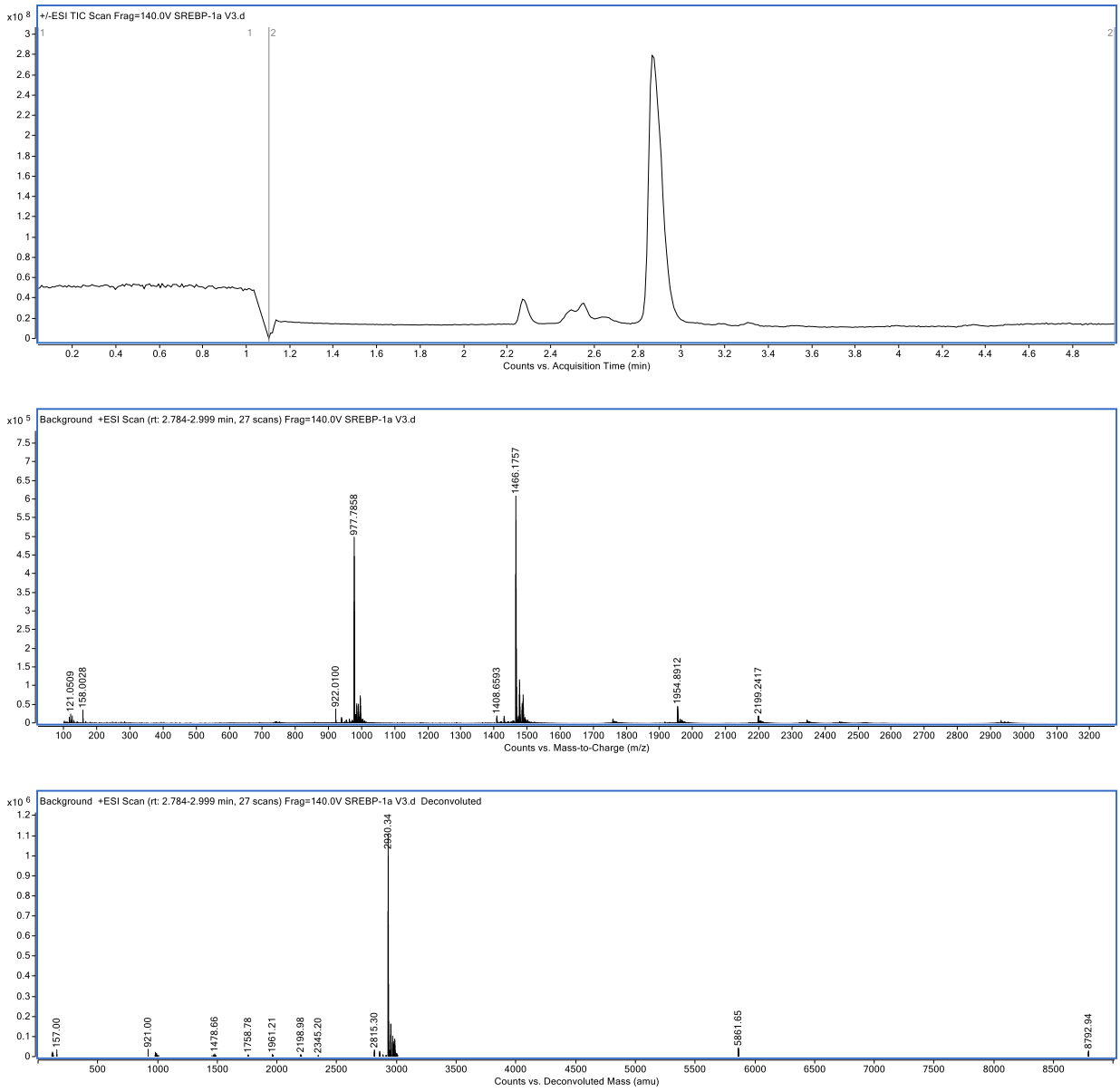


Figure A.10 Chromatogram and MS Spectrum for Ac-SREBP1a

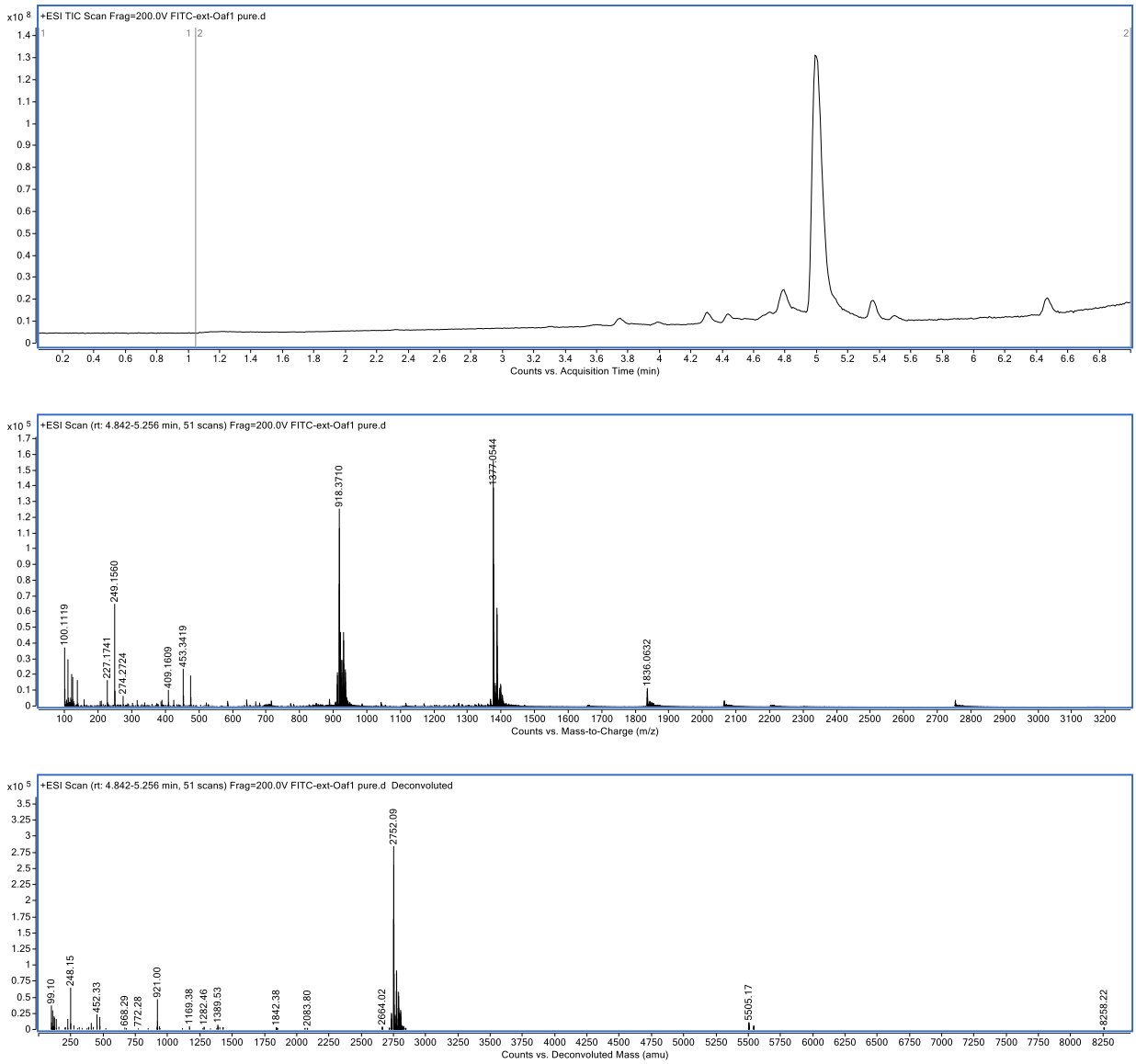


Figure A.11 Chromatogram and MS Spectra for FITC-Oaf1

Analytical High Performance Liquid Chromatography (HPLC) Data for Activator Peptides

Peptide	Purification Method
FITC-MLL	20-60% acetonitrile in 0.1% TFA water over 50 minutes
βAla-MLL	20-60% acetonitrile in 0.1% TFA water over 50 minutes
TR-MLL	20-60% acetonitrile in 0.1% TFA water over 50 minutes
βAla-Myb	10-50% acetonitrile in 0.1% TFA water over 40 minutes
FITC-Myb32	20-60% acetonitrile in 0.1% TFA water over 50 minutes
FITC-Pdr-1	20-40% acetonitrile in 0.1% TFA water over 40 minutes
Ac-Pdr-1	20-40% acetonitrile in 0.1% TFA water over 40 minutes
FITC-SREBP-1a	20-60% acetonitrile in 0.1% TFA water over 45 minutes
Ac-SREBP-1a	20-60% acetonitrile in 0.1% TFA water over 45 minutes
FITC-Oaf-1	20-60% acetonitrile in 0.1% TFA water over 60 minutes

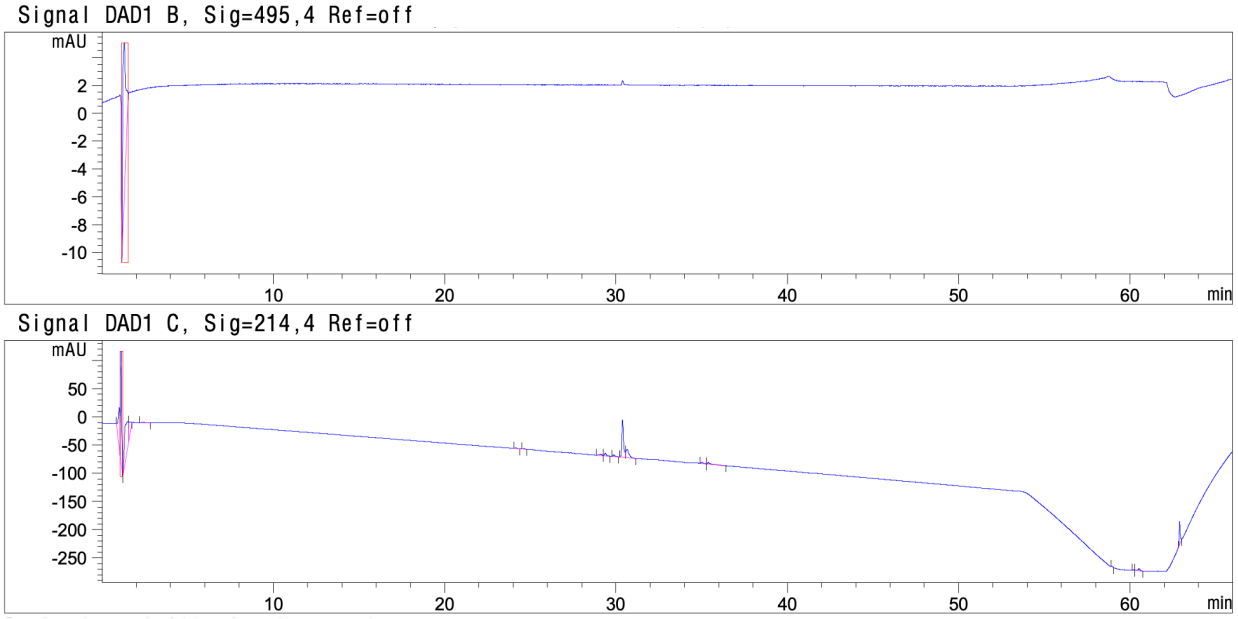


Figure A.12. Analytical HPLC trace of FITC-MLL monitored at 214 and 495 nm. Note the initial peak seen in the trace before the 2 minute mark is DTT, a reducing agent necessary for the effective purification of this peptide.

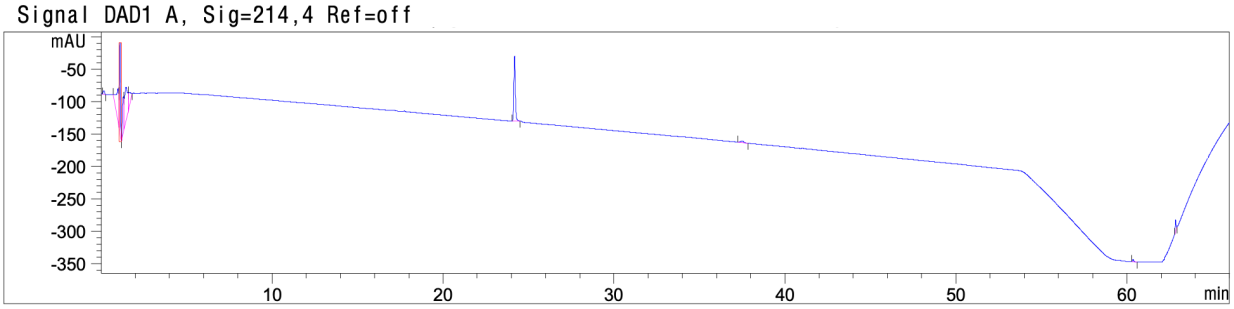


Figure A.13. Analytical HPLC trace of β-Ala-MLL monitored at 214 nm. Note the initial peak seen in the trace before the 2 minute mark is DTT, a reducing agent necessary for the effective purification of this peptide.

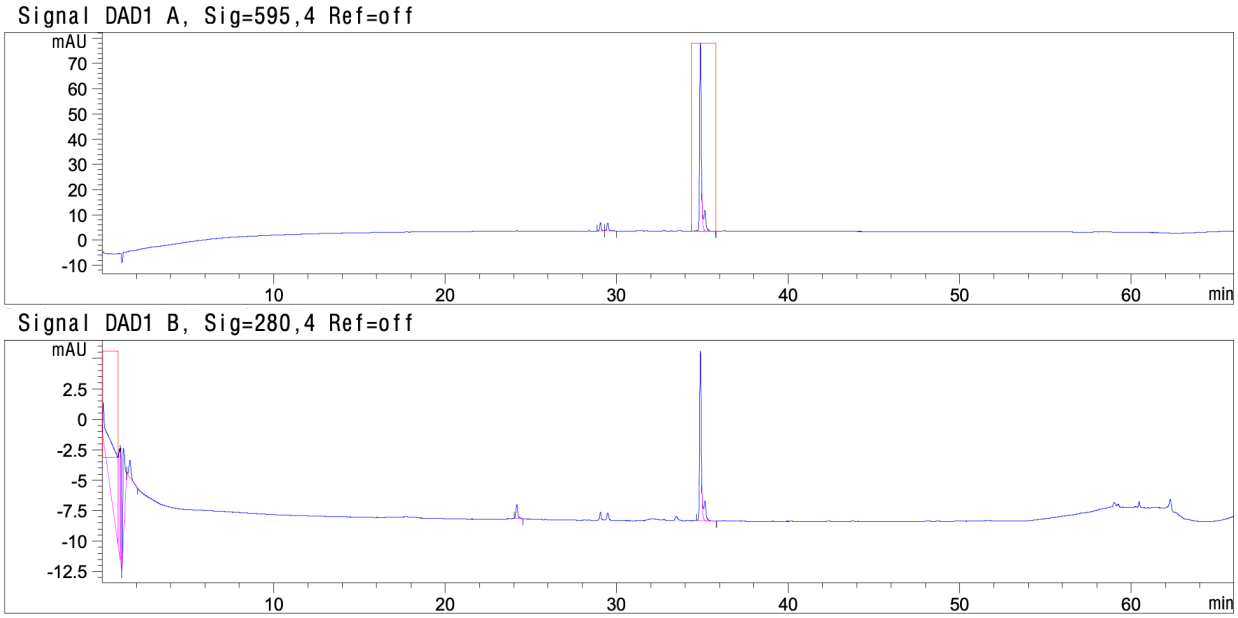


Figure A.14 Analytical HPLC trace of TR-MLL monitored at 280 and 595 nm.

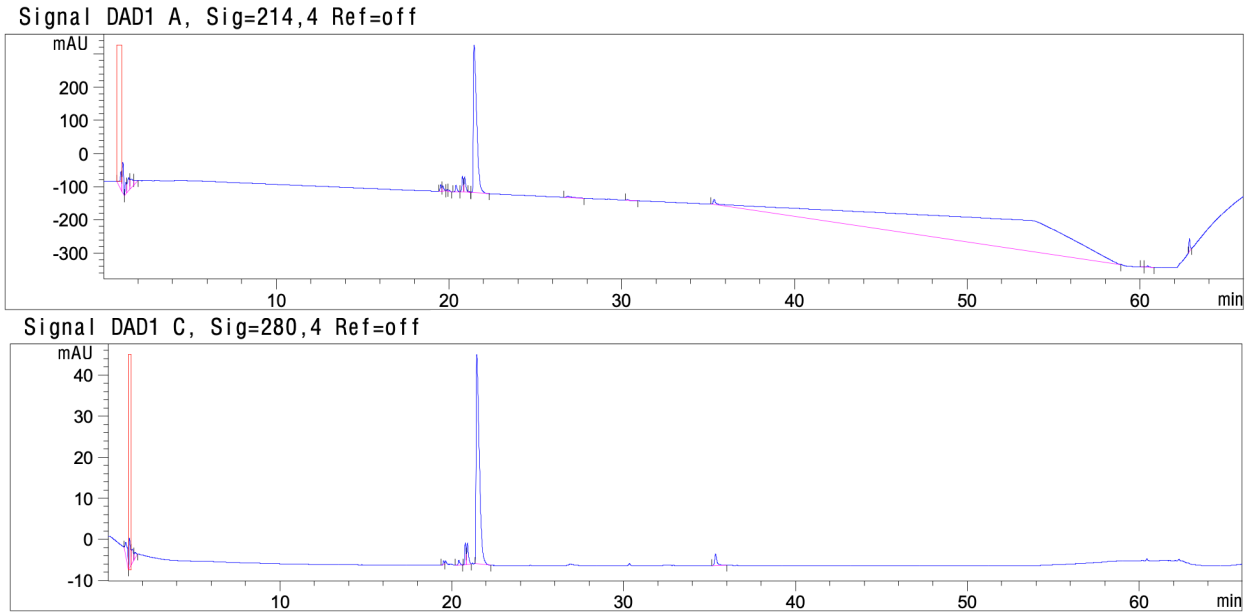


Figure A.15 Analytical HPLC trace of β-Ala-Myb monitored at 214 and 280 nm.

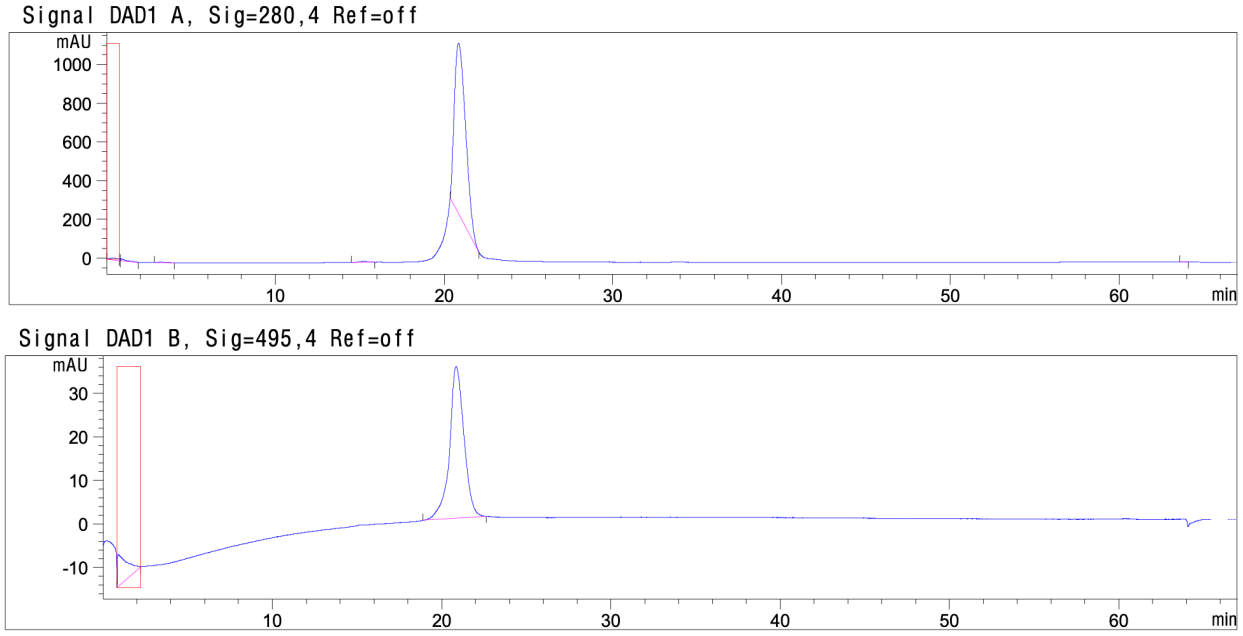


Figure A.16 Analytical HPLC trace of FITC-Myb32 monitored at 280 and 495 nm.

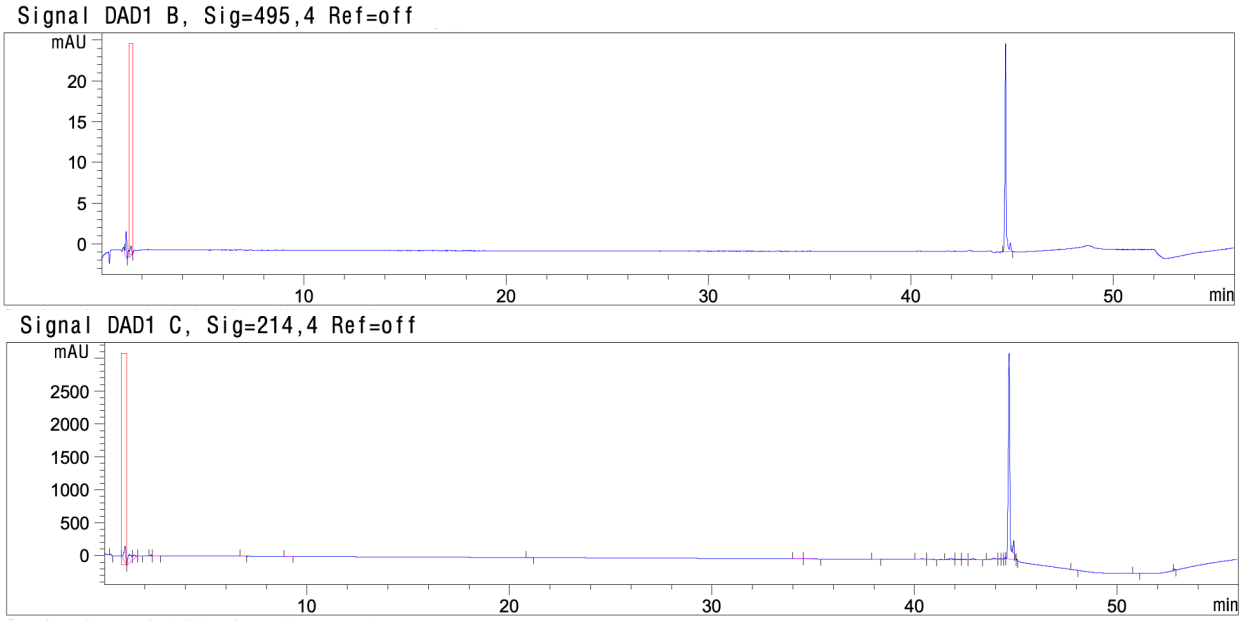


Figure A.17 Analytical HPLC trace of FITC-Pdr1 monitored at 214 and 495 nm. Note the initial peak seen in the trace before the 2 minute mark is DTT, a reducing agent necessary for the effective purification of this peptide.

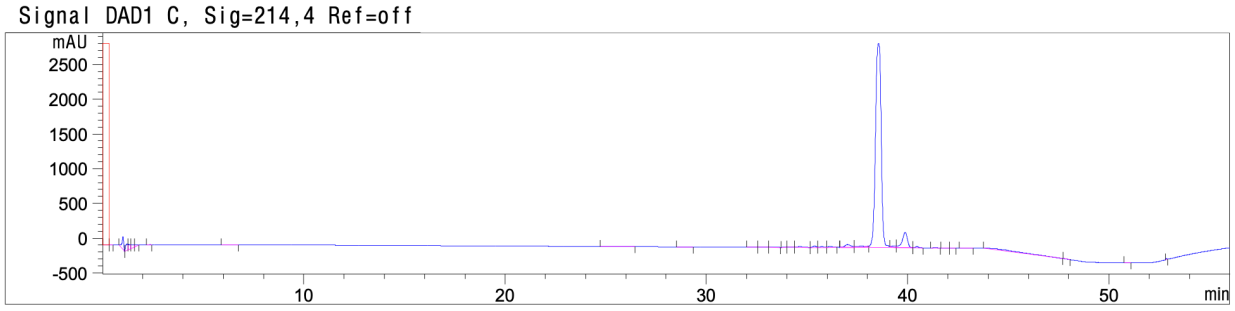


Figure A.18 Analytical HPLC trace of Ac-Pdr1 monitored at 214 nm. Note the initial peak seen in the trace before the 2 minute mark is DTT, a reducing agent necessary for the effective purification of this peptide.

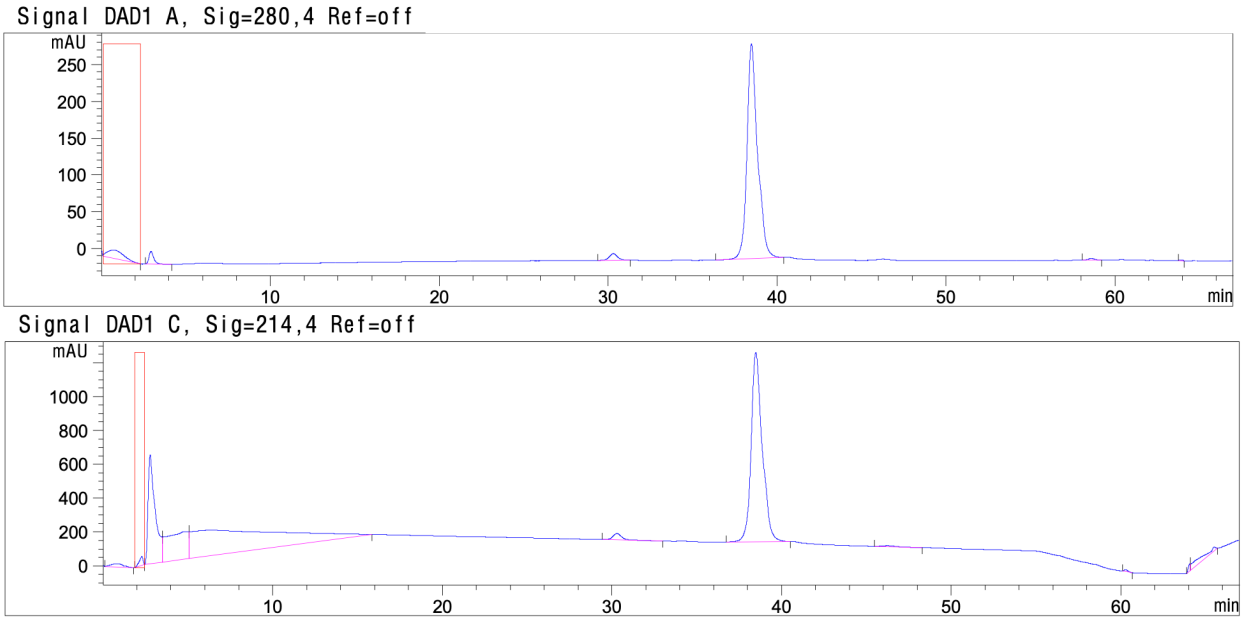


Figure A.19 Analytical HPLC trace of FITC-SREBP-1a monitored at 214 and 280 nm. Note the initial peak seen in the trace before the 2 minute mark is DTT, a reducing agent necessary for the effective purification of this peptide.

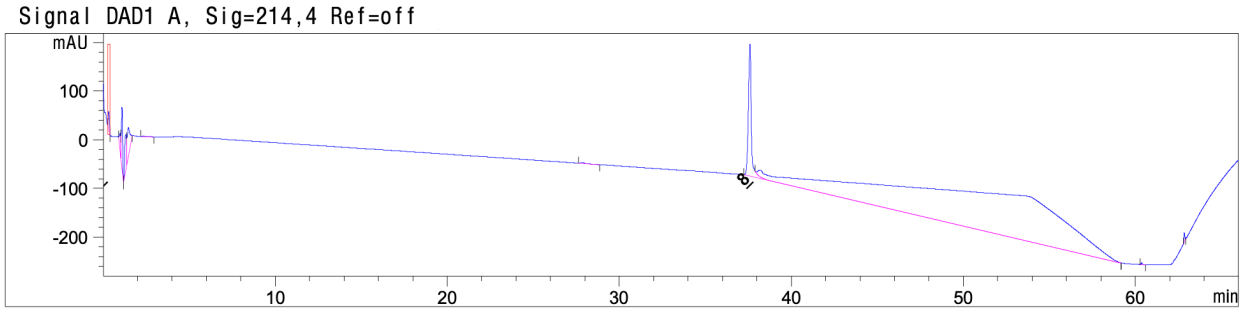


Figure A.20 Analytical HPLC trace of Ac-SREBP-1a monitored at 214 nm. Note the initial peak seen in the trace before the 2 minute mark is DTT, a reducing agent necessary for the effective purification of this peptide.

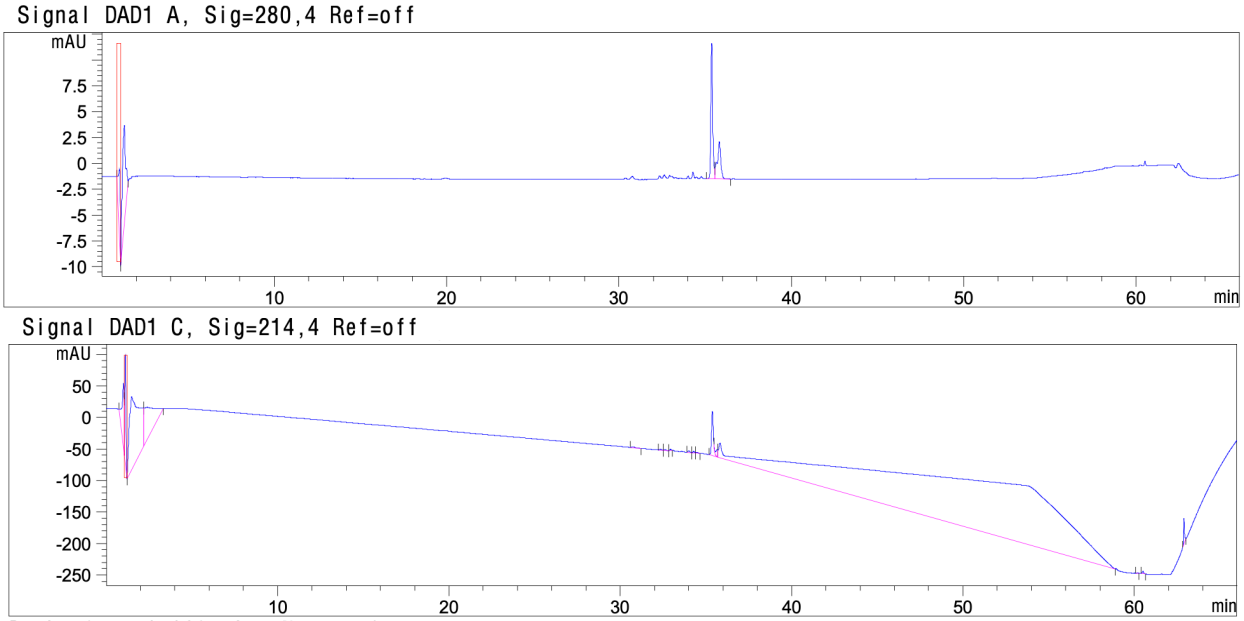


Figure A.21 Analytical HPLC trace of FITC-Oaf-1 monitored at 214 and 280 nm. Note the initial peak seen in the trace before the 2 minute mark is DTT, a reducing agent necessary for the effective purification of this peptide.

Appendix B: Supplemental Data for Chapter 2 – Targeting Loop Dynamics in the Search for Modulators for CBP KIX

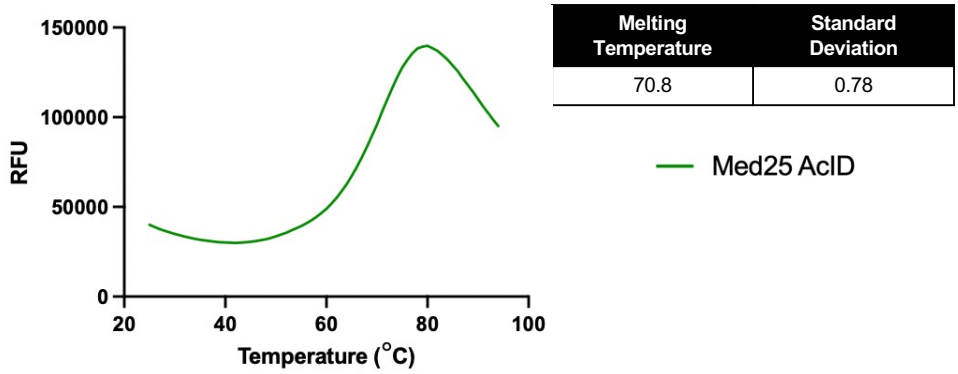


Figure B.1 Med25 AcID is a thermostable dynamic ABD. Med25 AcID thermal melting was measured by DSF in the standard storage buffer.

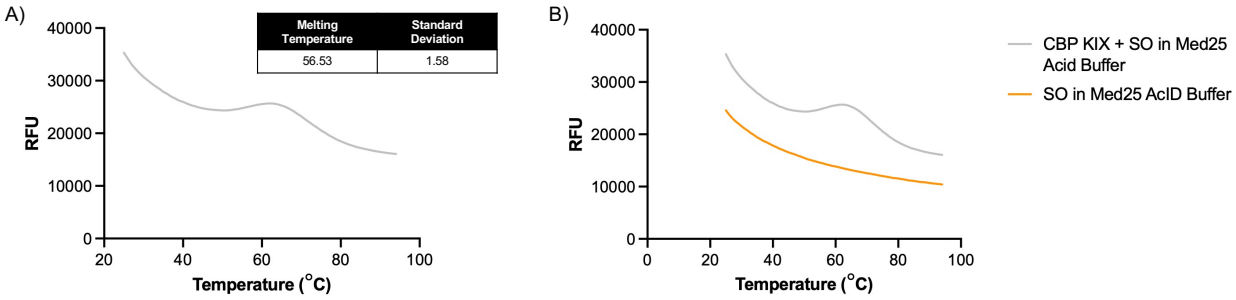
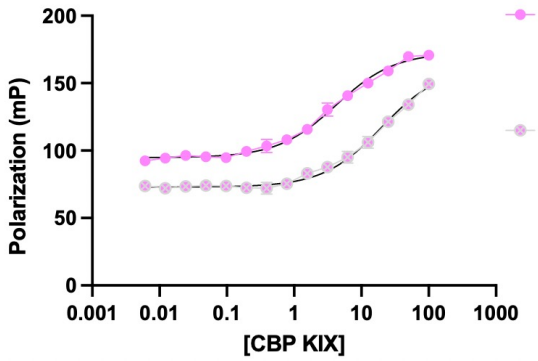


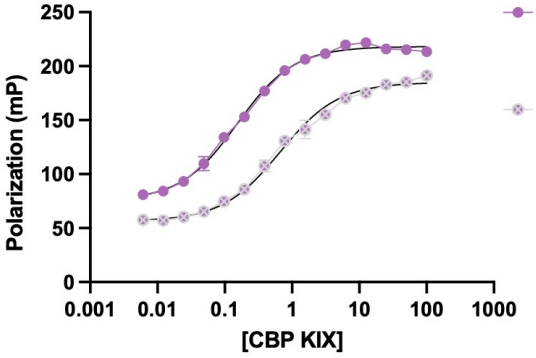
Figure B.2 DSF screening is not feasible with CBP KIX in Med25 AcID Buffer. A) In the standard storage buffer, also known as the Med25 AcID buffer, there is a high intrinsic fluorescence signal in the DSF assessment. B) Examination of the dye only control revealed that buffer is most likely interfering with the accurate measurement of CBP KIX melting temperature by DSF.

A)



Interaction	K_D (μM)
CBP KIX•c-Myb	4
	20

B)



Interaction	K_D (μM)
CBP KIX•MLL	0.14
	0.66

Figure B.3 Sodium phosphate concentration can shift TAD binding affinity. The calculated dissociation constants for A) Myb and B) MLL changed in conjunction with the change in sodium phosphate concentration.

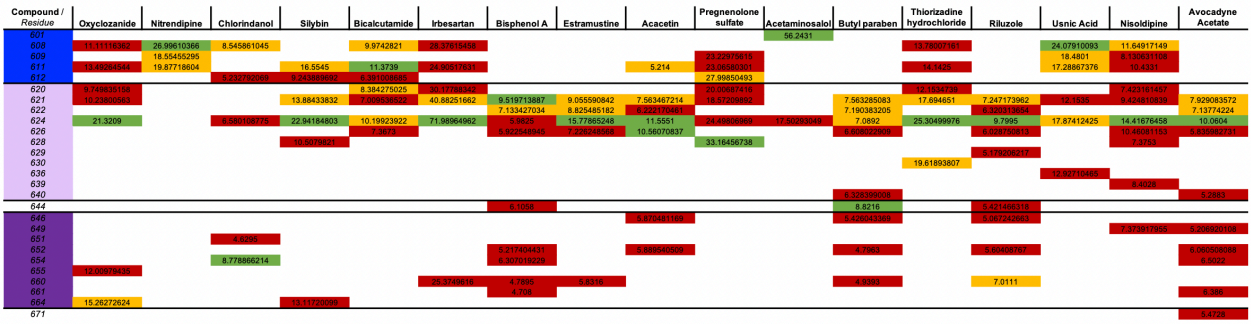


Figure B.4 Analysis of the regional chemical shifts for the significant CBP KIX modulators. Only those chemical shift changes of more than one standard deviation were noted and thus considered notable.

Appendix C: Supplemental Data for Chapter 3 – Setting the Stage for Targeting and Investigating the MED15 KIX Motifs

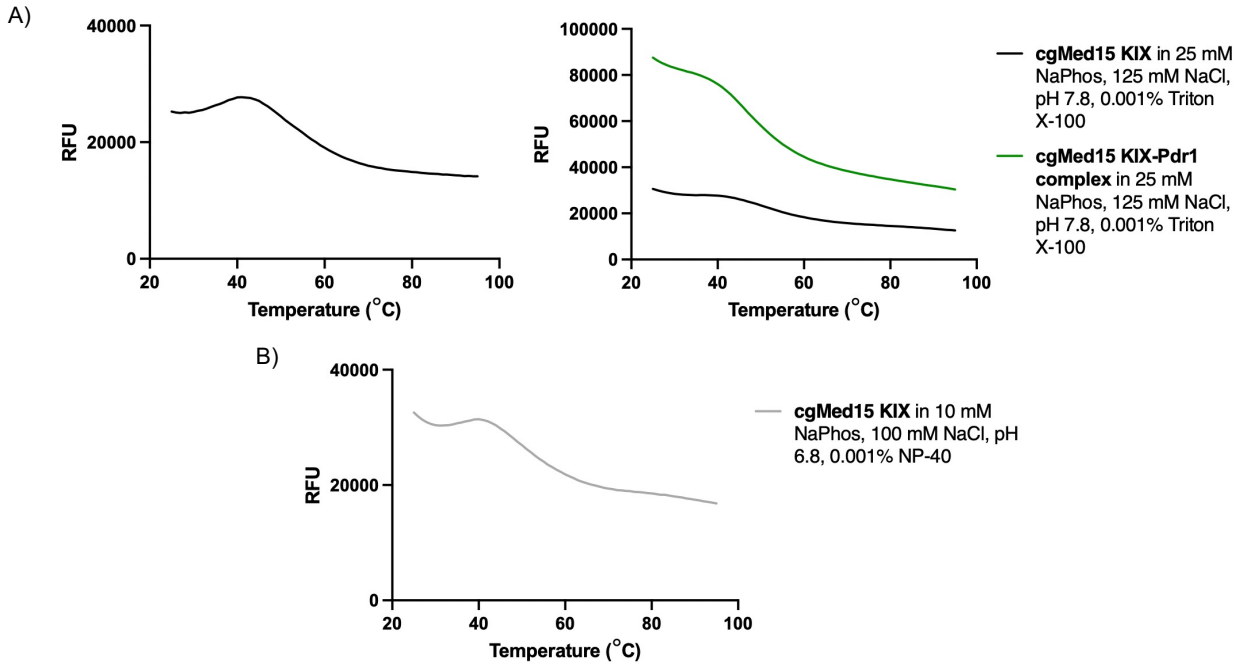
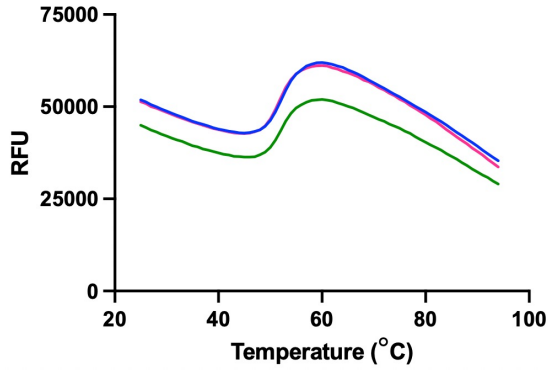


Figure C.1 Preliminary DSF assessment with cgMed15 KIX and SYPRO Orange. A) Use of the CBP KIX DSF conditions rendered visualization of ligand-induced thermostability changes impossible. B) However, simply changing the buffer conditions was not helpful in improving the apparent melting curve for cgMED15 KIX.



Buffer	Med25 AcID T_M (°C)
50 mM MOPS, 50 mM NaCl pH 6.5	52.3±0.1
50 mM MOPS, 50 mM NaCl pH 6.8	52.2±0.1
50 mM MES, 50 mM NaCl pH 6.5	51.8±0.1

Figure C.2 Top conditions for bis-ANS in Med25 AcID DSF assessment

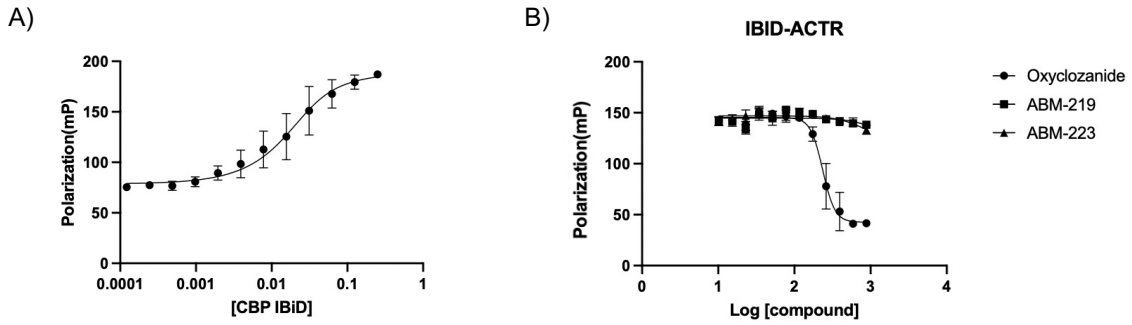


Figure C.3 The strong CBP IBiD and ACTR interaction is effectively inhibited by oxyclozanide. The A) direct binding FP experiments with ACTR set the protein concentration for B) the competitive FP assay with oxyclozanide and its analogs.

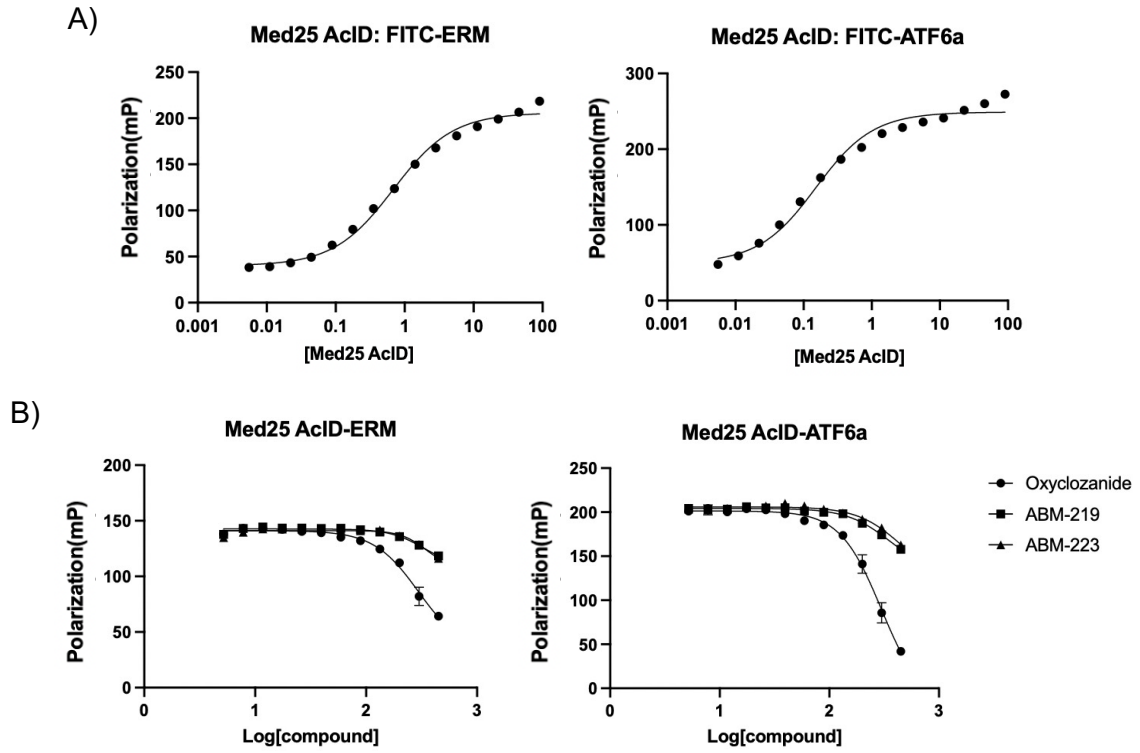


Figure C.4 Med25 AcID PPIs are largely unaffected by oxyclozanide. The A) direct binding FP experiments with ATF6α and ERM set the protein concentration for B) the competitive FP assay with oxyclozanide and its analogs.

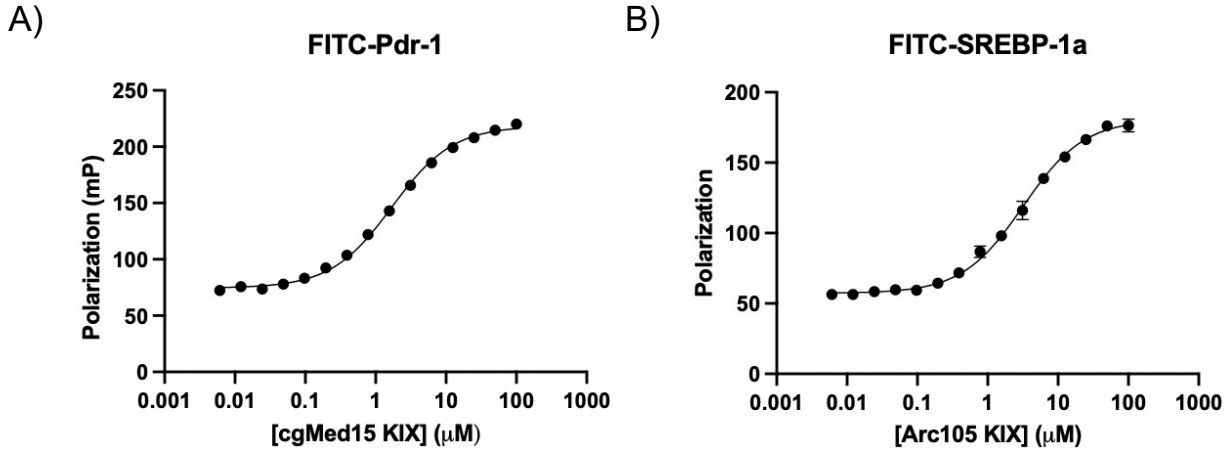
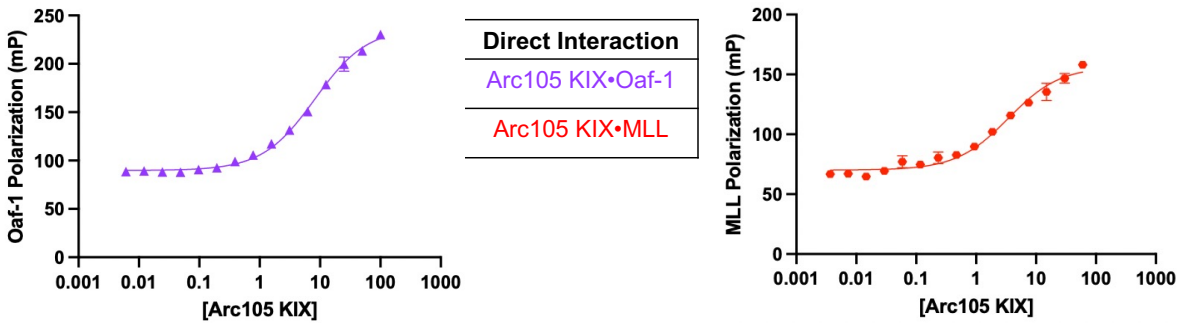


Figure C.5 FP Direct Binding Experiments with the known native ligands of A) cgMed15 KIX and B) Arc105 KIX.

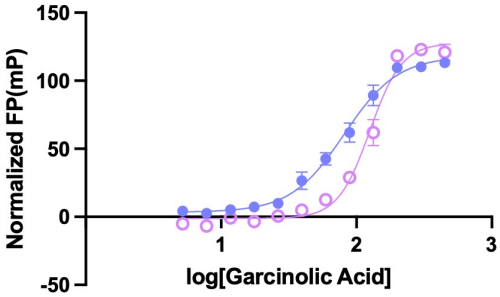
A)



B)

SREBP-1a	GPCDLDAALLTDIEDMLNLINNQDSD
Pdr-1	GDLEDLYSILWSDVYPDS
Oaf-1	GYFGGLDLFDYDFLFGNDFA
MLL	ADSGNILPSDIMDFVLKNTP

Figure C.6 Arc105 KIX Direct Binding with alternative TADs and TAD comparison. A) Oaf-1 and MLL interacts with ARC105 KIX in a weaker manner as compared to SREBP-1a and Pdr-1. B) The sequences and properties of the tested TADs varied significantly. Yellow letters represented the special case amino acids. Green letters represented those amino acids with negatively charged side chains. Red letters indicated those amino acids with hydrophobic side chains. The orange letters indicated those amino acids with positively charged side chains. The blue letters displayed those amino acids with aromatic side chains.



Interaction	K_I (μM)
Arc105 KIX•SREP-1a	22
Arc105 KIX•Pdr-1	35

Figure C.7 Garcinolic Acid inhibits Arc105 KIX interactions to similar degrees.

Appendix D: Supplemental Data for Chapter 4 – Uncovering Colorimetric Dye Sensors that Engage Conformationally Dynamic ABDs and Detect Their Binding Events

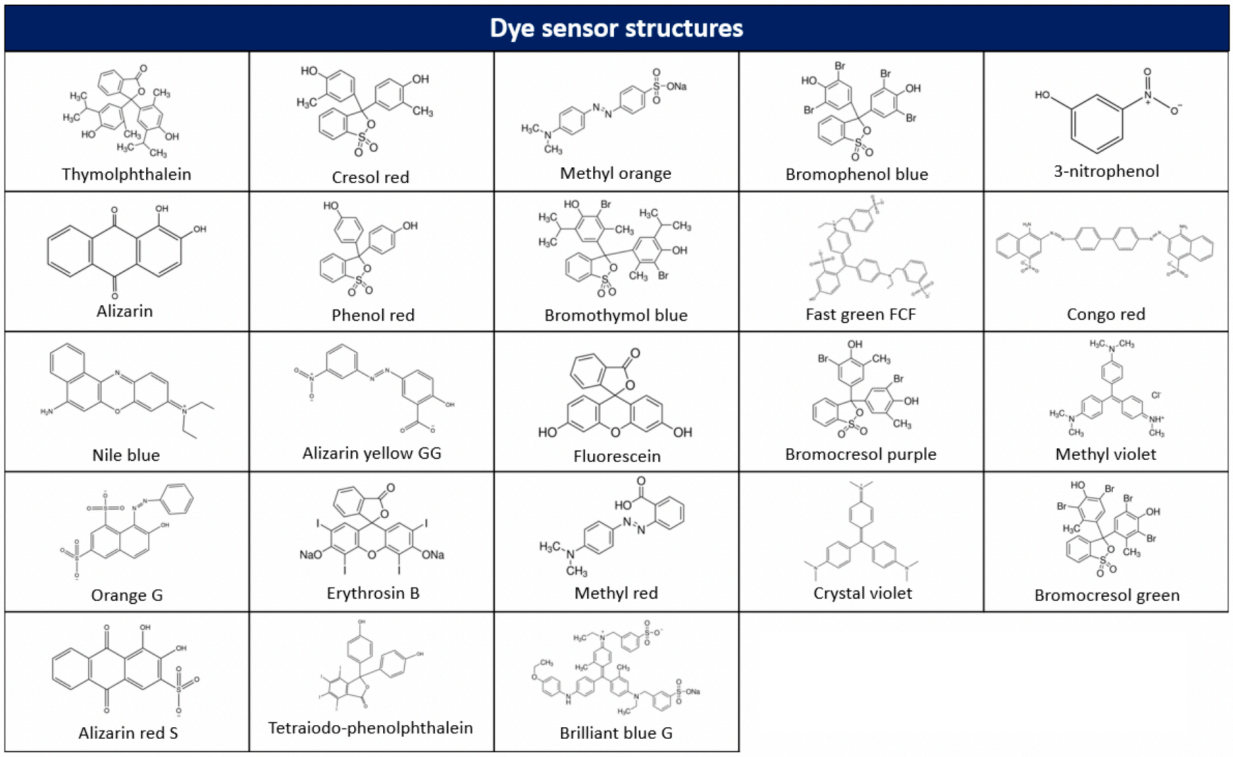


Figure D.1 The 23 dyes utilized in the colorimetric array screening

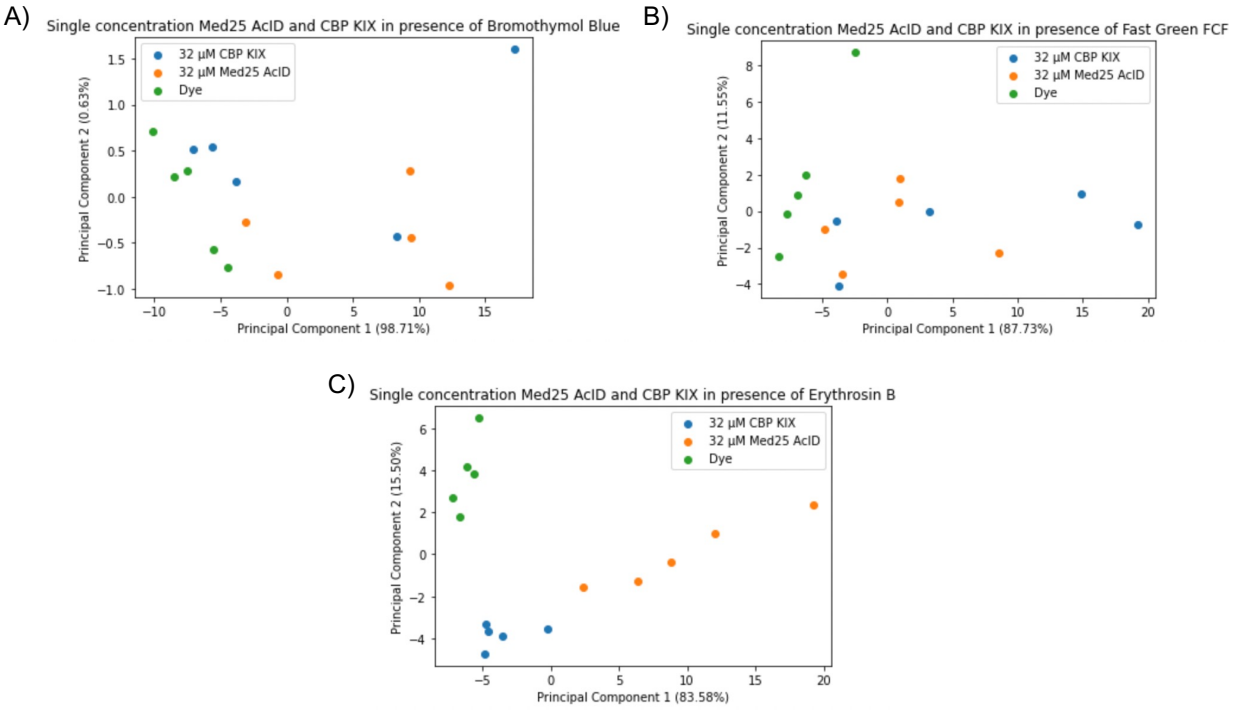


Figure D.2 PCA of the absorbance spectra for each ABD as single concentration compared to the dye alone

Table D.1 Dye concentrations for the initial colorimetric array screening

Dye number	Dye name	Final [uM]
1	Thymolphthalein	12.65
2	Cresol Red	10.66
3	Methyl Orange	10.25
4	Bromophenol Blue	6.42
5	3-Nitrophenol	485.71
6	Alizarin	33.03
7	Phenol Red	8.20
8	Bromothymol Blue	27.27
9	Fast Green FCF	4.45
10	Congo Red	13.14
11	Nile Blue	2.37
12	Alizarin yellow GG	39.62
13	Fluorescein	6.35
14	Bromocresol Purple	22.62
15	Methyl Violet	7.90
16	Orange G	35.09
17	Erythrosin B	5.48
18	Methyl Red	24.75
19	Crystal Violet	5.66
20	Bromocresol Green	26.47
21	Alizarin Red S	41.23
22	Tetraiodo-phenolphthalein	49.07
23	Brilliant Blue G	11.15